RICE UNIVERSITY

Correcting the Self-Interaction Error of Approximate Density Functionals

by

Oleg A. Vydrov

A Thesis Submitted
in Partial Fulfillment of the
Requirements for the Degree

Doctor of Philosophy

Approved, Thesis Committee:

Gustavo E. Scuseria, Chairman
Robert A. Welch Professor of Chemistry

Anatoly B. Kolomeisky
Assistant Professor of Chemistry

Peter J. Nordlander
Professor of Physics and
Electrical and Computer Engineering

Houston, Texas

May, 2007

Abstract

Correcting the Self-Interaction Error of Approximate Density Functionals

by

Oleg A. Vydrov

Common density functional approximations (DFAs) for the exchange-correlation energy suffer from self-interaction error (SIE), which is believed to be the cause of many of the failures of these approximations, such as poor description of charge transfer and transition states of chemical reactions. The standard self-interaction correction (SIC) of Perdew and Zunger (PZ) removes spurious self-interaction terms orbital-by-orbital. We implemented the Perdew–Zunger SIC self-consistently and carried out systematic tests of its performance. We found that PZ-SIC impairs the accuracy of semi-local functionals for equilibrium properties. PZ-SIC seems to overcorrect many-electron systems. We devised a modified version of the SIC, which is scaled down in many-electron regions. The scaled-down SIC has greatly improved performance for many molecular properties.

Studies of fractionally-charged systems led to the new definition of "many-electron self-interaction error", which is a generalization of the one-electron concept. An "M-electron self-interaction-free" functional is one that produces a realistic linear

variation of total energy with electron number N between the integers M–1 and M. Semi-local DFAs exhibit large many-electron SIE and therefore fail for systems with fractional average electron number. PZ-SIC and its scaled-down variants are one-electron SIE-free. PZ-SIC is often nearly many-electron SIE-free, but this property is lost in the scaled-down SIC.

Another consequence of the SIE is incorrect asymptotic behavior of the exchange-correlation potential in semi-local DFAs. PZ-SIC recovers the exact asymptote, but its scaled-down version does not. An efficient method to impose the exact asymptote in a hybrid functional is to introduce range separation into the exchange component and replace the long-range portion of the approximate exchange by the Hartree–Fock counterpart. We show that this long-range correction works particularly well in combination with the short-range variant of the Perdew, Burke, and Ernzerhof (PBE) exchange functional. This long-range-corrected hybrid, denoted LC-ωPBE, is remarkably accurate for a broad range of molecular properties, such as thermochemistry, barrier heights of chemical reactions, bond lengths, and most notably, description of processes involving long-range charge transfer. Although LC-ωPBE is not exactly one-electron SIE-free, it can be nearly many-electron SIE-free in many cases.

Acknowledgments

I would like to thank Prof. Gustavo Scuseria for his skillful mentoring and for providing considerable freedom in the choice of research direction and in the choice of working habits. I am indebted to Dr. Viktor Staroverov, Dr. Juan Peralta, and Dr. Sergey Maximoff for enlightening discussions, especially at the early stages of my research. I enjoyed fruitful collaborations with Prof. John Perdew, Prof. Gábor Csonka, Dr. Adrienn Ruzsinszky, and Dr. Jochen Heyd (aka JJ). I thank Dr. Ionut Prodan, Dr. Ed Brothers, Dr. Ben Janesko, and Artur Izmaylov for their contribution to creating an enjoyable work atmosphere. I greatly appreciate the continuous support of all my friends at Rice and outside, who are too numerous to mention individually.

Contents

Abstract ii

Acknowledgments iv

List of Illustrations viii

List of Tables x

Preface xii

List of Abbreviations xiv

1 Introduction and background 1

1.1 Kohn–Sham density functional theory 1

1.2 Approximate exchange-correlation functionals 3

  1.2.1 Semi-local approximations 4

  1.2.2 Hybrid functionals 5

1.3 One-electron self-interaction error 8

1.4 Many-electron self-interaction error and its relation to fractionally-charged systems 10

2 Self-interaction corrections utilizing orbital densities 13

2.1 Perdew–Zunger self-interaction correction 13

  2.1.1 Approximate implementations of the Perdew–Zunger SIC . . . 14

  2.1.2 Rigorous implementation of the Perdew–Zunger SIC 15

  2.1.3 Magnitudes of the correction 17

2.2 The effect of the Perdew–Zunger SIC on the performance of approximate density functionals 21

  2.2.1 Atomic ionization potentials and electron affinities 22

  2.2.2 Molecular ionization potentials and electron affinities 24

  2.2.3 Enthalpies of formation 27

2.3 Scaling down the Perdew–Zunger correction 28

2.3.1 Magnitudes of the scaling factors 31

2.3.2 Total energies of atoms 31

2.3.3 Atomization energies 34

2.3.4 Barrier heights of chemical reactions 36

2.3.5 Ionization potentials and electron affinities 38

2.3.6 Bond lengths 40

2.4 Discussion 42

2.4.1 Effects of using orbital densities 42

2.4.2 Formal properties of the SIC 43

2.5 Some alternative self-interaction corrections 46

3 Long-range-corrected hybrid functionals 47

3.1 Designing the optimal long-range-corrected hybrid 49

3.1.1 Tests on enthalpies of formation 50

3.1.2 Tests on barrier heights of chemical reactions 52

3.1.3 Tests on ionization potentials and electron affinities 55

3.2 Assessment of the LC-ωPBE functional 58

3.2.1 Total energies of atoms 59

3.2.2 Thermochemistry 60

3.2.3 Barrier heights of chemical reactions 63

3.2.4 Bond lengths 65

3.2.5 Hydrogen-bonded complexes 66

3.3 Discussion: long-range corrected vs. global hybrid functionals 67

4 Tests for fractionally-charged systems 70

4.1 Methodology and implementation 71

4.2 Varying the electron number in an atom 72

4.3 Dissociation of the NaCl molecule 77

4.4 Dissociation of the LiF molecule 80

4.5 Dissociation of symmetric radical cations 83
4.6 The effect of scaling down the SIC 89

5 Conclusions **93**

A Self-consistent implementation of the Perdew–Zunger SIC with Gaussian basis sets **95**

B Energy derivatives for the scaled-down SIC **98**

Bibliography **99**

Illustrations

1.1 Ground state energy E as a function of the electron number N. 11

2.1 Magnitudes of the Perdew–Zunger SIC for LSDA, PBE, TPSS, and PBE0 in atoms from H to Ar. 19

2.2 Contributions to E^{SIC} from individual shells in atoms. 20

2.3 Errors per electron in total energies of the atoms from Li to Ar 34

3.1 Mean absolute errors in the standard enthalpies of formation of the G2-1 set as a function of the exchange mixing parameter in global hybrids. 50

3.2 ω-dependence of mean absolute errors in the standard enthalpies of formation of the G2-1 set for the “long-range-corrected” hybrids. . . . 51

3.3 Mean absolute errors in the barrier heights of the BH42 set as a function of the exchange mixing parameter in global hybrids. 53

3.4 ω-dependence of mean absolute errors in the barrier heights of the BH42 set for the “long-range-corrected” hybrids. 54

3.5 Mean absolute errors in the ionization potentials and electron affinities of the G2 set as a function of the exchange mixing parameter in global hybrids of PBE. 56

3.6 ω-dependence of mean absolute errors in the ionization potentials and electron affinities of the G2 set for the “long-range-corrected” hybrids of PBE. 57

4.1 Total energy of the C atom as a function of the electron number N. . 73

4.2 Highest occupied orbital energy $\varepsilon_{\mathrm{HO}}$ of the C atom as a function of the electron number N. 74

4.3 Highest diagonal Lagrange multiplier ε_{ii} compared to the highest eigenvalue of the Lagrange multipliers matrix in PZ-SIC-PBE for the C atom as a function of the electron number N. 76

4.4 NaCl dissociation curves. 79

4.5 Energy difference $\Delta E = E(\mathrm{Li}^{+q}) + E(\mathrm{F}^{-q}) - E(\mathrm{Li}) - E(\mathrm{F})$ as a function of q. This represents the dissociation limit of LiF. 80

4.6 LiF dissociation curves. 81

4.7 Mulliken charge on the Li atom as a function of the internuclear distance in LiF. 82

4.8 Ar_2^+ dissociation curves. 86

4.9 Energy difference $\Delta E = E(\mathrm{Ne}^{+q}) + E(\mathrm{Ne}^{+(1-q)}) - E(\mathrm{Ne}) - E(\mathrm{Ne}^{+})$ as a function of q. This represents the dissociation limit of Ne_2^+. . . . 87

4.10 Ne_2^+ dissociation curves. 88

4.11 Ne_2^+ dissociation curves calculated with a scaled-down self-interaction correction. 90

4.12 Ne_2^+ dissociation curves calculated with a scaled-down self-interaction correction with a simplified scaling factor. 91

Tables

2.1 Mean absolute E^{SIC} per electron. 18

2.2 ΔSCF ionization potentials and electron affinities for atoms from H to Ar computed with self-interaction-corrected and uncorrected functionals. 24

2.3 Molecular benchmark set used to test the performance of PZ-SIC for ionization potentials and electron affinities. 25

2.4 ΔSCF ionization potentials and electron affinities for a molecular test set computed with self-interaction-corrected and uncorrected functionals 26

2.5 Standard enthalpies of formation ($\Delta_\mathrm{f}H^\circ_{298}$) for the G2-1 test set computed with self-interaction-corrected and uncorrected functionals. 27

2.6 Values of the scaling factors for different shells in the Ar atom. 32

2.7 Errors per electron in total energies of the atoms from Li to Ar. . . . 33

2.8 Errors in atomization energies for the AE6 test set. 35

2.9 Errors in barrier heights for the BH6 test set. 37

2.10 Deviations from experiment of ΔSCF ionization potentials and electron affinities for atoms from H to Ar 39

2.11 Deviations from experiment of equilibrium bond lengths for 12 molecules. 41

3.1 Total energies of atoms. 59

3.2 Deviations from experiment of standard enthalpies of formation ($\Delta_\mathrm{f}H^\circ_{298}$), ionization potentials, electron affinities, and proton affinities of the G2 and G3 test sets. 61

3.3 Deviations from experiment of barrier heights of chemical reactions. . 64

3.4 Summary of deviations from experiment of equilibrium bond lengths (r_e) for 95 molecules. 65
3.5 Errors in dissociation energies (D_e) of hydrogen-bonded complexes. . 66
3.6 Errors in hydrogen bond lengths (r_e) of hydrogen-bonded complexes. 67

4.1 Predicted dissociation limits of NaCl. 78
4.2 Dissociation of symmetric radical cations. 84

Preface

This thesis is based on parts of my research conducted at Rice University. Most of the results presented here have been previously published in a series of papers:

- Oleg A. Vydrov and Gustavo E. Scuseria,
  Effect of the Perdew–Zunger self-interaction correction on the thermochemical performance of approximate density functionals,
  J. Chem. Phys. **121**, 8187 (2004).

- Oleg A. Vydrov and Gustavo E. Scuseria,
  Ionization potentials and electron affinities in the Perdew–Zunger self-interaction corrected density functional theory,
  J. Chem. Phys. **122**, 184107 (2005).

- Oleg A. Vydrov, Gustavo E. Scuseria, John P. Perdew, Adrienn Ruzsinszky, and Gábor I. Csonka,
  Scaling down the Perdew–Zunger self-interaction correction in many-electron regions,
  J. Chem. Phys. **124**, 094108 (2006).

- Oleg A. Vydrov and Gustavo E. Scuseria,
  A simple method to selectively scale down the self-interaction correction,
  J. Chem. Phys. **124**, 191101 (2006).

- Oleg A. Vydrov, Jochen Heyd, Aliaksandr V. Krukau, and Gustavo E. Scuseria,
  Importance of short-range versus long-range Hartree–Fock exchange for the performance of hybrid density functionals,
  J. Chem. Phys. **125**, 074106 (2006).

- Adrienn Ruzsinszky, John P. Perdew, Gábor I. Csonka,
  Oleg A. Vydrov, and Gustavo E. Scuseria,
  Spurious fractional charge on dissociated atoms: Pervasive and resilient self-interaction error of common density functionals,
  J. Chem. Phys. **125**, 194112 (2006).

- Oleg A. Vydrov and Gustavo E. Scuseria,
  Assessment of a long-range corrected hybrid functional,
  J. Chem. Phys. **125**, 234109 (2006).

- Adrienn Ruzsinszky, John P. Perdew, Gábor I. Csonka, Oleg A. Vydrov, and Gustavo E. Scuseria,
  Density functionals that are one- and two- but not always many-electron self-interaction free, as shown for H_2^+, He_2^+, LiH^+, and Ne_2^+,
  J. Chem. Phys. **126**, 104102 (2007).

- Oleg A. Vydrov, Gustavo E. Scuseria, and John P. Perdew,
  Tests of functionals for systems with fractional electron number,
  J. Chem. Phys. **126**, 154109 (2007).

Abbreviations

AE — atomization energy
BH — barrier height
BLYP — Becke–Lee–Yang–Parr
DFA — density functional approximation
DFT — density functional theory
EA — electron affinity
GGA — generalized gradient approximation
HF — Hartree–Fock
HO — highest occupied
IP — ionization potential
KS — Kohn–Sham
LC — long-range correction
LR — long range
LSDA — local spin density approximation
MAE — mean absolute error
MAPE — mean absolute percentage error
ME — mean error
PBE — Perdew–Burke–Ernzerhof
PZ — Perdew–Zunger
SCF — self-consistent field
SIC — self-interaction correction
SIE — self-interaction error
SR — short range
St.Dev. — standard deviation
TPSS — Tao–Perdew–Staroverov–Scuseria
VSXC — Van Voorhis–Scuseria exchange-correlation
xc — exchange-correlation

Chapter 1

Introduction and background

1.1 Kohn–Sham density functional theory

Density functional theory (DFT) [1, 2, 3] is now the most widely used method for electronic structure calculations in quantum chemistry and condensed matter physics, providing useful predictions for atoms, molecules (including biomolecules), nanostructures, solids, and surfaces. Practical applications of DFT are typically performed within the Kohn–Sham framework [2], which reduces the many-electron ground-state problem to a tractable self-consistent one-electron form.

In Kohn–Sham DFT, the ground-state total energy E^{KS} and spin densities $\rho_\alpha(\mathbf{r})$, $\rho_\beta(\mathbf{r})$ for a system of N electrons with an external potential $v(\mathbf{r})$ (due to the nuclei in most practical cases) are found by the self-consistent solution of auxiliary (fictitious) one-electron Schrödinger equations:

$$\Big[-\frac{1}{2}\nabla^2 + v_s^\sigma(\mathbf{r})\Big]\varphi_{i\sigma}(\mathbf{r}) = \varepsilon_{i\sigma}\varphi_{i\sigma}(\mathbf{r}), \tag{1.1}$$

$$\rho_\sigma(\mathbf{r}) = \sum_i f_{i\sigma}\left|\varphi_{i\sigma}(\mathbf{r})\right|^2, \tag{1.2}$$

where $\varphi_{i\sigma}$ are the (orthonormal) spin-orbitals and $f_{i\sigma}$ are their occupation numbers. The total energy is found as

$$E^{\mathrm{KS}} = \sum_{\sigma=\alpha,\beta}\sum_i f_{i\sigma}\big\langle\varphi_{i\sigma}\big| -\frac{1}{2}\nabla^2\big|\varphi_{i\sigma}\big\rangle + \int\rho(\mathbf{r})v(\mathbf{r})\,d\mathbf{r} + J[\rho] + E_{\mathrm{xc}}[\rho_\alpha,\rho_\beta]. \tag{1.3}$$

The first two terms in Eq. (1.3) are the non-interacting kinetic energy and the interaction between the electron density $\rho(\mathbf{r})$ and the external potential $v(\mathbf{r})$. J is the mean-field Coulomb interaction of an electron density with itself,

$$J[\rho] = \frac{1}{2} \int\int \frac{\rho(\mathbf{r})\rho(\mathbf{r}')}{|\mathbf{r}-\mathbf{r}'|}\, d\mathbf{r}d\mathbf{r}', \tag{1.4}$$

also known as Hartree self-repulsion. E_{xc} is the exchange-correlation (xc) energy written as a functional of spin-densities $[\rho(\mathbf{r}) = \rho_\alpha(\mathbf{r}) + \rho_\beta(\mathbf{r})]$. E_{xc} is the only part of Eq. (1.3) that has to be approximated.

$v_s^\sigma(\mathbf{r})$ in Eq. (1.1) is the Kohn–Sham effective single-particle potential

$$v_s^\sigma(\mathbf{r}) = v(\mathbf{r}) + \int \frac{\rho(\mathbf{r}')}{|\mathbf{r}-\mathbf{r}'|}\, d\mathbf{r}' + v_{\mathrm{xc}}^\sigma(\mathbf{r}), \tag{1.5}$$

which includes the exchange-correlation potential $v_{\mathrm{xc}}^\sigma(\mathbf{r}) = \delta E_{\mathrm{xc}}/\delta\rho_\sigma(\mathbf{r})$.

$v_s(\mathbf{r})$ can be regarded as that unique, fictitious external potential which leads, for non-interacting particles, to the same physical density $\rho(\mathbf{r})$ as that of the interacting electrons in the physical external potential $v(\mathbf{r})$.

$\varepsilon_{i\sigma}$ in Eq. (1.1) are the Kohn–Sham orbital energies. Janak proved [4] that $\varepsilon_{i\sigma}$ satisfy

$$\frac{\partial E}{\partial f_{i\sigma}} = \varepsilon_{i\sigma}. \tag{1.6}$$

Eq. (1.6) holds both for the (unknown) exact functional and for all practical approximations. Using Eq. (1.6) it is easy to prove [4] that only the highest occupied (HO) spin-orbital (or HO orbitals in the case of degeneracy) can be fractionally occupied ($0 < f_{\mathrm{HO}} \leq 1$), and all spin-orbitals with $\varepsilon_{i\sigma} < \varepsilon_{\mathrm{HO}}$ must be singly occupied

$(f_{i\sigma} = 1)$. Since $N = \int \rho(\mathbf{r})\, d\mathbf{r} = \sum_{i\sigma} f_{i\sigma}$, it follows that

$$\frac{\partial E}{\partial N} = \varepsilon_{\text{HO}}. \tag{1.7}$$

The result of Eq. (1.7) will be useful in the discussion of fractionally-charged systems in Chapter 4.

1.2 Approximate exchange-correlation functionals

Kohn–Sham DFT is exact in principle, but in practice it requires an approximation to the exchange-correlation energy functional $E_{\text{xc}}[\rho_\alpha, \rho_\beta]$. In terms of total electron density $\rho(\mathbf{r})$ and exchange-correlation energy density per electron $\epsilon_{\text{xc}}(\mathbf{r})$, an approximation to E_{xc} is written as

$$E_{\text{xc}} = \int d\mathbf{r}\, \rho(\mathbf{r})\epsilon_{\text{xc}}(\mathbf{r}). \tag{1.8}$$

A ladder [5] of approximations constructs $\epsilon_{\text{xc}}(\mathbf{r})$ as a function of local ingredients at $\mathbf{r}$. The rungs are defined by the number and kind of the employed ingredients, with higher rungs increasingly more complex.

Rung 1: The local spin density approximation (LSDA) [2, 6, 7], which uses only $\rho_\alpha(\mathbf{r})$ and $\rho_\beta(\mathbf{r})$.

Rung 2: Generalized gradient approximations (GGAs), which introduce the density gradients $\nabla\rho_\alpha(\mathbf{r})$ and $\nabla\rho_\beta(\mathbf{r})$ as additional local ingredients.

Rung 3: Meta-GGAs, which further add the orbital kinetic energy densities $\tau_\alpha(\mathbf{r})$ and $\tau_\beta(\mathbf{r})$, and sometimes the Laplacians $\nabla^2\rho_\alpha(\mathbf{r})$ and $\nabla^2\rho_\beta(\mathbf{r})$.

Rung 4: Hyper-GGAs employ a fully non-local ingredient, the exact (ex) exchange energy density $\epsilon_{\mathrm{x}}^{\mathrm{ex}}(\mathbf{r})$.

The required computational cost does not increase much from the first to the third rung, but it increases rapidly on higher rungs.

1.2.1 Semi-local approximations

The first three rungs of the ladder of xc approximations are collectively known as semi-local approximations. Their $\epsilon_{\mathrm{xc}}(\mathbf{r})$ is found from the electron spin densities (and the occupied orbitals in the case of meta-GGAs) in an infinitesimal neighborhood of $\mathbf{r}$. Semi-local approximations are particularly popular due to their very favorable accuracy-to-computational cost ratio. For that reason, semi-local DFT is the method of choice to study relatively large systems, where wavefunction methods are unaffordable.

For the functionals of the first three rungs, there are nonempirical constructions, i.e. ϵ_{xc} can be constructed to satisfy universal constraints without fitting to datasets. The best nonempirical functional for a given rung satisfies as many exact theoretical constraints as possible while providing satisfactory numerical predictions for real systems. Additional local ingredients enable the satisfaction of additional constraints, therefore accuracy is expected to increase up the ladder.

LSDA is based on the model of the uniform electron gas. The most accurate parameterization of the uniform electron gas correlation energy was proposed by

Perdew and Wang [7]. A nonempirical GGA was constructed by Perdew, Burke, and Ernzerhof (PBE) [8]. A nonempirical meta-GGA functional was recently devised by Tao, Perdew, Staroverov, and Scuseria (TPSS) [9]. With LSDA, PBE, and TPSS, the first three rungs of the nonempirical ladder are essentially completed.

An alternative to "constraint satisfaction" is "semiempirical fitting", in which the functionals are fitted to selected data from experiment or from *ab initio* calculations. One of the most popular semiempirical GGAs is BLYP, combining Becke-88 exchange [10] with Lee–Yang–Parr correlation [11]. VSXC [12] is an example of a successful but heavily parameterized semiempirical meta-GGA.

1.2.2 Hybrid functionals

Hybrid functionals [13, 14, 15] is a special class of hyper-GGAs, where a certain portion of the exact non-local exchange is admixed to one of the common (usually semi-local) density functional approximations (DFAs) for the exchange-correlation energy. Exact exchange in Kohn–Sham DFT is defined by the same formal energy expression as in Hartree–Fock (HF) theory. We will use the terms "Hartree–Fock" and "exact" exchange interchangeably, since the difference in potentials and the resulting slight difference in orbitals are inessential for energetics. In the conventional one-parameter "global hybrid" mixing scheme [15] the xc-energy is written as

$$E_{\mathrm{xc}} = a_0 E_{\mathrm{x}}^{\mathrm{HF}} + (1 - a_0) E_{\mathrm{x}}^{\mathrm{DFA}} + E_{\mathrm{c}}^{\mathrm{DFA}}. \tag{1.9}$$

The value of the mixing parameter a_0 can sometimes be set *a priori* based on theoretical arguments [13, 16] but in most cases it is fitted to training datasets. The optimal value of a_0 can differ significantly depending on the property we wish to compute and on the particular DFA used. In a hybrid of LSDA, as much as 50% of Hartree–Fock exchange is needed to obtain acceptable thermochemistry [13]. A smaller fraction of HF exchange is generally used in hybrids of GGAs. It can be theoretically reasoned that $a_0 \approx 0.25$ should be optimal for predicting atomization energies by GGA hybrids [16]. Using PBE in Eq. (1.9) with $a_0 = 0.25$ has proven particularly successful [17, 18]. This hybrid is usually known under the acronyms of PBE0, PBE1PBE, or PBEh. Besides general-purpose hybrids (such as PBE0) there are specialized hybrids intended for a particular narrow purpose. For example, a proper description of transition states of chemical reactions requires admixture of a larger fraction of HF exchange than is optimal for equilibrium thermochemistry.

A hybrid of Eq. (1.9), where a_0 is a constant, is referred to as a "global hybrid". A more general exchange mixing technique is a so-called "local hybrid" [19] where the mixing parameter is not a constant but some function of coordinates, which is used to mix exchange energy densities at each point in space. Local hybrids have not been widely used because they are nontrivial to implement, computationally expensive, and have not yet yielded results significantly more accurate than global hybrids.

Another interesting and promising class of hybrid functionals involves separation of the exchange component into short-range (SR) and long-range (LR) parts. Such a decomposition can be accomplished by splitting the Coulomb operator with the help of the standard error-function (erf) [20, 21]:

$$\frac{1}{u} = \underbrace{\frac{1-\mathrm{erf}(\omega u)}{u}}_{\mathrm{SR}} + \underbrace{\frac{\mathrm{erf}(\omega u)}{u}}_{\mathrm{LR}}, \tag{1.10}$$

where $u = |\mathbf{r}_1 - \mathbf{r}_2|$ is the interelectronic distance and ω is a parameter defining the range of the separation. At a distance of about $2/\omega$ the short-range interactions become negligible. The choice of the splitting function is not unique and neither crucial. The error function is convenient because it allows analytic evaluation of two-electron repulsion integrals in Gaussian basis sets. For a given ω, HF and DFA exchange can be split as

$$E_{\mathrm{x}}^{\mathrm{HF}} = E_{\mathrm{x}}^{\mathrm{SR\text{-}HF}}(\omega) + E_{\mathrm{x}}^{\mathrm{LR\text{-}HF}}(\omega), \tag{1.11}$$

$$E_{\mathrm{x}}^{\mathrm{DFA}} = E_{\mathrm{x}}^{\mathrm{SR\text{-}DFA}}(\omega) + E_{\mathrm{x}}^{\mathrm{LR\text{-}DFA}}(\omega). \tag{1.12}$$

Mixing the SR and LR parts separately, one obtains a general expression for a hybrid functional with range separation:

$$\begin{aligned} E_{\mathrm{xc}} &= a\, E_{\mathrm{x}}^{\mathrm{SR\text{-}HF}}(\omega) + (1-a) E_{\mathrm{x}}^{\mathrm{SR\text{-}DFA}}(\omega) \\ &+ b\, E_{\mathrm{x}}^{\mathrm{LR\text{-}HF}}(\omega) + (1-b) E_{\mathrm{x}}^{\mathrm{LR\text{-}DFA}}(\omega) + E_{\mathrm{c}}^{\mathrm{DFA}}. \end{aligned} \tag{1.13}$$

The parameters a and b in Eq. (1.13) can be adjusted (between 0 and 1) for different purposes. For instance, setting $b = 0$ excludes the long-range portion of HF exchange. Such “exchange screening” greatly reduces computational cost for extended systems, especially for systems with a small band gap [22, 23, 24]. This technique enables hybrid DFT calculations on bulk metals, where conventional Hartree–Fock or global hybrid calculations are intractable. A PBE-based screened hybrid was recently developed and tested by Heyd, Scuseria, and Ernzerhof (HSE) [22, 23, 24]. HSE has proven to be a powerful tool for solid state studies [24, 25].

With a totally different goal in mind, it has been suggested that the long-range part of the exchange interaction be treated entirely by Hartree–Fock (which means setting $b = 1$) [20, 26, 27, 28]. In this scheme, $E_{\mathrm{x}}^{\text{LR-HF}}$ serves as an asymptotic correction for the exchange potential. This "long-range-correction" method will be discussed in detail in Chapter 3.

1.3 One-electron self-interaction error

As strange as it may sound, semi-local functionals are often more accurate for large many-electron systems than for systems with just one or a few electrons. A notorious example is the dissociation curve of the simplest one-electron molecule H_2^+, for which common functionals predict unphysical results [29]. This is one of the manifestations of a serious flaw in approximate xc functionals, known as self-interaction error (SIE).

It was noticed already in the early days of quantum mechanics [30, 31] that the Hartree energy J of Eq. (1.4) does not vanish even for a one-electron system due to the spurious self-interaction (SI) inherent in it. In Hartree–Fock theory this does not lead to any problem since all Coulomb self-interaction terms are exactly cancelled by the corresponding exchange self-interaction terms. A similar requirement is imposed on the exact exchange-correlation functional:

$$E_{\mathrm{xc}}[\rho_i, 0] + J[\rho_i] = 0, \tag{1.14}$$

where $\rho_i(\mathbf{r})$ is any one-electron density. In approximate xc functionals the cancellation is incomplete and the remainder is known as the self-interaction error. SIE is believed to be the cause of many of the failures of approximate density functionals.

The condition for a functional to be one-electron self-interaction-free given by Eq. (1.14) can be split into two separate conditions for the exchange and correlation components [32]:

$$E_{\mathrm{x}}[\rho_i, 0] \quad + \quad J[\rho_i] = 0, \tag{1.15}$$

$$E_{\mathrm{c}}[\rho_i, 0] \quad = \quad 0. \tag{1.16}$$

Because J of Eq. (1.4) is a fully non-local functional of the density, the requirement of Eq. (1.15) cannot be exactly satisfied on the first three rungs of the ladder of xc approximations. The requirement of Eq. (1.16) implies that the correlation energy must be equal to zero for any one-electron density. Eq. (1.16) can only be satisfied on the third or higher rungs of the ladder (e.g., it is satisfied in VSXC and TPSS correlation functionals).

1.4 Many-electron self-interaction error and its relation to fractionally-charged systems

If the SIE arose only in one-electron systems, it would be easy to correct: one can explicitly evaluate the spurious self-interaction terms and remove them. But the problem manifests itself in many-electron systems as well. Unfortunately, the SIE of a particular xc approximation is much more difficult to quantify in a many-electron system. There is no unique and general definition of the SIE and no unique way to correct it.

As shown below, study of fractionally-charged systems provides a way to quantify the many-electron SIE and get insight into its effects.

Consider an open system that can exchange electrons with its environment. In such a system, the electron number N can fluctuate between integers, and average N can be fractional. In the exact theory, the plot of the ground state energy E versus N is a series of straight line segments with derivative discontinuities at each integer [33], as shown in Fig. 1.1.

As a consequence of Eq. (1.7), in the exact Kohn–Sham DFT, ε_{HO} is constant for $M{-}1 < N \leq M$, where M is an integer, and equal to minus the electron removal energy from the ground state of the M-electron system [33].

Molecular fragments with effective fractional electron numbers can be found in systems and processes where a single electron is delocalized over spatially separated fragments. This is often the case in transition states of chemical reactions and charge

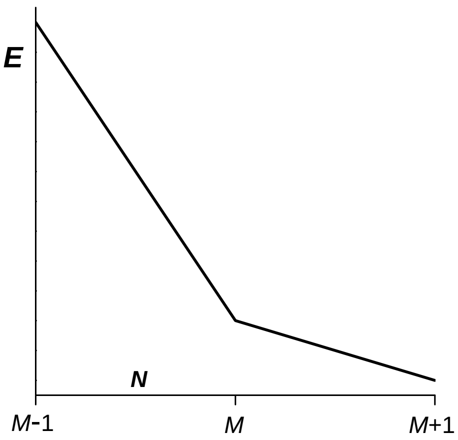

Figure 1.1 : Ground state energy E as a function of the electron number N.

transfer processes. Reproducing the correct dependence of E vs. fractional N is a prerequisite for proper description of such phenomena. Semi-local approximations predict highly non-linear N-dependence of the energy E: they give good total energies for integer N, but too low energies for non-integer N [29, 34]. In contrast to semi-local DFAs, Hartree–Fock theory often assigns too high relative energies for non-integer electron numbers [35, 36, 37]. These trends are directly reflected in relevant chemical properties: for instance, barrier heights of chemical reactions are too low in semi-local DFAs but too high in HF.

It has been demonstrated that failures of semi-local DFAs for systems with fractional occupations are related to the SIE in these approximations [29, 38]. Traditionally, the SIE has been defined as inexactness for one-electron systems (as described in the preceding section). However, as will be shown in Chapter 4 and as has been recently documented in Refs. [38, 39, 40], functionals that are exact for all one-electron systems can still fail for fractionally charged many-electron systems. This observation led to an extended definition of “many-electron SIE” [39, 40] complementing the conventional notion of “one-electron SIE”. A method is said to be nearly M-electron SIE-free if it yields a nearly linear variation of the total energy with electron number N between the integers M–1 and M, and the dependence has a realistic slope. In Chapter 4, we will study the many-electron SIE of common approximate functionals by plotting the ground state energies E for fractional N.

Chapter 2

Self-interaction corrections utilizing orbital densities

2.1 Perdew–Zunger self-interaction correction

More than two decades ago Perdew and Zunger (PZ) [32] proposed a (seemingly) simple self-interaction correction (SIC). In Perdew–Zunger self-interaction-corrected DFT, the ground state energy is written as

$$E^{\mathrm{PZ}} = E^{\mathrm{KS}} + E^{\mathrm{SIC}}. \tag{2.1}$$

E^{SIC} eliminates the self-interaction terms orbital by orbital:

$$E^{\mathrm{SIC}} = -\sum_{\sigma=\alpha,\beta} \sum_{i} \big(J[\rho_{i\sigma}] + E_{\mathrm{xc}}[\rho_{i\sigma}, 0] \big). \tag{2.2}$$

Orbital densities $\rho_{i\sigma}(\mathbf{r})$ in Eq. (2.2) are defined as $\rho_{i\sigma}(\mathbf{r}) = f_{i\sigma} \left|\varphi_{i\sigma}(\mathbf{r})\right|^2$.

E^{SIC} of Eq. (2.2) properly vanishes for the exact xc functional and for any functional that is one-electron SIE-free by construction.

Despite its apparent simplicity, practical implementation of the Perdew–Zunger self-interaction-corrected density functional theory (SIC-DFT) is complicated and that is the reason why it has not been widely used. SIC-DFT does not fit into the standard Kohn–Sham procedure because the SIC-DFT potential is orbital-dependent and the energy functional of Eq. (2.1) is not invariant under unitary transformations of the occupied orbitals.

2.1.1 Approximate implementations of the Perdew–Zunger SIC

Several approximate implementations of the Perdew–Zunger SIC in molecular codes have been reported in recent years. The correction can be applied in a post-SCF manner, subtracting self-interaction terms after a self-consistent Kohn–Sham calculation is done [41, 42, 43]. To maximize the removal of the error, a localization transformation is applied to the orbitals.

The simplest self-consistent approximate method is the so-called average-density SIC (ADSIC) [44, 45], based on the original idea of Fermi and Amaldi [31] to subtract a fraction $1/N$ from the total density. ADSIC uses one-electron densities $\rho_\sigma(\mathbf{r})/N_\sigma$, where N_σ is the number of σ-spin electrons. Hence, ADSIC is an extension of the Fermi–Amaldi correction [31] rather than an approximation to the Perdew–Zunger SIC. Unlike PZ-SIC, ADSIC is not size consistent. The magnitude of the ADSIC correction decreases as the electron number N increases. The correction will actually tend to zero for very large N. Thus ADSIC is expected to work well only in some intermediate range of N.

Several groups [46, 47, 48, 49, 50] have reported implementations of SIC-DFT using the Krieger–Li–Iafrate (KLI) [51] approximation to the optimized effective potential (OEP) method.

Implementing the PZ SIC for solids is an even greater challenge than for molecules. Most of the solid-state studies used various (often very crude) approximations. A review of solid state SIC-DFT techniques and studies can be found elsewhere [52, 53, 54]. Here we consider in detail only molecular studies.

2.1.2 Rigorous implementation of the Perdew–Zunger SIC

A rigorous implementation of SIC-DFT can be done by direct minimization of the energy functional of Eq. (2.1) under the constraint of orbital orthonormality

$$\langle \varphi_i | \varphi_j \rangle = \delta_{ij}. \tag{2.3}$$

The first self-consistent calculations for molecules were carried out by Pederson *et al.* [55], who minimized the SIC-DFT energies of a few homonuclear diatomics. Whitehead followed with some more molecular studies [56]. Goedecker and Umrigar derived the expression for the SIC-DFT energy gradient under the orthogonality restriction and performed direct minimization calculations for a few atoms and molecules using a plane-wave technique [57]. A self-consistent implementation of SIC-DFT with Gaussian-type orbitals was reported recently [35, 36, 58, 59]. It utilizes a univariate search method similar to that of Seeger and Pople [60].

Application of the variational principle to the Perdew–Zunger SIC-DFT energy functional leads to a system of self-consistent equations (with spin indices omitted)

$$H_i \varphi_i = \sum_j \varepsilon_{ji} \varphi_j, \tag{2.4}$$

where H_i is the effective one-electron Hamiltonian

$$H_i = -\frac{1}{2}\nabla^2 + v(\mathbf{r}) + \int \frac{\rho(\mathbf{r}')}{|\mathbf{r}-\mathbf{r}'|}\, d\mathbf{r}' + v_{\mathrm{xc}}\big([\rho_\alpha, \rho_\beta], \mathbf{r}\big) - \int \frac{\rho_i(\mathbf{r}')}{|\mathbf{r}-\mathbf{r}'|}\, d\mathbf{r}' - v_{\mathrm{xc}}\big([\rho_i, 0], \mathbf{r}\big). \tag{2.5}$$

Off-diagonal Lagrange multipliers $\varepsilon_{ji} = \langle\varphi_j|H_i|\varphi_i\rangle$ have to be introduced in Eq. (2.4) to maintain the orthogonality of the orbitals. The matrix of Lagrange multipliers $[\varepsilon_{ij}]$ is generally not Hermitian but at the minimum of the PZ-SIC energy functional it becomes Hermitian,

$$\varepsilon_{ij} = \varepsilon_{ji}^*, \tag{2.6}$$

and hence unitarily diagonalizable [57]. Eigenvalues of the Lagrange multipliers matrix are sometimes used as equivalents of Kohn–Sham orbital energies [55, 57, 61, 62]. However, in Section 4.2 we demonstrate that the diagonal elements ε_{ii} are the correct orbital energies in the sense of Eq. (1.6) and eigenvalues of the $[\varepsilon_{ij}]$-matrix do not have any physical meaning.

Eqs. (2.6) are sometimes called the localization conditions and can be utilized for energy minimization [55, 56] in a process known as "Jacobi sweeps", which has long been used for obtaining localized orbitals [63].

We adopt the procedure of Goedecker and Umrigar [57] as the most rigorous. To minimize the energy with respect to orbital variations, we use a gradient search technique. The energy gradient [57], in the molecular orbital basis, has the form (with the spin symbols omitted for brevity):

$$\frac{\partial E}{\partial\varphi_i(\mathbf{r})} = 2H_i\varphi_i(\mathbf{r}) - \sum_j \varphi_j(\mathbf{r})\Big(\langle\varphi_i|H_j|\varphi_j\rangle + \langle\varphi_j|H_i|\varphi_i\rangle\Big). \tag{2.7}$$

It is easy to see that when all $\partial E/\partial\varphi_i(\mathbf{r})$ vanish, localization conditions of Eq. (2.6) follow immediately.

Further details of our fully self-consistent implementation of the Perdew–Zunger SIC-DFT with Gaussian basis sets can be found in Appendix A.

Orbitals minimizing the PZ energy of Eq. (2.1) are usually localized in shape and look very much like Boys' orbitals [64]. Therefore, Boys' localization procedure is used to obtain the initial orbital guess, as described in Appendix A.

It should be stressed that our implementation works with any functional, including hybrids, whereas most of the previous studies focused on PZ-SIC-LSDA. There are only a few studies applying PZ-SIC to GGA functionals [41, 50, 58, 59, 35, 36]. For hybrid functionals, only post-SCF SIC-DFT calculations for the H_2 molecule [42] and H_2 + H reaction [43] were reported. No self-consistent SIC-hybrid-DFT calculations have been reported prior to this work.

2.1.3 Magnitudes of the correction

Using our self-consistent implementation of the Perdew–Zunger SIC-DFT, we minimized the total energies for atoms from H to Ar and 55 molecules of the standard thermochemical G2-1 test set [65]. Table 2.1 shows the mean absolute values of E^{SIC} per electron. The values are found by, first, dividing the absolute value of E^{SIC} of an atom (molecule) by the number of electrons and, then, averaging among all atoms (molecules) in the set. The mean absolute E^{SIC} of valence orbitals are shown in Table 2.1 separately. For thermochemistry, only the valence orbitals are important since core orbitals remain largely unchanged in chemical reactions and

Table 2.1 : Mean absolute Δ and E^{SIC} per electron (a.u.). The 6-311+G($3df, 2p$) basis set is used.

	18 Atoms (H-Ar)		
Functional	Δ^{a}	E^{SIC}	$E_{\text{val}}^{\text{SIC}\ b}$
LSDA	0.0983	0.0992	0.0165
VSXC	0.0259	0.0254	0.0125
TPSS	0.0205	0.0201	0.0116
BLYP	0.0173	0.0167	0.0110
PBE	0.0063	0.0059	0.0102
PBE0	0.0056	0.0053	0.0093
	55 Molecules (G2-1 set)		
Functional	Δ^{a}	E^{SIC}	$E_{\text{val}}^{\text{SIC}\ b}$
LSDA	0.0946	0.0957	0.0177
VSXC	0.0257	0.0250	0.0151
TPSS	0.0209	0.0203	0.0147
BLYP	0.0171	0.0161	0.0138
PBE	0.0058	0.0052	0.0119
PBE0	0.0056	0.0052	0.0108

[a] $\Delta = \text{Min}\{E^{\text{PZ}}\} - \text{Min}\{E^{\text{KS}}\}$.

[b] Contribution to E^{SIC} from valence orbitals.

contributions of core orbitals mostly cancel out in calculations of any thermochemical property. Indeed, we found that E^{SIC} of the core orbitals of a molecule is almost exactly equal to the sum of the E^{SIC} values of the core orbitals of the composing atoms. This observation is consistent with previous studies [47, 49]. Functionals in Table 2.1 are arranged in the order of decreasing average E^{SIC} for the valence orbitals. Since we directly minimize the energy functional of Eq. (2.1), E^{SIC} is not equal to $\Delta = \text{Min}\{E^{\text{PZ}}\} - \text{Min}\{E^{\text{KS}}\}$, but the difference between Δ and E^{SIC} is fairly small (Table 2.1).

Magnitudes of E^{SIC} for atoms are shown in Fig. 2.1. To analyze the breakdown of E^{SIC} into orbital contributions, we plot the corrections for individual atomic shells in Fig. 2.2. LSDA has a much greater total E^{SIC} than any other functional, however, most of it comes from the core region. E^{SIC} for the valence orbitals is of the same

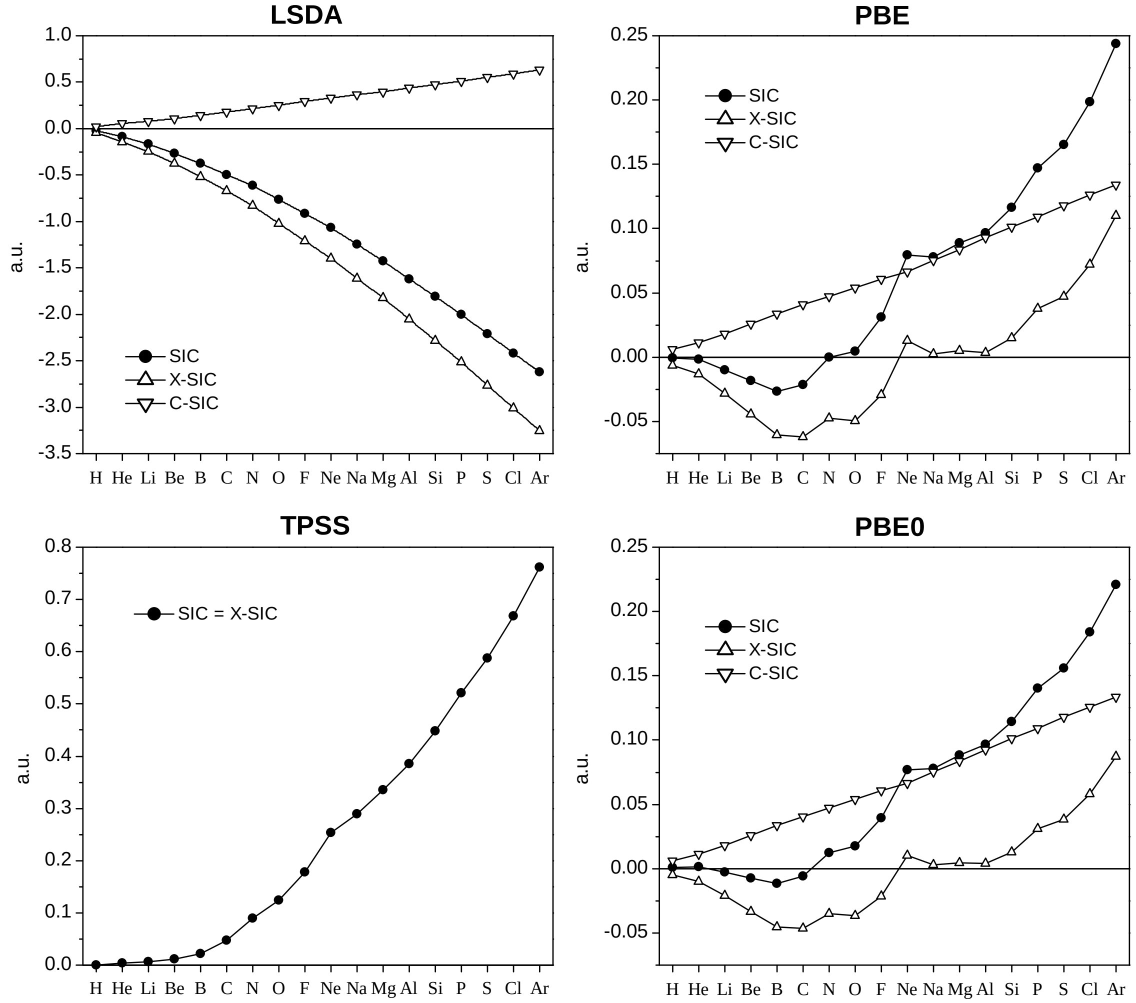

Figure 2.1 : Magnitudes of the Perdew–Zunger SIC for LSDA, PBE, TPSS, and PBE0 in atoms from H to Ar. The total SIC is broken down into the corrections for exchange (X-SIC) and correlation (C-SIC). C-SIC is zero in TPSS.

order of magnitude for all functionals. For some of the functionals (PBE, PBE0) the total average E^{SIC} in Table 2.1 is smaller than the corresponding value for the valence region. The reason for this is a partial cancellation of contributions from

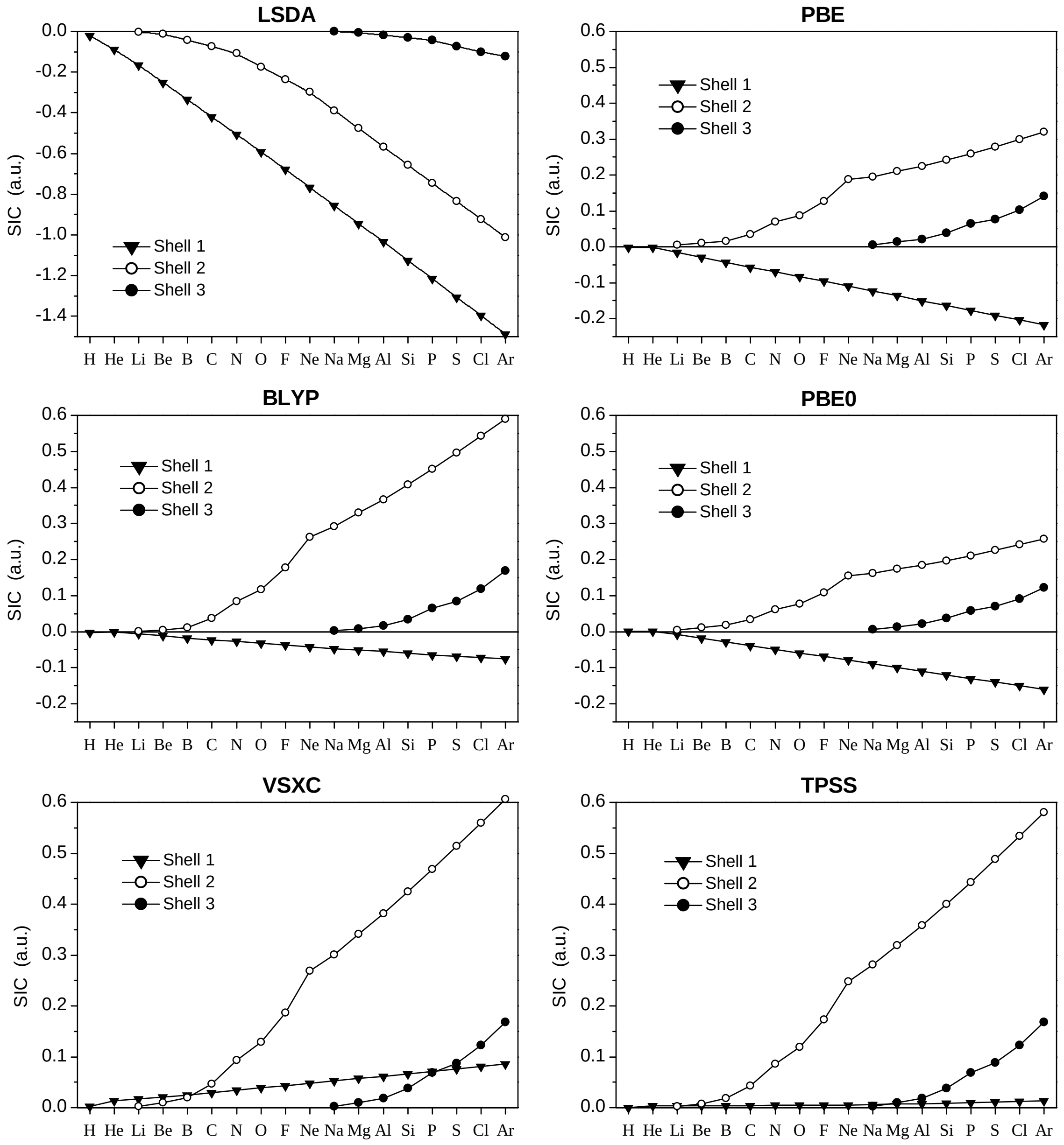

Figure 2.2 : Contributions to E^{SIC} from individual shells in atoms.

valence and core regions. For atoms, this effect is illustrated in Fig. 2.2. Such a cancellation reduces the total value of E^{SIC}. It should be stressed that for the exact xc functional not only the total E^{SIC} will be zero but also E^{SIC} of every orbital. From Fig. 2.2 we can tell which regions contribute most of E^{SIC} in atoms. In LSDA, the first shell ($1s$) is the largest contributor. In TPSS, E^{SIC} of the $1s$–orbitals is close to zero. This is not surprising because TPSS was constructed to reproduce the correct energy for the ground state density of the hydrogen atom [9].

Fig. 2.1 shows the breakdown of the total E^{SIC} into the corrections for exchange and correlation. We see that self-correlation in PBE and PBE0 has the same magnitude, while the error coming from the violation of Eq. (1.15) is slightly reduced in PBE0 due to the presence of the exact exchange.

2.2 The effect of the Perdew–Zunger SIC on the performance of approximate density functionals

Prior to this work, a systematic study of the performance of the Perdew–Zunger SIC had been lacking. Most tests of PZ-SIC have been done for atoms, due to the ease of implementation. There have been only a handful of molecular calculations, and most of them used approximate schemes. Limited previous studies suggested that the performance of the Perdew–Zunger SIC-DFT appeared to be ambivalent. It was found that PZ-SIC improves the description of transition states of chemical reactions [41, 43, 50] and dissociation curves of odd-electron systems [35, 36, 50], but it provides little or no improvement for reaction energies [35, 50, 57] and predicts too short bonds in molecules [41, 43, 57]. The majority of the previous studies applied PZ-SIC only to LSDA. There are very few reports using PZ-SIC with GGAs.

2.2.1 Atomic ionization potentials and electron affinities

Perdew and Zunger in their original work [32] carried out a few atomic calculations using a "central field" approximation, in which not only the total density but every orbital density was spherically averaged. This "sphericalization" is not an intrinsic feature of the method, but rather a simplification facilitating the minimization of the energy, since only the radial dimension has to be considered. Spherical averaging was also used in most of the later atomic PZ-SIC calculations [66, 67, 68, 69]. However, there is some degree of arbitrariness in how spherical averaging is done in PZ-SIC. Several different techniques have been proposed [70, 71], which yield slightly different total energies. Moreover, orbital densities that give lower total energy are not necessarily those that give the best results. This inconsistency undermines the validity of the method itself. There is no consensus about the effects of PZ-SIC on atomic properties.

In atoms with only s-electrons (H to Be), all orbitals are already spherically symmetric. For atoms with p-electrons, spherical averaging implies using the density

$$\tilde{\rho}_i(\mathbf{r}) = \frac{1}{3}[p_x^2(\mathbf{r}) + p_y^2(\mathbf{r}) + p_z^2(\mathbf{r})]. \tag{2.8}$$

In atoms with more than one p-orbital, spherical averaging may considerably lower the total energy E^{PZ} since it eliminates the orthogonality constraint. In such cases, there will be several equivalent orbital densities $\tilde{\rho}_i(\mathbf{r})$ of Eq. (2.8).

Spherical averaging obviously cannot be applied to molecules. If a uniform treatment of both atoms and molecules is needed, any sphericalization is unacceptable.

Up to date, almost all of the studies of the performance of PZ-SIC in atoms have been performed using spherical averaging of orbital densities. To the best of our knowledge, there has been only one report applying the rigorous variational approach to atomic calculations with PZ-SIC [71]. A variational solution obeying the Pauli exclusion principle requires imposing the orthogonality of orbitals. Under orthogonality restriction, a full energy minimization yields a set of "hybridized local orbitals", as was found by Pederson and Lin [71]. These orbitals are very similar in shape to Boys' localized orbitals [64]. For instance, the valence orbitals of the Ne atom will be a set of equivalent sp^3-hybrid orbitals. To expand upon the work of Pederson and Lin (who used PZ-SIC with exchange-only LSDA), we conducted a comprehensive study using various exchange-correlation functionals. The rigorous self-consistent method with orthonormal orbitals is used throughout.

Table 2.2 provides a summary of performance of various self-interaction-corrected and uncorrected functionals for ΔSCF[*] ionization potentials (IPs) and electron affinities (EAs) in atoms. Table 2.2 shows that only LSDA results benefit from the PZ-

---

[*] ΔSCF indicates that the difference of the two self-consistent field energies is computed.

Table 2.2 : Deviations from experiment of ΔSCF ionization potentials and electron affinities for atoms from H to Ar computed with self-interaction-corrected and uncorrected functionals using the 6-311++G* basis set. No spherical averaging is applied. All values are in eV.

	18 IPs		12 EAs	
Functional	ME	MAE	ME	MAE
LSDA	0.17	0.30	0.29	0.29
BLYP	0.05	0.18	0.01	0.11
PBE	0.10	0.15	0.09	0.13
PBE0	0.06	0.12	−0.02	0.09
TPSS	0.08	0.12	0.03	0.05
PZ-SIC-LSDA	0.21	0.24	−0.15	0.18
PZ-SIC-BLYP	−0.41	0.48	−0.68	0.68
PZ-SIC-PBE	−0.34	0.39	−0.57	0.57
PZ-SIC-PBE0	−0.30	0.33	−0.53	0.53
PZ-SIC-TPSS	−0.28	0.34	−0.45	0.47

SIC, while the performance of all other functionals deteriorates. Some EAs become negative after the Perdew–Zunger correction is made: the B^- anion is unbound in all beyond-LSDA PZ-SIC-corrected functionals. In addition, Al^- is unbound in PZ-SIC-BLYP.

2.2.2 Molecular ionization potentials and electron affinities

Prior to this work, no ΔSCF IPs or EAs with a self-interaction correction had been reported for molecules. We have constructed a benchmark set of molecular IPs and EAs as a subset of the G2 ion test set of Curtiss *et al.* [72]. Aiming to decrease the computational effort, we have dropped the larger molecules and species causing

Table 2.3 : Molecular benchmark set used to test the performance of PZ-SIC for ionization potentials and electron affinities. It is a subset of the G2 set (Ref. [72]).

Ionization Potentials (44 Molecules):
CH_2, CH_3, NH, NH_2, NH_3, OH, H_2O, HF, SiH_2, SiH_3, SiH_4, PH, PH_2, PH_3,
SH, H_2S, HCl, C_2H_2, C_2H_4, CO, N_2, O_2, P_2, S_2, Cl_2, ClF, CS, CF_2, COS,
C_2H_5, CHO, CH_2OH, CH_3O, CH_3OH, CH_3F, CH_2SH, CH_3SH, CH_3Cl,
CH_3CHO, CH_3OF, B_2H_4, N_2H_2, N_2H_3, HOF.
Electron Affinities (32 Molecules):
CH, CH_2, CH_3, NH, NH_2, OH, SiH, SiH_2, SiH_3, PH, PH_2, SH, NO,
CN, S_2, CF_2, NCO, NO_2, OF, C_2H, C_2H_3, CHO, HCF, CH_3O,
CH_3S, CH_2CN, CH_2NC, CHCO, CH_3CO, LiH, HNO, HOO.

convergence problems for PZ-SIC-DFT. The final test set consisting of 44 ionization potentials and 32 electron affinities is shown in Table 2.3.

ΔSCF IPs and EAs were evaluated as the difference in total energies at 0 K of the ion and the corresponding neutral, at their respective B3LYP/6-31G($2df,p$) geometries using scaled B3LYP/6-31G($2df,p$) zero-point energies. Deviations from experiment for both self-interaction-corrected and uncorrected functionals are summarized in Table 2.4. In the case of LSDA, PZ-SIC provides no significant improvement for IPs and EAs. The situation is more unfavorable for PBE and TPSS, where the correction substantially increases the errors. Some of the EAs in the test set even become negative. The number of predicted negative EAs is 2 for PZ-SIC-LSDA, 6 for PZ-SIC-TPSS, and 9 for PZ-SIC-PBE.

Table 2.4 : Deviations from experiment of ΔSCF ionization potentials and electron affinities for the molecular test set defined in Table 2.3 computed with self-interaction-corrected and uncorrected functionals using the 6-311+G($3df, 2p$) basis set. The geometries and zero-point energies were obtained at the B3LYP/6-31G($2df, p$) level using a frequency scale factor of 0.9854. All values are in eV.

	44 Ionization Potentials				32 Electron Affinities			
Functional	ME	MAE	Max (+)	Max (−)	ME	MAE	Max (+)	Max (−)
LSDA	0.04	0.20	0.46 (HF)	−0.49 (CH_3F)	0.20	0.21	0.47 (CH)	−0.15 (NO_2)
PBE	−0.10	0.20	0.25 (CHO)	−0.58 (CH_3OF)	0.01	0.10	0.28 (CH)	−0.29 (NO_2)
TPSS	−0.14	0.20	0.26 (CHO)	−0.55 (CH_3OF)	−0.09	0.15	0.22 (CF_2)	−0.32 (NO_2)
PZ-SIC-LSDA	0.24	0.25	1.10 (N_2)	−0.25 (COS)	−0.11	0.21	0.58 (CN)	−0.67 (CH_3O)
PZ-SIC-PBE	−0.41	0.42	0.17 (N_2)	−1.18 (HF)	−0.60	0.60	None	−1.44 (OH)
PZ-SIC-TPSS	−0.37	0.39	0.18 (N_2)	−1.18 (HF)	−0.50	0.52	0.27 (CF_2)	−1.34 (OH)

Table 2.5 : Deviations from experiment of standard enthalpies of formation ($\Delta_\mathrm{f}H^\circ_{298}$) for the G2-1 test set computed with self-interaction-corrected and uncorrected functionals using the 6-311+G($3df,2p$) basis set. The geometries and zero-point energies were obtained at the B3LYP/6-31G($2df,p$) level using a frequency scale factor of 0.9854. All values are in kcal/mol.

Functional	ME	MAE	Max (+)	Max (−)
LSDA	−36.0	36.1	0.5 (Li_2)	−86.1 (CO_2)
PBE	−6.6	8.1	10.7 (Si_2H_6)	−28.9 (CO_2)
PBE0	1.4	2.9	9.8 (SiO)	−5.9 (BeH)
BLYP	−2.8	4.8	10.7 (Si_2H_6)	−15.4 (O_2)
VSXC	−0.4	2.3	8.0 (N_2H_4)	−7.5 (O_2)
TPSS	−3.6	4.5	5.6 (SiO)	−18.1 (Si_2H_6)
PZ-SIC-LSDA	−21.5	22.8	8.4 (SiO)	−89.2 (C_2H_6)
PZ-SIC-PBE	10.0	12.5	63.6 (CO_2)	−11.5 (PH_2)
PZ-SIC-PBE0	13.6	14.9	63.5 (CO_2)	−7.7 (PH_2)
PZ-SIC-BLYP	18.6	21.0	99.7 (CO_2)	−13.9 (PH_2)
PZ-SIC-VSXC	13.6	16.5	69.4 (CO_2)	−24.7 (Si_2H_6)
PZ-SIC-TPSS	15.0	19.5	83.9 (CO_2)	−27.9 (Si_2H_6)

Our results indicate that the performance of the Perdew–Zunger SIC for molecules is even worse than for atoms. It seems that PZ-SIC overcorrects many-electron systems and overcorrection intensifies with increase in system size.

2.2.3 Enthalpies of formation

Using both self-interaction-corrected and uncorrected functionals, we computed the standard enthalpies of formation for the G2-1 set using methodology described by Curtiss *et al.* [65]. Table 2.5 shows the summary of the deviations of $\Delta_\mathrm{f}H^\circ_{298}$ from the experimental values. As one can see, the PZ correction improves agreement with experiment only for the LSDA functional, whereas all other functionals show worse performance upon introducing the PZ-SIC. This behavior appears reasonable for semiempirical functionals since they are fitted to reproduce experimental data with self-interaction terms included. However, the self-interaction correction leads to a decrease in accuracy for both empirical and nonempirical functionals. Possible reasons for that will be discussed in Sec. 2.4.1.

2.3 Scaling down the Perdew–Zunger correction

As was shown in the previous section, the Perdew–Zunger SIC seems to "overcorrect" many-electron systems, which results in poor performance for thermochemistry. It has been suggested [5] that scaling the PZ-SIC down may improve its performance. However, adding a simple constant scaling factor in front of Eq. (2.2) leads to the loss of the useful property of being exact for any one-electron density. It is preferable to scale down the SIC only in many-electron systems, leaving the full correction in one-electron systems. This can be accomplished by introducing a scaling factor for every occupied orbital,

$$E^{\mathrm{SIC}} = -\sum_{i\sigma} X_{i\sigma}^{k} \big(J[\rho_{i\sigma}] + E_{\mathrm{xc}}^{\mathrm{DFA}}[\rho_{i\sigma}, 0] \big), \tag{2.9}$$

and requiring that $X_{i\sigma}^{k} = 1$ for one-electron systems and $0 \leq X_{i\sigma}^{k} \leq 1$ otherwise.

A scaling factor with good formal properties can be constructed as

$$X_{i\sigma}^{k} = \frac{1}{f_{i\sigma}} \int \left(\frac{\tau_{\sigma}^{W}}{\tau_{\sigma}} \right)^{k} \rho_{i\sigma}(\mathbf{r})\, d\mathbf{r}, \tag{2.10}$$

where τ_σ is the non-interacting kinetic energy density of σ-spin electrons

$$\tau_\sigma(\mathbf{r}) = \frac{1}{2}\sum_i f_{i\sigma} \left|\nabla\varphi_{i\sigma}(\mathbf{r})\right|^2, \tag{2.11}$$

τ_σ^W is the von Weizsäcker kinetic energy density

$$\tau_\sigma^W(\mathbf{r}) = \frac{|\nabla\rho_\sigma(\mathbf{r})|^2}{8\rho_\sigma(\mathbf{r})}, \tag{2.12}$$

$f_{i\sigma} = \int \rho_{i\sigma}(\mathbf{r})\, d\mathbf{r}$ is the orbital occupation number, and k is a non-negative real number. τ_σ^W and τ_σ in Eq. (2.10) are evaluated at the total spin-density ρ_σ. It is known that $\tau_\sigma(\mathbf{r}) = \tau_\sigma^W(\mathbf{r})$ in regions containing only one electron of spin σ (or more generally containing only orbitals of spin σ with the same shape), and that $\tau_\sigma(\mathbf{r}) \geq \tau_\sigma^W(\mathbf{r})$ otherwise. For a uniform density, $\tau_\sigma^W(\mathbf{r}) = 0$. The ratio $\tau_\sigma^W/\tau_\sigma$ is customarily used in construction of self-correlation-free [i.e., obeying Eq. (1.16)] meta-GGA functionals [9, 12, 73]. This ratio was also recently used as a mixing function in a local hybrid [19], with intent to eliminate the self-interaction error in the exchange component.

Eq. (2.10) is not the only possible choice of a scaling factor. Using the fact that $\rho_{i\sigma}(\mathbf{r}) \leq \rho_\sigma(\mathbf{r})$, an even simpler version can be constructed:

$$X_{i\sigma}^m = \frac{1}{f_{i\sigma}} \int \left(\frac{\rho_{i\sigma}}{\rho_\sigma}\right)^m \rho_{i\sigma}\, d\mathbf{r} = \frac{1}{f_{i\sigma}} \int \frac{\rho_{i\sigma}^{m+1}}{\rho_\sigma^m}\, d\mathbf{r}, \tag{2.13}$$

where m is a non-negative real number. For $m > 0$, the scaling factor $X_{i\sigma}^m$ of Eq. (2.13) will be less than one if an orbital density $\rho_{i\sigma}(\mathbf{r})$ overlaps with other orbital densities of same-spin electrons.

The Perdew–Zunger SIC is obtained as a special case of Eq. (2.9) when $k = 0$ in Eq. (2.10) or when $m = 0$ in Eq. (2.13). In the limit of $k \to \infty$ (or $m \to \infty$), both scaling factors will approach 0. One-electron and spin-compensated two-electron systems are the exceptions from the latter rule: in such systems (e.g. H, He, and H_2) the scaling factors of Eqs. (2.10) and (2.13) will be 1 for any k or m.

The scaling factor X_i^k of Eq. (2.10) with $k > 0$ ensures that the correction vanishes for a uniform density, independent of the type of orbitals used. Most of the xc functionals we test in this work are exact in the uniform density limit, so that no correction is needed. The alternative choice X_i^m of Eq. (2.13), however, is not guaranteed to vanish in the uniform density limit. Thus, Eq. (2.10) has better formal properties (as will be further shown in Section 2.4.2), but Eq. (2.13) is simpler since it only uses orbital densities and no density derivatives.

The correction of Eq. (2.9) properly vanishes when $E_{\mathrm{xc}}^{\mathrm{DFA}}$ is replaced by the exact xc-functional, irrespective of which scaling factor is used (provided that $k \geq 0$ and $m \geq 0$).

The derivatives of Eq. (2.9) with respect to orbital variations can be easily obtained analytically, as shown in Appendix B. The self-consistent implementation of the scaled-down SIC is straightforward and requires only minor changes in the PZ-SIC code.

2.3.1 Magnitudes of the scaling factors

Table 2.6 shows how the SIC is scaled down for different shells in the Ar atom. The scaling factors of Eqs. (2.10) and (2.13) do not explicitly include any dependence on the xc functional. Magnitudes of the scaling factors are determined solely from the shapes of the orbital densities. Hence, we can infer from Table 2.6 that, for a given k in Eq. (2.10) or a given m in Eq. (2.13), the minimizing orbitals look similar in SIC-LSDA and SIC-PBE, since the scaling factor assumes similar values for corresponding orbitals.

2.3.2 Total energies of atoms

The nonrelativistic total energies of all the atoms up to Ar are known accurately [74]. We computed the errors in the total energies of 16 atoms from Li to Ar. The error for each atom was divided by the number of electrons N and averaged among the atoms in the set. After this division by N, the absolute error can still grow with N, but more slowly than before. The statistics thus obtained are presented in Table 2.7. To estimate the effect of incompleteness of the 6-311+G($3df$) basis set, we calculated total energies of several atoms with a much larger aug-cc-pVQZ basis set. We found that, for all theoretical methods studied, the increase of basis set size results in energy lowering of less than 0.002 hartree per electron, which will not dramatically change the qualitative trends observed in Table 2.7.

It is clear that scaling down the SIC reduces the errors in total energies as com-

Table 2.6 : Values of the scaling factors for different shells in the Ar atom. The 6-311+G(3df) basis set was used.

Functional	Shell 1[a]	Shell 2[b]	Shell 3[b]
Scaling factor of Eq. (2.10)			
SIC-LSDA ($k = 1$)	0.675	0.443	0.528
SIC-LSDA ($k = 2$)	0.514	0.238	0.350
SIC-LSDA ($k = 3$)	0.412	0.140	0.252
SIC-PBE ($k = 1$)	0.674	0.443	0.527
SIC-PBE ($k = 2$)	0.511	0.238	0.349
SIC-PBE ($k = 3$)	0.410	0.140	0.251
Scaling factor of Eq. (2.13)			
SIC-LSDA ($m = 1$)	0.791	0.492	0.531
SIC-LSDA ($m = 2$)	0.692	0.323	0.363
SIC-LSDA ($m = 3$)	0.626	0.238	0.273
SIC-PBE ($m = 1$)	0.790	0.490	0.518
SIC-PBE ($m = 2$)	0.687	0.321	0.342
SIC-PBE ($m = 3$)	0.616	0.236	0.253

[a] First shell (1s) includes two electrons.

[b] Second and third shells each include eight electrons in equivalent sp^3-hybrid orbitals.

pared to the original Perdew–Zunger SIC. The most remarkable improvement is observed in the case of LSDA. The uncorrected LSDA functional predicts total energies that are too high, and the deviation ($calculated - exact$) increases with the atomic number. On the other hand, PZ-SIC-LSDA energies are too low with an increasingly negative deviation. Total energies obtained with the scaled-down SIC fall in between LSDA and PZ-SIC-LSDA, and thus much closer to the accurate values. Figure 2.3 illustrates the errors in total energies for SIC-LSDA with the scaling

Table 2.7 : Errors per electron in total energies of the atoms from Li to Ar computed with the 6-311+G($3df$) basis set. All values are in hartrees.

Functional	ME	MAE	RMSE
LSDA	0.073	0.073	0.074
PBE	0.009	0.009	0.009
PZ-SIC-LSDA	−0.033	0.033	0.037
PZ-SIC-PBE	0.014	0.014	0.016
Scaling factor of Eq. (2.10)			
SIC-LSDA ($k = 1/2$)	−0.014	0.014	0.014
SIC-LSDA ($k = 1$)	−0.001	0.004	0.005
SIC-LSDA ($k = 2$)	0.014	0.015	0.018
SIC-LSDA ($k = 3$)	0.022	0.023	0.028
SIC-PBE ($k = 1/2$)	0.011	0.011	0.012
SIC-PBE ($k = 1$)	0.010	0.010	0.010
SIC-PBE ($k = 2$)	0.008	0.008	0.008
SIC-PBE ($k = 3$)	0.007	0.007	0.007
Scaling factor of Eq. (2.13)			
SIC-LSDA ($m = 1$)	−0.008	0.008	0.008
SIC-LSDA ($m = 2$)	0.003	0.007	0.007
SIC-LSDA ($m = 3$)	0.009	0.011	0.014
SIC-LSDA ($m = 4$)	0.013	0.015	0.018
SIC-PBE ($m = 1/2$)	0.011	0.011	0.012
SIC-PBE ($m = 1$)	0.009	0.009	0.010
SIC-PBE ($m = 3/2$)	0.008	0.008	0.009
SIC-PBE ($m = 2$)	0.007	0.007	0.008

factor of Eq. (2.10).

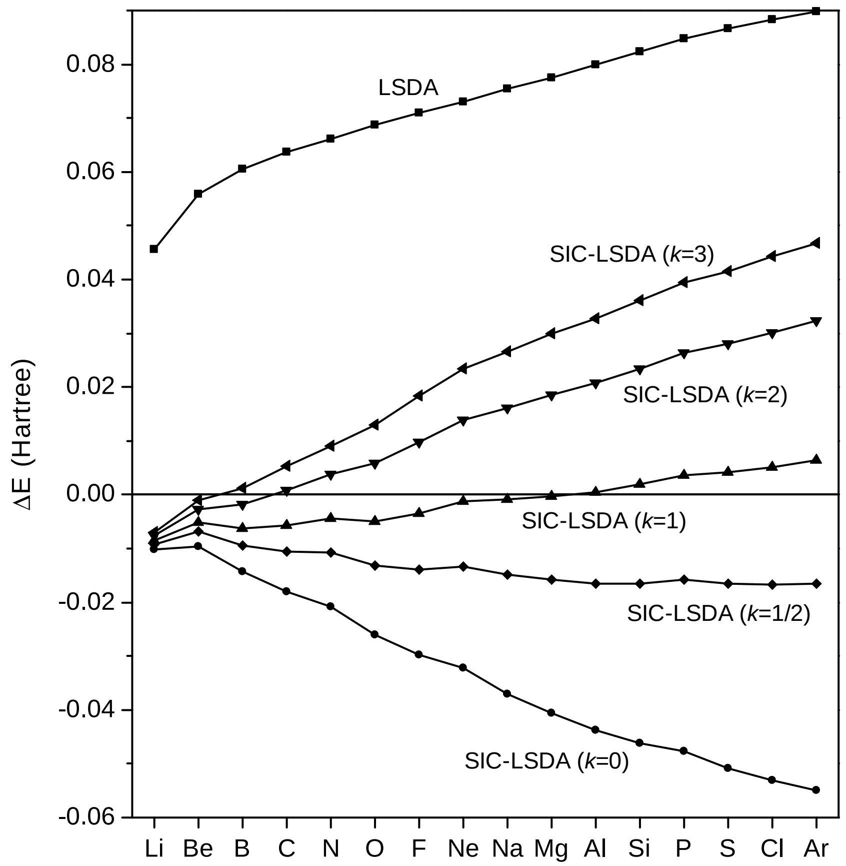

Figure 2.3 : Errors per electron in total energies of the atoms from Li to Ar computed with the 6-311+G(3*df*) basis set. The scaling factor of Eq. (2.10) is used.

2.3.3 Atomization energies

A benchmark set of molecular atomization energies or enthalpies of formation is one of the standard tests habitually applied to a newly developed density functional. To assess the thermochemical performance of the new SIC scheme, we computed atomization energies for the AE6 set developed by Lynch and Truhlar [75]. This set includes only six molecules [SiH_4, S_2, SiO, C_3H_4 (propyne), $C_2H_2O_2$ (glyoxal), and C_4H_8 (cyclobutane)], but it is quite diverse and was constructed to be representa-

Table 2.8 : Errors in atomization energies for the AE6 test set computed with the 6-311+G($3df, 2p$) basis set. All values are in kcal/mol.

Functional	ME	MAE	RMSE
LSDA	77.3	77.3	92.2
PBE	12.4	15.5	17.8
PZ-SIC-LSDA	57.7	60.3	79.4
PZ-SIC-PBE	−13.6	17.0	21.7
	Scaling factor of Eq. (2.10)		
SIC-LSDA ($k = 1/2$)	31.3	34.0	42.9
SIC-LSDA ($k = 1$)	18.6	21.0	25.1
SIC-LSDA ($k = 2$)	6.7	8.6	10.0
SIC-LSDA ($k = 3$)	0.8	7.2	8.7
SIC-PBE ($k = 1/2$)	0.7	8.6	12.4
SIC-PBE ($k = 1$)	7.8	12.6	14.7
SIC-PBE ($k = 2$)	13.5	16.0	19.3
SIC-PBE ($k = 3$)	14.8	17.2	20.6
	Scaling factor of Eq. (2.13)		
SIC-LSDA ($m = 1$)	32.6	35.5	44.9
SIC-LSDA ($m = 2$)	22.3	25.2	31.1
SIC-LSDA ($m = 3$)	15.4	18.2	22.4
SIC-LSDA ($m = 4$)	10.2	13.0	16.6
SIC-LSDA ($m = 5$)	6.7	11.5	13.2
SIC-PBE ($m = 1/2$)	−1.7	7.7	10.1
SIC-PBE ($m = 1$)	4.3	8.8	9.8
SIC-PBE ($m = 3/2$)	10.7	12.4	15.3

tive, that is to reproduce errors in much larger sets. We used QCISD/MG3 molecular geometries suggested by the authors of the set [75, 76]. The deviations of the theoretical methods from the best estimates of atomization energies are summarized in

Table 2.8.

Note that an error in an atomization energy is equal to the negative of the error in the enthalpy of formation for the same molecule. Thus, mean errors (ME) reported in Table 2.8 for the PZ-SIC have opposite signs to the ones reported in Table 2.5 for enthalpies of formation.

As compared to the Perdew–Zunger SIC, the scaled-down corrections provide much better thermochemical performance. The improvement is particularly noticeable in the case of LSDA. For the scaling factor of Eq. (2.10), the optimal value of the parameter k happens to be around 1/2 for PBE, whereas LSDA needs higher values of k, such as $k = 2$ or $k = 3$. For the scaling factor of Eq. (2.13), $m = 1/2$ works well in SIC-PBE, but a value of m as large as 5 is needed in SIC-LSDA.

The strong LSDA overbinding of molecules (Table 2.8) arises largely because the self-interaction error of LSDA raises the energies of the separated atoms more than it raises the energy of the molecule. Reducing this error in the atoms (as in Table 2.7) strongly reduces the LSDA error of the atomization energy of the molecule.

2.3.4 Barrier heights of chemical reactions

Barrier heights of chemical reactions are seriously underestimated by semi-local functionals. In fact, barrier heights are often predicted to be negative, erroneously suggesting that the transition state is more stable than either reactants or products. Self-interaction error is often assumed to be responsible for this fault. Hybrid func-

Table 2.9 : Errors in barrier heights for the BH6 test set computed with the 6-311+G($3df, 2p$) basis set. All values are in kcal/mol.

Functional	ME	MAE	RMSE
LSDA	−17.9	17.9	18.8
PBE	−9.5	9.5	10.0
PZ-SIC-LSDA	−5.2	5.2	6.6
PZ-SIC-PBE	−0.1	4.2	5.4
Scaling factor of Eq. (2.10)			
SIC-LSDA ($k = 1/2$)	−3.8	3.8	5.0
SIC-LSDA ($k = 1$)	−3.2	3.5	4.7
SIC-LSDA ($k = 2$)	−2.8	4.7	5.4
SIC-LSDA ($k = 3$)	−2.9	5.7	6.3
SIC-PBE ($k = 1/2$)	−2.5	2.9	4.9
SIC-PBE ($k = 1$)	−4.2	4.3	5.8
SIC-PBE ($k = 2$)	−6.5	6.5	7.7
SIC-PBE ($k = 3$)	−7.7	7.7	8.9
Scaling factor of Eq. (2.13)			
SIC-LSDA ($m = 1$)	−3.7	3.9	5.3
SIC-LSDA ($m = 2$)	−3.2	4.2	5.3
SIC-LSDA ($m = 3$)	−2.9	4.6	5.6
SIC-LSDA ($m = 4$)	−2.7	5.0	5.9
SIC-LSDA ($m = 5$)	−2.5	5.4	6.3
SIC-PBE ($m = 1/2$)	−2.2	2.5	4.4
SIC-PBE ($m = 1$)	−3.2	3.2	4.3
SIC-PBE ($m = 3/2$)	−3.9	3.9	4.7

tionals specifically designed for thermochemical kinetics usually contain a large fraction of exact exchange, which reduces the SIE. Although the Perdew–Zunger SIC does improve barrier heights [50], it cannot compete with specialized hybrids.

To assess the performance of the new SIC, we computed barrier heights for the BH6 benchmark set [75], which consists of the forward and reverse barriers for three reactions: $OH + CH_4 \rightarrow CH_3 + H_2O$, $H + OH \rightarrow H_2 + O$, and $H + H_2S \rightarrow H_2 + HS$. Like the AE6 set, this small data set was optimized to be representative. Geometries of all species as well as the best estimates of barrier heights were taken from Refs. [75, 76]. The summary of deviations is given in Table 2.9.

Table 2.9 shows that the scaled-down SIC performs better than the PZ-SIC, if $k = 1/2$ or $k = 1$ is chosen in Eq. (2.10). For the scaling factor of Eq. (2.13), $m = 1/2$ works well for SIC-PBE and $m \sim 2$ is optimal for SIC-LSDA. For all self-interaction corrected methods, the largest error corresponds to the reverse barrier of the first reaction. That is not surprising since this reaction has the CH_3 radical as one of the products. We used the planar geometry for CH_3, optimized in a high-level quantum chemistry method. However PZ-SIC erroneously predicts CH_3 to be pyramidal [35]. Scaling the SIC down alleviates but does not completely solve this problem. The SIC also produces an unwanted large correction to the reaction energy of the first reaction.

2.3.5 Ionization potentials and electron affinities

In Section 2.2, we tested the Perdew–Zunger SIC for atomic and molecular ionization potentials and electron affinities. For IPs and EAs evaluated as differences in total energies (the ΔSCF method), we found that PZ-SIC provides a little improvement

Table 2.10 : Deviations from experiment of ΔSCF ionization potentials and electron affinities for atoms from H to Ar computed with the 6-311++G(d) basis set. All values are in eV.

	18 IPs		12 EAs	
Functional	ME	MAE	ME	MAE
LSDA	0.17	0.30	0.29	0.29
PBE	0.10	0.15	0.09	0.13
PZ-SIC-LSDA	0.21	0.24	−0.15	0.18
PZ-SIC-PBE	−0.34	0.39	−0.57	0.57
Scaling factor of Eq. (2.10)				
SIC-LSDA ($k = 1$)	0.07	0.15	−0.08	0.11
SIC-LSDA ($k = 2$)	0.00	0.13	−0.05	0.09
SIC-LSDA ($k = 3$)	−0.04	0.14	−0.03	0.10
SIC-PBE ($k = 1$)	−0.14	0.22	−0.29	0.29
SIC-PBE ($k = 2$)	−0.06	0.15	−0.15	0.15
SIC-PBE ($k = 3$)	−0.01	0.12	−0.07	0.10
Scaling factor of Eq. (2.13)				
SIC-LSDA ($m = 1$)	0.06	0.20	−0.13	0.17
SIC-LSDA ($m = 2$)	0.01	0.22	−0.11	0.15
SIC-LSDA ($m = 3$)	−0.02	0.22	−0.10	0.14
SIC-LSDA ($m = 4$)	−0.04	0.22	−0.09	0.14
SIC-LSDA ($m = 5$)	−0.05	0.22	−0.07	0.14
SIC-PBE ($m = 1/2$)	−0.20	0.26	−0.36	0.36
SIC-PBE ($m = 1$)	−0.13	0.19	−0.25	0.25
SIC-PBE ($m = 3/2$)	−0.08	0.15	−0.17	0.17
SIC-PBE ($m = 2$)	−0.06	0.13	−0.12	0.14

for LSDA, whereas the performance of beyond-LSDA functionals is deteriorated by the PZ-SIC.

We have tested the performance of the scaled-down SIC for IPs and EAs of atoms up to argon. The deviations of theoretical predictions from the experimental data [77] are summarized in Table 2.10.

We can clearly see that scaling down the SIC improves atomic IPs and EAs. The optimal values of k in Eq. (2.10) for IPs and EAs seem to be around $k = 2 \dots 3$, which is somewhat higher than the optimal values for atomization energies or barrier heights. In the case of SIC-LSDA with the scaling factor of Eq. (2.13), we observe only a weak dependence of the accuracy on the parameter m and any value of $m \geq 1$ is acceptable. In the case of SIC-PBE scaled down by Eq. (2.13), the value of $m \sim 2$ performs well for IPs and EAs. The EA of the boron atom is negative in Perdew–Zunger-corrected PBE. But it becomes correctly positive once the SIC is sufficiently scaled down.

2.3.6 Bond lengths

In order to test the performance of the new SIC in predicting molecular bond lengths, we compiled a set of 12 small molecules: LiH, BeH, BH, CH_4, CO, NH, NO, N_2, OH, O_2, HF, and F_2. The equilibrium bond lengths for all these species are known from experiment [77].

We optimized the geometries of all the molecules in the set using self-interaction-corrected and uncorrected functionals. Since analytic gradients with respect to nuclear displacements are not available in our SIC code, all the geometry optimiza-

Table 2.11 : Deviations from experiment of equilibrium bond lengths for 12 molecules computed with the 6-311+G($3df, 2p$) basis set. All values are in Å.

Functional	ME	MAE	RMSE
LSDA	0.006	0.013	0.015
PBE	0.010	0.010	0.011
PZ-SIC-LSDA	−0.045	0.045	0.051
PZ-SIC-PBE	−0.024	0.024	0.032
Scaling factor of Eq. (2.10)			
SIC-LSDA ($k = 1$)	−0.015	0.015	0.020
SIC-LSDA ($k = 2$)	−0.003	0.007	0.010
SIC-PBE ($k = 1$)	−0.012	0.014	0.019
SIC-PBE ($k = 2$)	−0.006	0.007	0.012
Scaling factor of Eq. (2.13)			
SIC-LSDA ($m = 1$)	−0.022	0.022	0.024
SIC-LSDA ($m = 2$)	−0.012	0.012	0.014
SIC-LSDA ($m = 3$)	−0.008	0.008	0.010
SIC-LSDA ($m = 4$)	−0.004	0.006	0.008
SIC-LSDA ($m = 5$)	−0.002	0.006	0.007
SIC-PBE ($m = 1/2$)	−0.014	0.014	0.019
SIC-PBE ($m = 1$)	−0.007	0.007	0.009
SIC-PBE ($m = 3/2$)	−0.004	0.005	0.006
SIC-PBE ($m = 2$)	−0.003	0.004	0.005

tions with SIC functionals were done by means of bond length variation, followed by quadratic interpolation. Table 2.11 sums up the deviations of predicted bond lengths from experiment.

In agreement with previous observations [57, 43], we found that the PZ-SIC predicts too short bonds in molecules. For every molecule in the set, as the SIC is scaled-down, the predicted bond length becomes longer and thus better agrees with experiment. Scaling factor of Eq. (2.10) with $k = 2$ works well for both SIC-LSDA and SIC-PBE. For the scaling factor of Eq. (2.13), $m \geq 3$ in SIC-LSDA and $m \geq 1$ in SIC-PBE give particularly accurate results.

2.4 Discussion

2.4.1 Effects of using orbital densities

In Section 2.2, we found that the Perdew–Zunger SIC works better for LSDA than for other functionals. This conclusion seems to hold for the scaled-down correction as well: remarkable improvements are observed for LSDA, whereas the performance of the SIC is less satisfactory for beyond-LSDA functionals. Our tests clearly show that the SIC (either PZ or scaled-down) works worse with PBE GGA than with LSDA, and it works even worse with TPSS meta-GGA (for that reason we did not include TPSS into the tables in Section 2.3).

These observations may be explained as results of using orbital densities in Eqs. (2.2) and (2.9). Orbital densities often have nodes and minute details, such as so-called "orthogonalization tails". Thus orbital densities can be much more rapidly-varying than normal ground-state densities. Our corrections involve evaluation of the xc energy for an orbital density. LSDA has a limited sensitivity to density variations. Functionals explicitly dependent on the density derivatives (GGA, meta-GGA) are more sensitive to density variations. The reduced gradient $\sim |\nabla\rho|/\rho^{4/3}$ and the reduced Laplacian $\sim \nabla^2\rho/\rho^{5/3}$ diverge at the nodes. Thus, corrections utilizing orbital densities are better suited for LSDA than for higher-level functionals.

In Eqs. (2.2) and (2.9), $E_{\text{xc}}^{\text{DFA}}[\rho_{i\sigma}, 0]$ is the ground-state exchange-correlation energy for an orbital density $\rho_{i\sigma}(\mathbf{r}) = |\varphi_{i\sigma}(\mathbf{r})|^2$. In many cases, $\rho_{i\sigma}(\mathbf{r})$ is found from an orbital $\varphi_{i\sigma}(\mathbf{r})$ that changes sign or phase and so is not a ground-state wavefunction. The corresponding ground-state orbital would be $|\varphi_{i\sigma}(\mathbf{r})|$, which belongs to a highly singular and rapidly-varying external potential $\frac{1}{2}\nabla^2 |\varphi_{i\sigma}(\mathbf{r})| / |\varphi_{i\sigma}(\mathbf{r})| + constant$, even when $\varphi_{i\sigma}(\mathbf{r})$ belongs to a smooth external potential $\frac{1}{2}\nabla^2\varphi_{i\sigma}(\mathbf{r})/\varphi_{i\sigma}(\mathbf{r}) + constant$. We may expect semi-local approximations to be significantly less accurate for $E_{\text{xc}}[\rho_{i\sigma}, 0]$ than for $E_{\text{xc}}[\rho_\alpha, \rho_\beta]$, which may cause some accuracy loss in orbital-density-dependent corrections like Eq. (2.2) or (2.9).

Use of orbital densities in Eqs. (2.2) and (2.9) also has computational disadvantages. The exchange-correlation energy has to be evaluated at each orbital density, which is one of the major factors slowing down the calculation. Evaluation of SIC requires dense unpruned integration grids since orbital densities can be rather rapidly varying.

2.4.2 Formal properties of the SIC

As stated earlier, Eqs. (2.2) and (2.9) are exact for any one-electron density, and give no correction to the exact density functional. For $k = 0$ in Eq. (2.10) or $m = 0$ in Eq. (2.13), Eq. (2.9) reduces to the original Perdew–Zunger self-interaction correction of Eq. (2.2), and for $k > 0$ or $m > 0$ the SIC is scaled down in many-electron regions. Both Eq. (2.2) and Eq. (2.9) are size-consistent (separable and extensive in the sense of Ref. [78]).

In the Perdew–Zunger SIC, there is a formal problem [78] which is not widely appreciated. We do not know if the orbitals that minimize the PZ-SIC total energy for a uniform density are localized or delocalized [79, 80, 81] (1) If they are localized, then the PZ-SIC, applied to an approximate functional that is exact for the energy of a uniform density, produces an energy that is lower than the exact one. (2) If the SIC orbitals for a uniform density are delocalized, then the PZ-SIC energy of a large finite chunk of uniform density has a "false surface energy" that is correctly proportional to the area of its surface but incorrectly depends upon its shape.

With any $k > 0$ in Eq. (2.10), the above problems are corrected, since τ^W/τ vanishes for a uniform density. But we still do not know if the orbitals that minimize the SIC ($k > 0$) energy for an electron gas of slow or small density variation are localized or delocalized. If they are delocalized, then no further constraint on k is implied. But if they are localized, then k must be an integer ≥ 1 to guarantee the existence of a gradient expansion for $E_{\mathrm{xc}}^{\mathrm{DFA}}$. In particular, $k \geq 2$ is needed to preserve all the correct formal properties of LSDA and PBE under self-interaction correction, while $k \geq 3$ is needed to preserve all the correct properties of TPSS.

Let us focus specifically upon self-interaction correction of LSDA, for the reasons described in Section 2.4.1. Consider a uniform electron gas perturbed by a density variation of small amplitude A: $\rho(\mathbf{r}) = \textit{constant} + Af(\mathbf{r})$. LSDA is known to give a rather good description of the energy variation through order A^2, and indeed the PBE GGA was constructed [8] to preserve this good LSDA behavior. If we want our SIC to do the same even if the SIC orbitals are localized, we must take $k \geq 2$ in Eq. (2.10) to make $(\tau^W/\tau)^k$ of order A^4 or higher, since $\tau^W \sim |\nabla\rho(\mathbf{r})|^2 \sim A^2$. In a sense, SIC-LSDA scaled down by Eq. (2.10) with $k = 2$ is not only a successful approximation, but a particularly well-justified one. The simplified scaling factor Eq. (2.13) does not have such good formal properties.

Unfortunately, scaling down the SIC using the factors of Eq. (2.10) or Eq. (2.13) leads to violation of some exact constraints satisfied in the PZ-SIC. For example, the original Perdew–Zunger SIC exchange-correlation potential has the correct asymptotic behavior $-1/r$, while the xc potential in the scaled-down SIC has a $-X_{\mathrm{HO}}/r$ asymptote, where X_{HO} is the scaling factor for the highest occupied orbital, and X_{HO} is usually less than one in many-electron systems. In Section 4.6 we will also show that the scaled-down SIC is often inferior to the original PZ-SIC in terms of the many-electron SIE. It appears that the full correction may be needed for the highest occupied orbital to provide a good description of charge transfer. Thus, we do not yet have here an all purpose self-interaction correction.

2.5 Some alternative self-interaction corrections

$\tau_\sigma^W/\tau_\sigma$ was first proposed as a scaling factor for the self-interaction correction in Eq. (22) of Ref. [5], and our Eq. (2.9) was intended as a computationally practical test of the principle for that approach. The alternative SIC of Ref. [5] is invariant under unitary transformations of orbitals. However, this nice feature comes at the price of a great increase in computational complexity. The SIC of Ref. [5] uses energy densities that are not unique and may not be mutually consistent. The explicit and intricate dependence on energy densities also makes this method non-trivial (if at all possible) to implement and, even if implemented, will make it prohibitively expensive computationally.

It sounds obvious that any kind of correction must not modify the exact xc functional (which is itself unknown, but many of its formal properties are known). All the corrections considered above are constructed to vanish when applied to the exact functional. This feature seems to be absent from a recently proposed alternative self-interaction correction of Lundin and Eriksson [82]. Thus, the SIC of Ref. [82] does not really qualify to be called a “correction”.

Chapter 3

Long-range-corrected hybrid functionals

A common shortcoming of all semi-local approximations is the incorrect asymptotic behavior of the exchange-correlation potential. In molecules, the xc potential of semi-local functionals decays exponentially along with the density, while the asymptotic form of the exact xc potential is $-1/r$ [83, 84]. The problem of poor asymptotics is considered to be a consequence of SIE. Indeed, the Perdew–Zunger SIC recovers the exact asymptote of the xc potential. However, as was shown in Section 2.4.2, it is possible to define a method (such as the scaled-down SIC of Eq. (2.9)) that will be exact for all one-electron densities but will not yield the correct asymptotics for the xc potential of a many-electron system. Conversely, there are correction schemes that treat the long-range asymptote of the xc potential directly [85, 86], without correcting the SIE.

In the global hybrid of Eq. (1.9), the xc potential decays asymptotically as $-a_0/r$, where a_0 is the fraction of HF exchange. To recover the exact $-1/r$ asymptote, it has been suggested to introduce a range separation into the exchange component [see Eqs. (1.10)—(1.13)] and replace the long-range portion of the DFA exchange by the Hartree–Fock counterpart [20, 87, 26, 27, 28]. Such a long-range-corrected (LC) hybrid is defined as

$$E_{\mathrm{xc}}^{\text{LC-DFA}} = E_{\mathrm{x}}^{\text{SR-DFA}}(\omega) + E_{\mathrm{x}}^{\text{LR-HF}}(\omega) + E_{\mathrm{c}}^{\text{DFA}}. \tag{3.1}$$

This long-range correction was shown to improve such properties as polarizabilities of long chains [26, 88], charge-transfer and Rydberg excitations [27], nonlinear optical properties [89], and dissociation of 2-center 3-electron bonds [28]. This scheme can also be utilized to describe the repulsive part of van der Waals potentials [90, 91, 92, 93].

The short-range component of an exchange DFA, required in Eq. (3.1), can be straightforwardly derived if the expression for the corresponding exchange hole is known. Given a spherically-averaged exchange hole $h_{\mathrm{x}}^{\mathrm{DFA}}(\mathbf{r}, u)$, the short-range part of the exchange energy is evaluated as

$$E_{\mathrm{x}}^{\text{SR-DFA}}(\omega) = 2\pi \int d\mathbf{r}\, \rho(\mathbf{r}) \int_0^\infty du\, \big(1 - \operatorname{erf}(\omega u)\big)\, u\, h_{\mathrm{x}}^{\mathrm{DFA}}(\mathbf{r}, u). \tag{3.2}$$

We have implemented and tested the SR and LR components for three exchange DFAs. The short-range Dirac/Slater exchange functional (which we will denote as SR-LSDA) was derived [20, 94] a decade ago and it is easy to implement. The SR-PBE exchange was obtained using the model PBE exchange hole [95], as described in Refs. [22, 23]. The TPSS exchange hole has been recently engineered [96] and used to implement the corresponding SR component [97]. The details of the implementation of all the terms in Eq. (3.1) can be found in Refs. [22, 23].

We note that a derivation analogous to Eq. (3.2) cannot be used for most of the available DFAs, since the explicit expression for the exchange hole $h_{\mathrm{x}}^{\mathrm{DFA}}(\mathbf{r}, u)$ is usually unknown. In fact, most of the studies of SR GGAs used various approximations [26, 27, 93].

Handy and coworkers [98] and later Tozer and coworkers [99, 100] noted that the long-range correction of Eq. (3.1) can in some cases worsen the accuracy of a DFA, if the scheme is implemented approximately. As a remedy, they proposed to decrease the fraction of HF exchange at long range. This, however, leads to the loss of the exact asymptote of the exchange potential. In the next section, we will show that such problems do not occur when the rigorous implementation of SR-DFA of Eq. (3.2) is used.

For $\omega = 0$, the hybrid of Eq. (3.1) reduces to the underlying semi-local DFA. In the limit $\omega \to \infty$, the hybrid of Eq. (3.1) becomes HF exchange with DFA correlation.

When the error function is used in Eq. (1.10), the transition between the short-range and the long-range parts is very smooth. Note also that, as u approaches zero, $\mathrm{erf}(\omega u)/u$ does not go to zero but to a constant $2\omega/\sqrt{\pi}$. In other words, short-range interactions are not completely removed from the long-range part. In Ref. [101], $\mathrm{erf}(\omega u)/u$ is actually referred to as "background", rather than "long-range" interaction.

3.1 Designing the optimal long-range-corrected hybrid

In this section we attempt to determine which semi-local DFA is best suited to use in Eq. (3.1) and which range parameter ω is optimal. We also compare the performance of the long-range correction scheme of Eq. (3.1) to the conventional global hybrid scheme of Eq. (1.9).

3.1.1 Tests on enthalpies of formation

Predicting accurate enthalpies of formation (or atomization energies) has traditionally been the major survival criterion in the natural selection of constantly appearing exchange-correlation approximations. In fact, a set of standard enthalpies of formation is often used to fit parameters in semiempirical functionals. Hybrid functionals hold the leading position in this "survival of the fittest" contest. Admixture of HF exchange has long been an effective means of improving thermochemical performance [14, 15].

As a benchmark set of standard enthalpies of formation ($\Delta_\mathrm{f} H^\circ_{298}$), we use the G2-1 set of 55 small molecules [65]. The geometries and zero-point energies are obtained

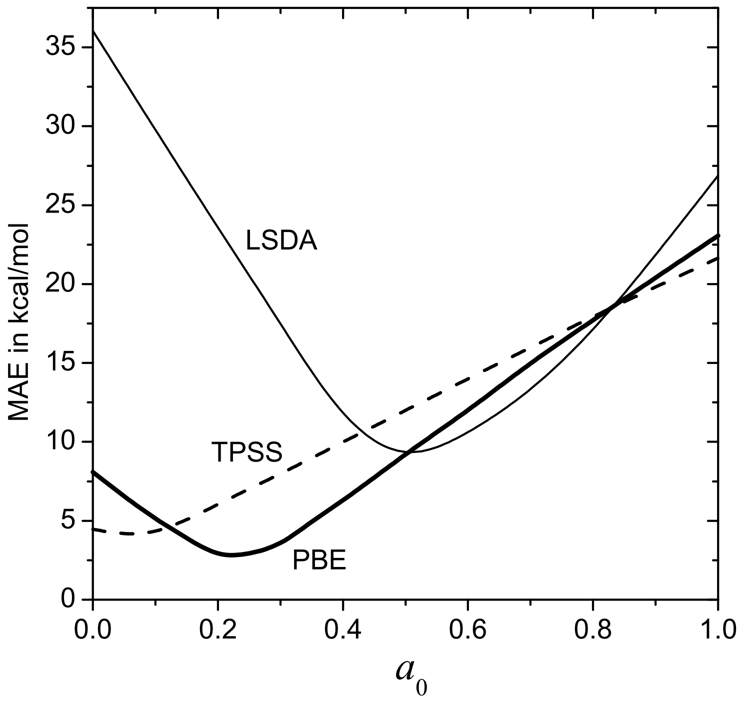

Figure 3.1 : Mean absolute errors in the standard enthalpies of formation of the G2-1 set as a function of the exchange mixing parameter in global hybrids.

at the B3LYP/6-31G($2df, p$) level. A frequency scale factor of 0.9854 is used in calculation of zero-point energies and thermal corrections. We find enthalpies of formation of molecules by calculating the atomization energies and employing the experimental enthalpies of formation of free atoms. Hence, the errors reported in this section reflect the errors in computed atomization energies.

The comparison of the performance of pure DFAs for the enthalpies of formation reveals how the errors are reduced while ascending the ladder of xc approximations. For the G2-1 set, the MAE of LSDA is 36 kcal/mol, while it is 8 kcal/mol in PBE and just 4.5 kcal/mol in TPSS. Figure 3.1 shows the errors of the global hybrids of Eq. (1.9) for the G2-1 set as a function of the HF exchange mixing parameter. In the

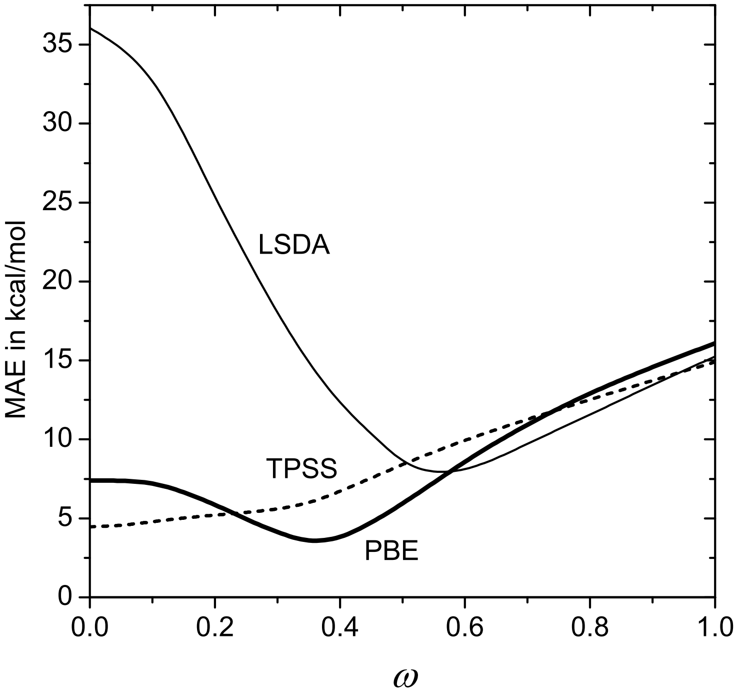

Figure 3.2 : ω-dependence of mean absolute errors in the standard enthalpies of formation of the G2-1 set for the “long-range-corrected” hybrids. ω is in a.u.$^{-1}$.

hybrid of LSDA, the best performance is attained with about 50% of HF exchange: the MAE is lowered to 9.4 kcal/mol. For the PBE hybrid, the typically used value of $a_0 = 0.25$ (as in PBE0) provides optimal accuracy with a MAE of only 2.9 kcal/mol. In the case of TPSS, an admixture of HF exchange does not lead to any considerable improvement for the G2-1 set.

Next, we consider the long-range-corrected hybrids of Eq. (3.1). Figure 3.2 shows how the long-range correction influences the errors in the enthalpies of formation. The ω-dependence of the errors is quite different for LSDA, PBE, and TPSS hybrids, but is quite reminiscent of the a_0-dependence in the global hybrids (Figure 3.1). In the LSDA curve in Figure 3.2, there is a deep minimum around $\omega = 0.55$ with MAE of 8.0 kcal/mol. This result is consistent with the work of Gerber and Ángyán [28], within the difference in computational details. For PBE, the minimal MAE of 3.6 kcal/mol is obtained when $\omega = 0.35$. The long-range correction method applied to TPSS provides no improvement for the enthalpies of formation, irrespective of the value of ω.

3.1.2 Tests on barrier heights of chemical reactions

Significant underestimation of reaction barrier heights is a well known deficiency of common DFAs. Transition states of chemical reactions are characterized by unusual, stretched bonds. In such systems, the self-interaction error of a DFA may be particularly large [29]. A greater fraction of HF exchange (usually between 40 and 60%) is needed for a global hybrid functional to obtain accurate barrier heights [102]. Becke's half-and-half functional [13], one of the earliest and simplest hybrids, contains 50% of HF exchange and it is surprisingly successful in predicting barrier heights, despite being not very accurate for other properties.

A benchmark set of barrier heights was recently assembled by Truhlar and coworkers [102, 76]. It consists of the forward and reverse barrier heights for 21 reactions. We will refer to it as the BH42 set. The best estimates of the barrier heights as well as the geometries of all the species in the BH42 set, are available from the Truhlar group database website [76].

The performance of the pure functionals for barrier heights is improved going

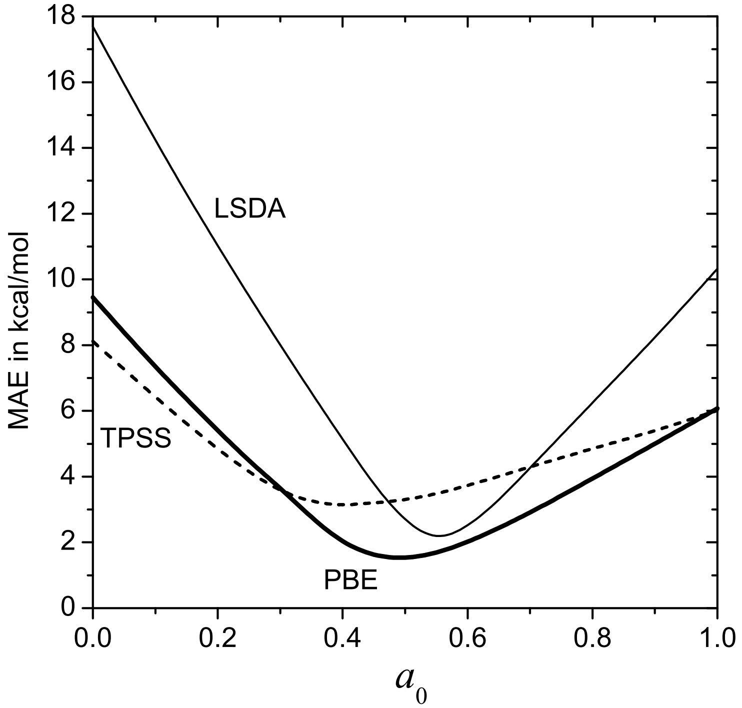

Figure 3.3 : Mean absolute errors in the barrier heights of the BH42 set as a function of the exchange mixing parameter in global hybrids.

from LSDA (MAE = 17.7 kcal/mol) to PBE (MAE = 9.4 kcal/mol) to TPSS (MAE = 8.1 kcal/mol). But even the accuracy of TPSS is still unsatisfactory. Figure 3.3 shows the errors of the global hybrids for the BH42 set. Admixture of 55% of HF exchange to LSDA brings its error down to 2.2 kcal/mol. We note that in LSDA global hybrids, about 50% of HF exchange is optimal for both enthalpies of formation and barrier heights. Global hybrids of PBE and TPSS are not that consistent: a significantly larger fraction of HF exchange is required to accurately predict barrier heights. Figure 3.3 shows that $a_0 = 0.5$ is needed in the PBE hybrid, which gives the lowest MAE of just 1.5 kcal/mol. TPSS global hybrid with $a_0 = 0.4$ has MAE of 3.1 kcal/mol.

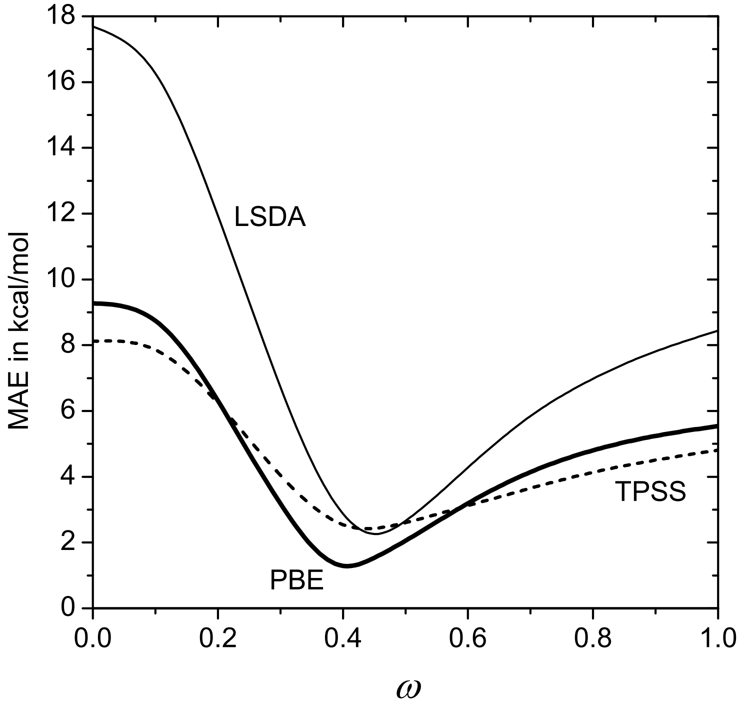

Figure 3.4 : ω-dependence of mean absolute errors in the barrier heights of the BH42 set for the "long-range-corrected" hybrids. ω is in a.u.$^{-1}$.

Figure 3.4 shows that long-range corrected hybrids can be quite successful in describing barrier heights: the LSDA curve has the minimum at $\omega = 0.45$ with MAE = 2.3 kcal/mol; for PBE, the minimal MAE of only 1.3 kcal/mol is obtained with $\omega = 0.4$; for TPSS, the minimum occurs at $\omega = 0.45$ with MAE = 2.4 kcal/mol.

It is known to be quite challenging to construct a functional that would work well for barrier heights and for enthalpies of formation at the same time. As we mentioned above, global hybrids of beyond-LSDA functionals are not well fit for that. Long-range corrected functionals seem to be more successful. As Figures 3.1 and 3.4 show, the long-range-corrected hybrid of PBE with $\omega = 0.4$ is consistently accurate for barrier heights as well as for equilibrium thermochemistry.

3.1.3 Tests on ionization potentials and electron affinities

In this section we only consider hybrids of PBE, since PBE seems to benefit the most from an admixture of HF exchange, as can be seen from Figures 3.1, 3.2, 3.3, and 3.4.

All the benchmark calculations of ionization potentials (IPs) and electron affinities (EAs) were performed on the G2 ion test set [72]. The calculations of the H_2S^+ and N_2^+ cations do not converge with pure DFT methods [72] and these two species were dropped from the set. Our test set thus comprises 86 ionization potentials and 58 electron affinities. IPs and EAs were evaluated as the difference in total energies at 0 K of the ion and the corresponding neutral, at their respective B3LYP/6-31G($2df, p$) geometries. Zero-point energies were obtained at the B3LYP/6-31G($2df, p$) level with a frequency scale factor of 0.9854.

The mean absolute errors in IPs and EAs of the global hybrids of PBE are shown in Figure 3.5. Ionization potentials are only slightly improved by the admixture of HF exchange. The dependence of the errors in IPs on the mixing parameter a_0 is weak: with a_0 ranging from 0 to 0.8, the MAE varies by less than 0.05 eV. For $0.2 \leq a_0 \leq 0.5$, the MAE nearly levels off at 0.20 eV.

EAs, on the other hand, do not benefit from the admixture of HF exchange. The error in EAs grows with increasing a_0. This observation is somewhat counter

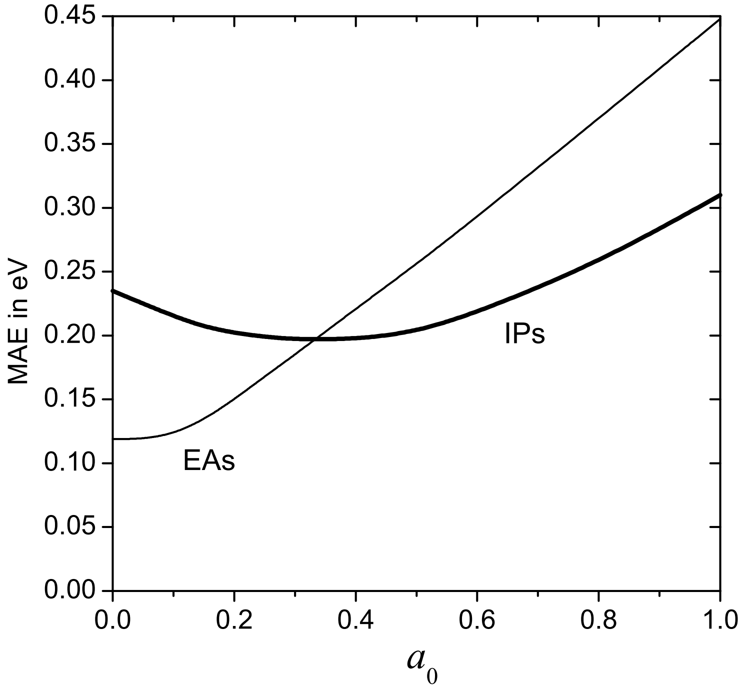

Figure 3.5 : Mean absolute errors in the ionization potentials and electron affinities of the G2 set as a function of the exchange mixing parameter in global hybrids of PBE.

intuitive. Pure DFAs predict positive highest occupied orbital energies in anions, meaning that the outermost electron is effectively unbound (for the detailed discussion see Section 4.2). Admixture of a certain amount of HF exchange makes all occupied orbital energies properly negative. However, as seen from Figure 3.5, this is not accompanied by any improvement in ΔSCF EAs. When a finite basis set is used, the highest occupied orbital seems artificially stabilized irrespective of the sign of the orbital eigenvalue. The success of pure DFAs in predicting EAs seems to rest on basis set effects and error cancellations, which do not necessarily comply to a theoretical justification.

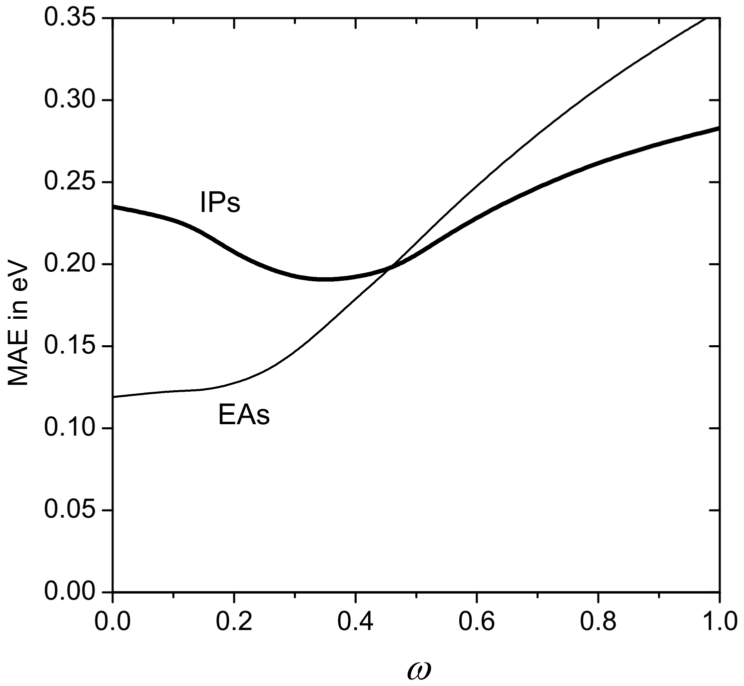

Figure 3.6 : ω-dependence of mean absolute errors in the ionization potentials and electron affinities of the G2 set for the “long-range-corrected” hybrids of PBE. ω is in a.u.$^{-1}$.

Figure 3.6 presents the performance of the long-range corrected PBE hybrid for IPs and EAs. There is a shallow minimum in the IP curve at $\omega \approx 0.35$ with a MAE of 0.19 eV. For EAs, the long-range correction provides no improvement.

Summarizing the results for IPs and EAs: the error in IPs can be only slightly reduced by adding a fraction of HF exchange. For EAs, an admixture of HF exchange in any form increases the errors. The best performance for electron affinities is achieved by the pure PBE.

3.2 Assessment of the LC-ωPBE functional

As shown in Figures 3.2, 3.4, and 3.6, the long-range corrected hybrid of PBE with $\omega = 0.4$ bohr^{-1} happens to work well for enthalpies of formation, barrier heights, and IPs. The correct asymptote of the exchange potential, recovered by the long-range correction, may not be very important for these benchmark properties, but it is very important for other properties, such as charge transfer, which are discussed in Chapter 4.

In this section, we present a more comprehensive assessment of the performance of the long-range corrected PBE with $\omega = 0.4$ bohr^{-1}. We will denote this hybrid functional as LC-ωPBE. The acronym ωPBE, introduced in Refs. [22] and [23], refers to the short-range exchange functional derived by integration of the model PBE exchange hole [95]. Note that most of other studies used very different derivations of short-range DFAs [26, 27, 90, 89, 88, 91, 93, 98, 99, 100].

Table 3.1 : Total energies of atoms (hartree) computed with the UGBS2P basis set.

Atom	Accurate[a]	PBE	PBE0	LC-ωPBE
H	-0.500	-0.500	-0.501	-0.506
He	-2.904	-2.893	-2.895	-2.905
Li	-7.478	-7.462	-7.467	-7.472
Be	-14.667	-14.630	-14.637	-14.641
B	-24.654	-24.612	-24.620	-24.630
C	-37.845	-37.799	-37.807	-37.825
N	-54.589	-54.536	-54.547	-54.571
O	-75.067	-75.015	-75.023	-75.054
F	-99.734	-99.676	-99.682	-99.722
Ne	-128.938	-128.866	-128.872	-128.918
Na	-162.255	-162.173	-162.185	-162.219
Mg	-200.053	-199.955	-199.971	-199.994
Al	-242.346	-242.236	-242.257	-242.277
Si	-289.359	-289.234	-289.259	-289.281
P	-341.259	-341.116	-341.146	-341.169
S	-398.110	-397.953	-397.986	-398.013
Cl	-460.148	-459.975	-460.012	-460.042
Ar	-527.540	-527.346	-527.388	-527.420
ME/ē [b]		0.0076	0.0061	0.0034
MAE/ē [c]		0.0076	0.0063	0.0042

[a] Ref. [74].

[b] Mean error per electron.

[c] Mean absolute error per electron.

3.2.1 Total energies of atoms

For PBE and its hybrids, we have computed the total energies of atoms up to Ar. We used the UGBS2P basis set [103] which is expected to yield energies close to the basis set limit. Table 3.1 compares the total energies with the accurate nonrelativistic values [74]. LC-ωPBE gives a smaller average error per electron than both PBE and PBE0. However, for the total energy of the hydrogen atom, LC-ωPBE has the largest error. This error is entirely contained in the correlation energy. The LC-ωPBE exchange energy in the hydrogen atom is accurate to within less than a millihartree, but there is a spurious self-correlation of -0.006 hartree. We note that the pure PBE functional yields very accurate total energy for the H atom due to fortuitous cancellation of errors between the exchange and correlation components.

3.2.2 Thermochemistry

Critically evaluated experimental thermochemical data for the compounds of the first- and second-row elements have been compiled by Curtiss *et al.* [65, 72, 104] into standard test sets, known as G2/97 and G3/99. Adopting the procedure of Ref. [105], we use the equilibrium B3LYP/6-31G($2df,p$) geometries and zero-point energies for all the species in the test sets. A frequency scale factor of 0.9854 is used in calculation of zero-point energies and thermal corrections. The 6-311++G($3df,3pd$) basis set is used in computing the energies. All the computational details in this section are intentionally chosen the same as in Ref. [106] to enable a direct comparison with all the functionals tested in that paper.

Table 3.2 : Deviations from experiment of standard enthalpies of formation ($\Delta_{\mathrm{f}}H^{\circ}_{298}$), ionization potentials (IP), electron affinities (EA), and proton affinities (PA) of the G2 and G3 test sets computed using the 6-311++G(3*df*, 3*pd*) basis set. The geometries and zero-point energies were obtained at the B3LYP/6-31G(2*df*, *p*) level using a frequency scale factor of 0.9854.

	$\Delta_{\mathrm{f}}H^{\circ}_{298}$ (kcal/mol)									
	G2 set (148 mols.)		G3 set (223 mols.)		86 IP (eV)		58 EA (eV)		8 PA (kcal/mol)	
Method	ME	MAE	ME	MAE	ME	MAE	ME	MAE	ME	MAE
PBE	−16.1	16.9	−21.7	22.2	−0.11	0.24	0.06	0.12	−0.8	1.6
PBE0	−2.4	4.9	−4.7	6.7	−0.06	0.20	−0.03	0.17	0.2	1.1
LC-ωPBE	−0.4	3.7	−0.9	4.2	0.07	0.19	0.02	0.18	0.9	1.4

Standard enthalpies of formation ($\Delta_\mathrm{f}H^\circ_{298}$) for the molecules in the G2 and G3 sets are found by calculating the atomization energies and employing the experimental enthalpies of formation of free atoms, as prescribed in Ref. [65]. Hence, the errors in $\Delta_\mathrm{f}H^\circ_{298}$ reflect the errors in computed atomization energies. Table 3.2 shows that LC-ωPBE is very accurate in predicting enthalpies of formation. It outperforms PBE0. LC-ωPBE has a very low mean signed error and therefore provides an unbiased estimate for $\Delta_\mathrm{f}H^\circ_{298}$. In LC-$\omega$PBE, the errors do not change considerably from the G2 to the G3 set. The G3 set mostly augments the G2 set with larger organic molecules. Thus, the errors of LC-ωPBE do not significantly increase with molecular size, as PBE and PBE0 errors do.

Ionization potentials (IPs) and electron affinities (EAs) of the G2 ion test set [72] were evaluated as the difference in total energies at 0 K of the ion and the corresponding neutral molecule. Table 3.2 shows that, for both IPs and EAs, LC-ωPBE is comparable in accuracy to PBE0. PBE0 has a tendency to underestimate IPs and EAs, while LC-ωPBE tends to overestimate them.

The eight proton affinities (PAs) included in the G3/99 test set were computed as the differences between the energies of neutral and protonated molecules in their lowest vibrational states. As Table 3.2 shows, PBE0 gives the smallest errors in PAs, followed by LC-ωPBE.

3.2.3 Barrier heights of chemical reactions

Truhlar and coworkers have compiled several benchmark sets of barrier heights of chemical reactions [102, 107]. The HTBH38/04 set comprises forward and reverse barrier heights for 19 hydrogen transfer reactions [107]. The HTBH38/04 set is a subset of an earlier BH42/04 set [102]. Forward and reverse barriers of 19 non-hydrogen-transfer reactions constitute the NHTBH38/04 set [107], which is further subdivided into the sets of 6 heavy-atom transfer reactions, 8 nucleophilic substitution reactions, and 5 association and unimolecular reactions. The best estimates of the barrier heights as well as the geometries of all the species are taken from Ref. [107]. We use the 6-311++G($3df, 3pd$) basis set for computing the barriers.

Table 3.3 shows that LC-ωPBE is remarkably accurate for the barriers of hydrogen-transfer and heavy-atom-transfer reactions. For these types of barrier heights, the PBE0 hybrid yields unacceptably large errors, showing that the admixture of 25% of HF exchange is insufficient. On the other hand, for the barriers of nucleophilic substitution, association, and unimolecular reactions, PBE0 performs fairly well and LC-ωPBE is somewhat less accurate.

Table 3.3 : Deviations from experiment of barrier heights of chemical reactions computed using the 6-311++G($3df, 3pd$) basis set. All values are in kcal/mol.

	HTBH38		non-hydrogen-transfer reactions of the NHTBH38 set							
	hydrogen-transfer (38)		heavy-atom-transfer (12)		nucleophilic substitution (16)		unimolecular and association (10)		full NHTBH38	
Functional	ME	MAE	ME	MAE	ME	MAE	ME	MAE	ME	MAE
PBE	−9.7	9.7	−15.3	15.3	−6.8	6.8	−3.1	3.5	−8.5	8.6
PBE0	−4.6	4.6	−7.0	7.0	−1.7	1.9	−0.8	2.3	−3.1	3.6
LC-ωPBE	−0.5	1.3	−0.6	1.9	2.9	2.9	1.4	2.3	1.4	2.4

Table 3.4 : Summary of deviations from experiment of equilibrium bond lengths (r_e) for 95 molecules of the T-95R test set (excludes Be_2 from the T-96R set of Ref. [106]) computed using the 6-311++G($3df, 3pd$) basis. All values are in Å.

Method	ME	MAE	St.Dev.	Max.(+)	Max.(−)
PBE	0.0156	0.0160	0.0113	0.055 (Li_2)	−0.009 (F_2^+)
PBE0	−0.0013	0.0091	0.0133	0.055 (Li_2)	−0.052 (F_2^+)
LC-ωPBE	−0.0087	0.0139	0.0164	0.044 (Li_2)	−0.055 (P_4)

3.2.4 Bond lengths

To test the predictive power of the LC-ωPBE functional for molecular geometries, we use a test set of equilibrium bond lengths (r_e) compiled in Ref. [106]. We have excluded Be_2 from that set, since Be_2 is bound primarily by van der Waals interaction and does not belong in a set of covalently bound molecules. The resulting test set comprises 95 molecules and is referred to as T-95R. The set consists mostly of diatomics, but includes several polyatomic molecules of high symmetry whose geometry is completely determined by a single bond length. All geometry optimizations were carried out using the 6-311++G($3df, 3pd$) basis.

Table 3.4 shows that all tested functionals are reasonably accurate in predicting bond lengths. PBE0 performs only slightly better than the others. The largest deviations from experiment are observed, as one would expect, for weakly bound molecules, such as F_2^+, and metal dimers.

Table 3.5 : Errors in dissociation energies (D_e) of hydrogen-bonded complexes. The aug-cc-pVQZ basis set is used. All values are in kcal/mol.

		Deviation = Functional – Reference		
Complex	Reference	PBE	PBE0	LC-ωPBE
$(H_2O)_2$	4.98	0.12	−0.01	−0.56
$(H_3O^+)(H_2O)$	33.74	3.29	2.52	1.66
$(H_2O)(NH_3)$	6.41	0.57	0.26	−0.42
$(NH_3)_2$	3.13	0.01	−0.16	−0.69
$(FH)(NH_3)$	12.45	1.84	1.21	0.58
$(ClH)(NH_3)$	8.34	2.50	1.57	−0.14
$(HF)_2$	4.57	0.29	0.13	−0.44
$(HCl)_2$	2.01	0.07	−0.23	−0.81
(CO)(HF)	1.69	−0.07	−0.09	−0.48
(OC)(HF)	3.53	1.05	0.52	−0.06
ME		0.97	0.57	−0.13
MAE		0.98	0.67	0.58
MAPE (%)		11.0	8.0	13.1

3.2.5 Hydrogen-bonded complexes

A test set of ten hydrogen-bonded complexes has been compiled in Ref. [108]. The reference geometries and dissociation energies were obtained at a high level of correlated wave function theory [108]. We use this set to assess the performance of LC-ωPBE in describing hydrogen bonds. We employed the aug-cc-pVQZ basis to optimize the geometries. Since this basis set is fairly large, we did not include basis set superposition error corrections in D_e values.

Table 3.5 shows that LC-ωPBE performs rather well for the dissociation energies of hydrogen-bonded complexes. LC-ωPBE is also accurate in predicting hydrogen

Table 3.6 : Errors in hydrogen bond lengths (r_e) of hydrogen-bonded complexes. The aug-cc-pVQZ basis set is used. All values are in Å.

		Deviation = Functional − Reference		
Complex	Reference	PBE	PBE0	LC-ωPBE
$(H_2O)_2$	1.954	−0.030	−0.024	0.003
$(H_3O^+)(H_2O)$	1.195	0.016	0.001	0.002
$(H_2O)(NH_3)$	1.978	−0.059	−0.041	−0.013
$(NH_3)_2$	2.302	−0.053	−0.034	0.032
$(FH)(NH_3)$	1.697	−0.070	−0.051	−0.049
$(ClH)(NH_3)$	1.793	−0.196	−0.153	−0.057
$(HF)_2$	1.823	−0.037	−0.025	0.000
$(HCl)_2$	2.559	−0.122	−0.067	0.070
(CO)(HF)	2.072	−0.001	−0.001	0.074
(OC)(HF)	2.081	−0.111	−0.069	−0.035
ME		−0.066	−0.046	0.003
MAE		0.070	0.047	0.034
MAPE (%)		3.5	2.4	1.7

bond lengths, as shown in Table 3.6. LC-ωPBE clearly outperforms both PBE and PBE0 in the description of hydrogen-bonded complexes. Note that LC-ωPBE has very small mean errors (ME) for both dissociation energies (Table 3.5) and hydrogen bond lengths (Table 3.6).

3.3 Discussion: long-range corrected vs. global hybrid functionals

In LC-ωPBE the admixture of HF exchange is governed by the range separation parameter ω that we keep fixed at 0.4 bohr^{-1}. The actual effective percentage of

HF-type exchange depends on the size of the system to some degree. For instance, as will be shown in Chapter 4, more HF exchange is included for atomic anions, which are diffuse, than for cations, which are more compact. For some small cations, the percentage of HF exchange in LC-ωPBE seems to be insufficient. On the other hand, LC-ωPBE seems to include too much HF exchange for some larger molecules. Presumably, the performance of LC-ωPBE could be improved by making ω dependent on the system size. This, however, may lead to size-inconsistency. Alternatively, ω could be made a function of spatial coordinates, but this may render the functional computationally intractable. For the time being, we recommend to use $\omega = 0.4$ bohr^{-1}, which works well in many cases. LC-ωPBE with $\omega = 0.4$ bohr^{-1} is at least as good as PBE0 for most equilibrium properties of molecules, and is clearly better than PBE0 for many non-equilibrium properties. The range-separated exchange mixing used in LC-ωPBE appears to be a considerably more advantageous way to admix a portion of HF exchange, as compared to the conventional global hybrid scheme. A global hybrid with less than 100% of HF exchange does not satisfy any universal constraints beyond those satisfied by the underlying semi-local functional. In contrast, the long-range correction scheme used in LC-ωPBE recovers the exact asymptote of the exchange potential in molecules, which is expected to improve the description of the density tail regions.

For the long-range part of the exchange-correlation hole density around an electron, LC-ωPBE combines full HF exchange with (typically short-ranged) semi-local

PBE correlation. For compact systems of integer electron number, this choice is very plausible. For inhomogeneous solid metals, however, where the most long-ranged parts of the exact exchange and correlation holes are known to cancel [118], it would be less well justified.

Chapter 4

Tests for fractionally-charged systems

As we have shown above, semi-local and hybrid functionals can be quite accurate for equilibrium thermochemistry. A set of atomization energies is often used as a measure of accuracy. Atomization energies are normally computed with respect to separated neutral atoms. It is not widely realized that some binding energy curves or energy surfaces can show much bigger errors, because semi-local approximations can dissociate a neutral molecule XY (Y$\neq$X), to fragments $\mathrm{X}^{+q}\cdots\mathrm{Y}^{-q}$ with spurious fractional charge $q > 0$, and with an energy below that of $\mathrm{X}^{0}\cdots\mathrm{Y}^{0}$. For example, in LSDA, NaCl can dissociate to $\mathrm{Na}^{+0.4}\cdots\mathrm{Cl}^{-0.4}$ with an energy lowering of about 25 kcal/mol relative to $\mathrm{Na}^{0}\cdots\mathrm{Cl}^{0}$. A similar effect will occur in a polyatomic molecule built in part from atoms X and Y.

From the simplest perspective, the spurious fractional-charge dissociation arises from the self-interaction error inherent to all the semi-local functionals [34]. As we will show here, however, for a correct dissociation it is not enough to make the functionals exact for all one-electron densities. More importantly, one must ensure that the energy of an open system with fractional electron number N has a realistic linear variation [33] with N between any two integers $M-1$ and M.

In this chapter, we study the performance of various density functionals as well as HF theory in description of the properties of fractionally-charged systems. By plotting the ground state energies E for fractional N, we directly quantify many-electron SIE of these methods.

4.1 Methodology and implementation

In the majority of molecular Kohn–Sham codes, in systems with integer net number of electrons, orbitals are allowed to have only integer occupations. This approach works well if no symmetry restrictions are applied to the electron density, e.g. the total density in atoms is not required to be spherical. To obtain proper dissociation limits, spin-densities are allowed to be unequal even if the dissociating molecule is closed-shell. Such an approach may not be theoretically perfect, but it is practical and well-suited [109] to the available approximations for E_{xc}.

In this chapter we consider the direct extension of the Kohn–Sham formalism to systems with non-integer total electron number. We occupy orbitals according to the *aufbau* principle. Only the HO spin-orbital is allowed to be fractionally occupied, as prescribed by Janak's theorems [4]. Since we do not require the electron density in atoms to be spherical, a fractionally occupied HO spin-orbital ends up being non-degenerate in all cases we have studied. As we show below, such a technique for fractionally charged atoms is consistent with dissociation limits of diatomics predicted by typical molecular codes.

Hartree–Fock calculations with fractional occupations are performed using the formalism of Refs. [32] and [37].

We note that all our results have been obtained with nucleus-centered finite Gaussian basis sets. Predictions made within this "model chemistry" may in some cases substantially differ from the complete basis set limit. Implications of using finite atom-centered basis sets will be particularly evident in the discussion of the results for anions.

We find that all semi-local xc functionals give qualitatively very similar results for systems with fractional electron number. Therefore, we will show only PBE results in most cases.

4.2 Varying the electron number in an atom

Fig. 4.1 shows the ground state energy of the C atom as a function of the electron number N. The exact straight lines are obtained using the experimental ionization potential (IP) and electron affinity (EA) of the C atom. The exact derivative dE/dN is equal to –IP for $5 < N \leq 6$ and to –EA for $6 < N \leq 7$ (see Fig. 4.2). Early plots of these types, for the H atom in the local spin density approximation, can be found in Fig. 5 of Ref. [34].

The PBE curve in Fig. 4.1 has almost quadratic shape and the derivative discontinuity at $N = 6$ is almost but not completely missing. A very small discontinuity that is seen in the plot of $\varepsilon_{\mathrm{HO}}$ for PBE in Fig. 4.2 is due to the spin-dependence in the PBE xc functional and to the fact that the calculations are spin-unrestricted. In PBE0, the discontinuity at $N = 6$ is widened (Fig. 4.2) but is still only about a third of the exact one. PBE and PBE0 exhibit large negative deviations from the exact linear curves for non-integer N. As can be seen from Fig. 4.1, this leads to instability of the C$^-$ anion. PBE predicts that C$^-$ disintegrates into C$^{-0.7}$ and 0.3 of a free electron. PBE0 does not improve much upon PBE. Instabilities of anions in approximate functionals are indicated by positive values of $\varepsilon_{\mathrm{HO}}$ [110]. Note that positive $\varepsilon_{\mathrm{HO}}$ are artifacts of using finite atom-centered basis sets, which confine the electron

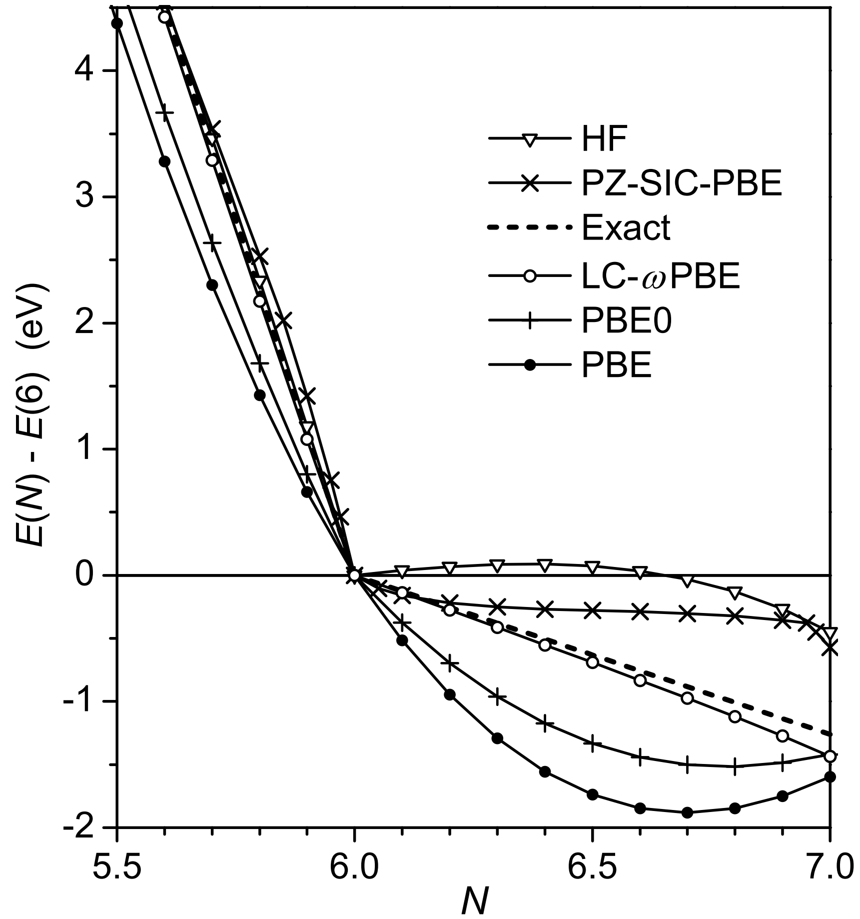

Figure 4.1 : Total energy (eV) of the C atom as a function of the electron number N. The energy is zeroed out at $N = 6$. The aug-cc-pV5Z basis set is used in all calculations except PZ-SIC, where the 6-311+G($3df$) basis set is used. The “exact” lines are obtained from the experimental IP and EA.

near the nucleus [110]. If we were to do a PBE calculation in the complete basis set, we would find that a fraction of an electron (0.3 in the case of C^-) leaves the anion and goes to the bottom of the free-electron continuum and for the combined system $\varepsilon_{\text{HO}} \to 0_+$. It is interesting to note, that despite such instabilities, PBE happens to predict rather accurate EAs, if calculated as differences in energies between a neutral atom and its anion in a limited basis set (as shown in Section 3.1.3).

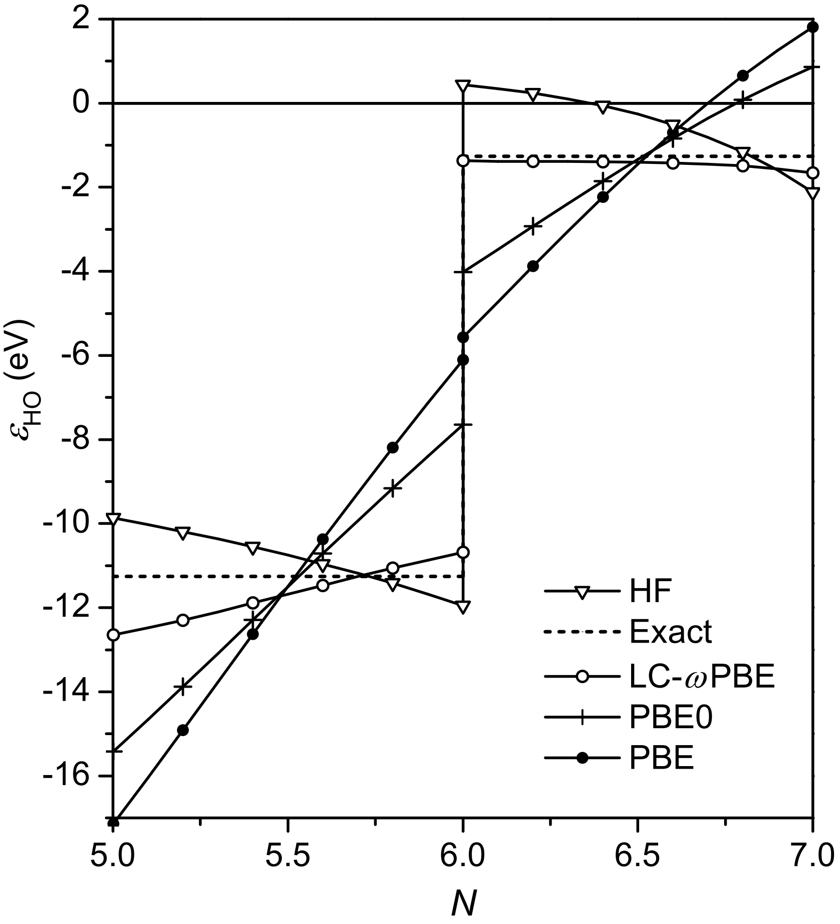

Figure 4.2 : Highest occupied orbital energy ε_{HO} (eV) of the C atom as a function of the electron number N. The aug-cc-pV5Z basis set is used. “Exact” ε_{HO} are the exact –IP and –EA. Note that ε_{HO} crosses zero at $N = 6.70$ in PBE and at $N = 6.78$ in PBE0.

As Fig. 4.1 shows, Hartree–Fock theory deviates from linearity in the direction opposite to PBE: HF yields a downward curved dependence of E vs. N and overestimates the derivative discontinuity at $N = 6$ (see Fig. 4.2).

LC-ωPBE gives rather accurate total energies for the C atom and its ions and predicts almost linear dependence of E vs. N, particularly for $6 < N < 7$. The size of the derivative discontinuity at $N = 6$ in LC-ωPBE is very close to the exact one (see Fig. 4.2). The C^- anion in LC-ωPBE is bound and stable. Tests for other atomic anions show that if an anion is experimentally stable, LC-ωPBE not only predicts it to be bound ($\varepsilon_{\mathrm{HO}} < 0$), but also gives a good estimate for the EA.

The PZ-SIC-PBE curves in Fig. 4.1 deviate from linearity in a rather unexpected way. We have found that PZ-SIC-PBE yields S-like curves for the N dependence of the ground state energies of atoms, with the largest curvatures near integer N. For instance, the energy dependence for the C atom is upward curved for $6 < N < 6.5$ and downward curved for $6.5 < N < 7$. Fig. 4.3 shows the highest diagonal Lagrange multiplier $\{\max(\varepsilon_{ii})\}$ compared to the highest eigenvalue of the Lagrange multipliers matrix $\{\max(\mathrm{eig}[\varepsilon_{ij}])\}$ as a function of N. We find that numerical differentiation of the PZ-SIC-PBE energy curve in Fig. 4.1 yields the derivatives exactly equal to $\max(\varepsilon_{ii})$. Thus, diagonal Lagrange multipliers ε_{ii} are the correct orbital energies in the sense of Eq. (1.6). Eigenvalues of the Lagrange multipliers matrix do not seem to have any physical meaning. The only reason why $\max(\mathrm{eig}[\varepsilon_{ij}])$ is often used as effective $\varepsilon_{\mathrm{HO}}$ is that the highest eigenvalue happens to be closer to the exact

$\varepsilon_{\mathrm{HO}}$ for integer N (see Fig. 4.3). Note the kinks in the plots of both $\max(\varepsilon_{ii})$ and $\max(\mathrm{eig}[\varepsilon_{ij}])$ at $N = 5.85$ and $N = 6.95$ in Fig. 4.3. These kinks appear when the shape of the self-consistent orbitals changes abruptly. For $5 < N \leq 5.85$, two α-spin valence electrons occupy sp-hybrid orbitals and a fraction of an electron goes to an unhybridized p orbital. For $5.85 < N \leq 6$, the valence α-spin electrons occupy three almost equivalent sp^2-hybrid orbitals. For $6 < N \leq 6.95$, three valence α

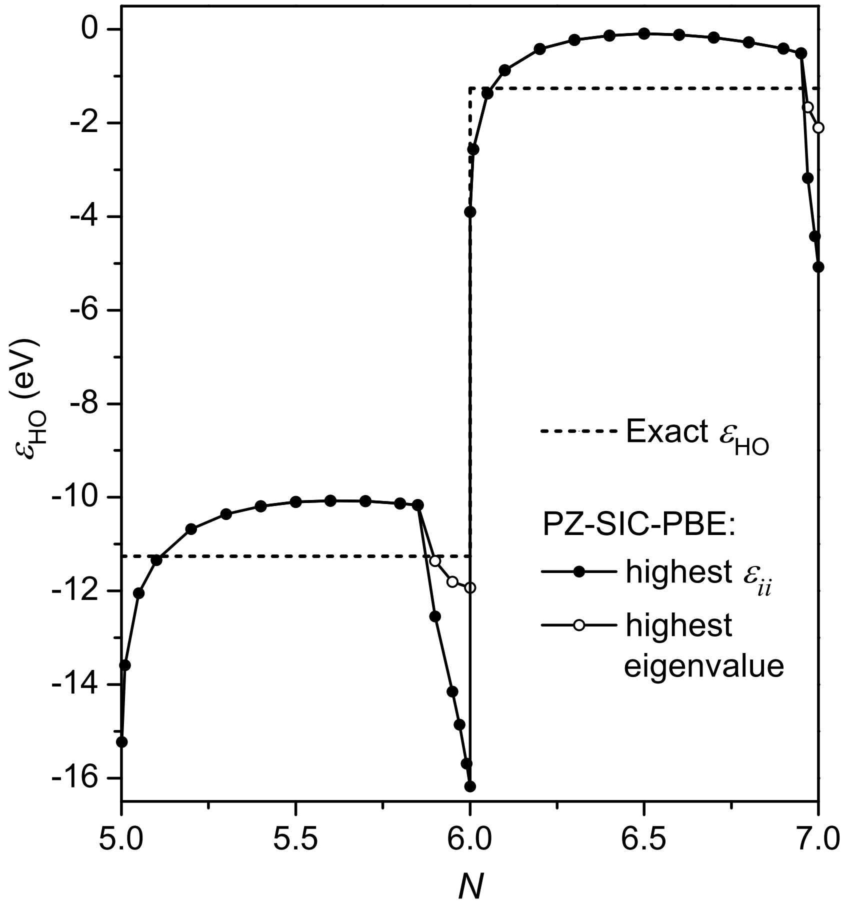

Figure 4.3 : Highest diagonal Lagrange multiplier ε_{ii} compared to the highest eigenvalue of the Lagrange multipliers matrix in PZ-SIC-PBE for the C atom as a function of the electron number N. All numbers are in eV. The 6-311+G($3df$) basis set is used. "Exact" $\varepsilon_{\mathrm{HO}}$ are the exact –IP and –EA.

electrons occupy sp^2-hybrid orbitals and a fraction of an electron goes to a p orbital. For $6.95 < N \leq 7$, the valence α electrons occupy four sp^3-hybrid orbitals. When a fraction of an electron occupies an unhybridized p orbital ($5 < N \leq 5.85$ and $6 < N \leq 6.95$), off-diagonal Lagrange multipliers corresponding to that orbital are nearly zero and therefore $\max(\varepsilon_{ii}) \approx \max(\mathrm{eig}[\varepsilon_{ij}])$, as can be seen in Fig. 4.3. We have tested PZ-SIC with a few other semi-local DFAs and found results qualitatively very similar to PZ-SIC-PBE.

4.3 Dissociation of the NaCl molecule

At interatomic separations R not very far from equilibrium, the NaCl molecule is an ionic pair. But in the dissociation limit, when the two nuclei are infinitely separated, we should obtain the neutral Na and Cl atoms since $\mathrm{IP_{Na}} > \mathrm{EA_{Cl}}$. At a certain critical separation R_c, a sudden charge transfer occurs [33]:

$$\mathrm{Na^+ + Cl^- \rightleftarrows Na + Cl}.$$

In other words, the ground state of the system is the neutral atom state for $R > R_c$, and the singly charged ionic state for $R < R_c$. At the critical separation, the electrostatic attraction of the ions balances out the difference in energy between the ions and neutrals: $-e^2/R_c + \mathrm{IP_{Na}} - \mathrm{EA_{Cl}} = 0$. Thus we find [33]

$$R_c = e^2/(\mathrm{IP_{Na}} - \mathrm{EA_{Cl}}). \tag{4.1}$$

In the derivation of Eq. (4.1) we assumed that all types of interatomic interactions except electrostatic are negligible at R_c. Using the experimental [77] $\mathrm{IP_{Na}}$ and $\mathrm{EA_{Cl}}$

Table 4.1 : Predicted dissociation limits of NaCl. The 6-311+G(3*df*) basis set is used.

	Charge	Δ (kcal/mol)[a]
HF	0.0	0.0
PBE	0.37	−20.0
PBE0	0.31	−9.6
LC-ωPBE	0.0	0.0

[a] $\Delta = E(\text{predicted dissoc. limit}) - E(\text{Na}) - E(\text{Cl})$.

in Eq. (4.1), we obtain (after the proper unit conversion) $R_c \approx 9.4$ Å.

As we mentioned in the Introduction, semi-local functionals tend to assign too low relative energies for non-integer electron numbers. As a result, common approximate functionals erroneously predict NaCl to dissociate into fractionally-charged species [111, 39]. To find the predicted dissociation limits, we carried out spin-unrestricted energy minimizations with the 6-311+G(3*df*) basis set at a very large internuclear separation of 1000 Å and analyzed the Mulliken charges on the atoms. The results are summarized in Table 4.1. PBE minimizes the energy at the configuration $\text{Na}^{+0.37}$ $\text{Cl}^{-0.37}$, which is 20 kcal/mol lower in energy than the neutral atoms. PBE0 hybrid is only a little improvement over PBE.

HF predicts the correct dissociation limit, but R_c is significantly underestimated (5.7 Å) because HF overestimates the $(\text{IP}_{\text{Na}} - \text{EA}_{\text{Cl}})$ difference. LC-ωPBE predicts $(\text{IP}_{\text{Na}} - \text{EA}_{\text{Cl}})$ very accurately, and as a result, yields a very precise R_c (see Fig. 4.4). LC-ωPBE finds two isoenergetic electronic states at $R \approx 9$ Å. Analysis of Mulliken charges shows that one of them corresponds to the neutral atoms, the other to the singly-charged ions. Thus, LC-ωPBE provides an excellent description of the NaCl dissociation, both in qualitative and quantitative sense (Fig. 4.4). In HF and LC-ωPBE, the dissociation curve for $3\text{Å} < R < R_c$ closely follows the formula $(\text{IP}_{\text{Na}} - \text{EA}_{\text{Cl}}) - e^2/R$, which is the expected correct behavior.

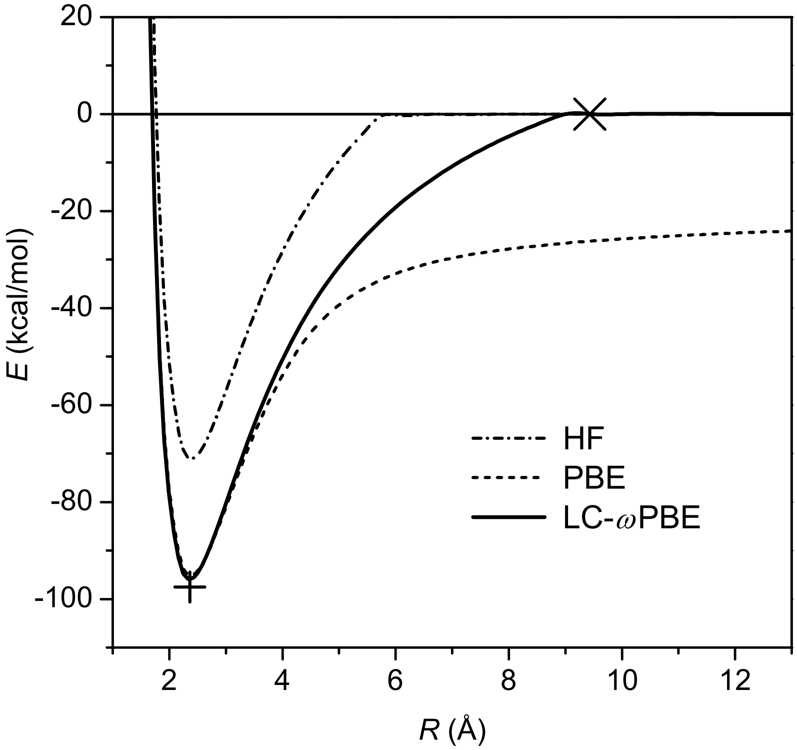

Figure 4.4 : NaCl dissociation curves obtained with the 6-311+G(3*df*) basis set. Only lowest-energy spin-unrestricted solutions are shown. Zero level is set to $E(\text{Na}) + E(\text{Cl})$ in each method. Experimental equilibrium bond length and atomization energy is marked by symbol "+". Symbol "×" marks the expected critical distance $R_c = 9.4$ Å.

4.4 Dissociation of the LiF molecule

Just like in the case of NaCl, the LiF molecule must dissociate into neutral atoms, since $\mathrm{IP}_{\mathrm{Li}} > \mathrm{EA}_{\mathrm{F}}$. In Fig. 4.5 we study possible dissociation limits for LiF using purely atomic calculations. We plot $\Delta E = E(\mathrm{Li}^{+q}) + E(\mathrm{F}^{-q}) - E(\mathrm{Li}) - E(\mathrm{F})$ as a function of q. The minimum on each curve shows the dissociation limit predicted by that particular method. HF, PZ-SIC-PBE and LC-ωPBE all correctly yield the neutral atoms limit, whereas PBE and PBE0 predict fractionally charged dissociation

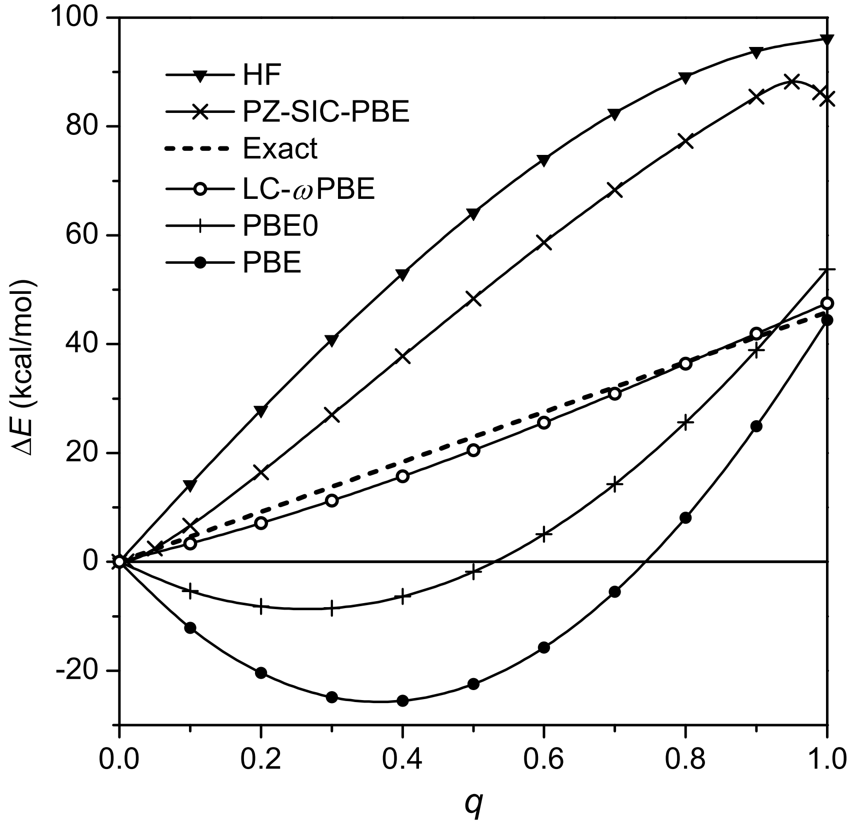

Figure 4.5 : Energy difference $\Delta E = E(\mathrm{Li}^{+q}) + E(\mathrm{F}^{-q}) - E(\mathrm{Li}) - E(\mathrm{F})$ in kcal/mol as a function of q. This represents the dissociation limit of LiF. The aug-cc-pV5Z basis set is used in all calculations except PZ-SIC, where the 6-311+G(3*df*) basis set is used. The "exact" curve is $q(\mathrm{IP}_{\mathrm{Li}} - \mathrm{EA}_{\mathrm{F}})$ with the experimental IP and EA.

limits. In PBE, LiF dissociates into $\mathrm{Li}^{+0.4}\cdots\mathrm{F}^{-0.4}$, and in PBE0, into $\mathrm{Li}^{+0.3}\cdots\mathrm{F}^{-0.3}$. The point $q = 1$ in Fig. 4.5 represents $\mathrm{IP}_{\mathrm{Li}} - \mathrm{EA}_{\mathrm{F}}$. This difference is well reproduced by PBE, PBE0 and LC-ωPBE, which are known to perform rather well for equilibrium thermochemistry. Remarkably, LC-ωPBE reproduces not only $q = 0$ and $q = 1$ points, but also predicts a nearly exact linear dependence for $0 \leq q \leq 1$.

To find at which R_c the charge transfer $\mathrm{Li}^+ + \mathrm{F}^- \rightarrow \mathrm{Li} + \mathrm{F}$ is expected occur, we plugged the experimental [77] $\mathrm{IP}_{\mathrm{Li}}$ and EA_{F} into Eq. (4.1). This gives $R_c \approx 7.2$ Å.

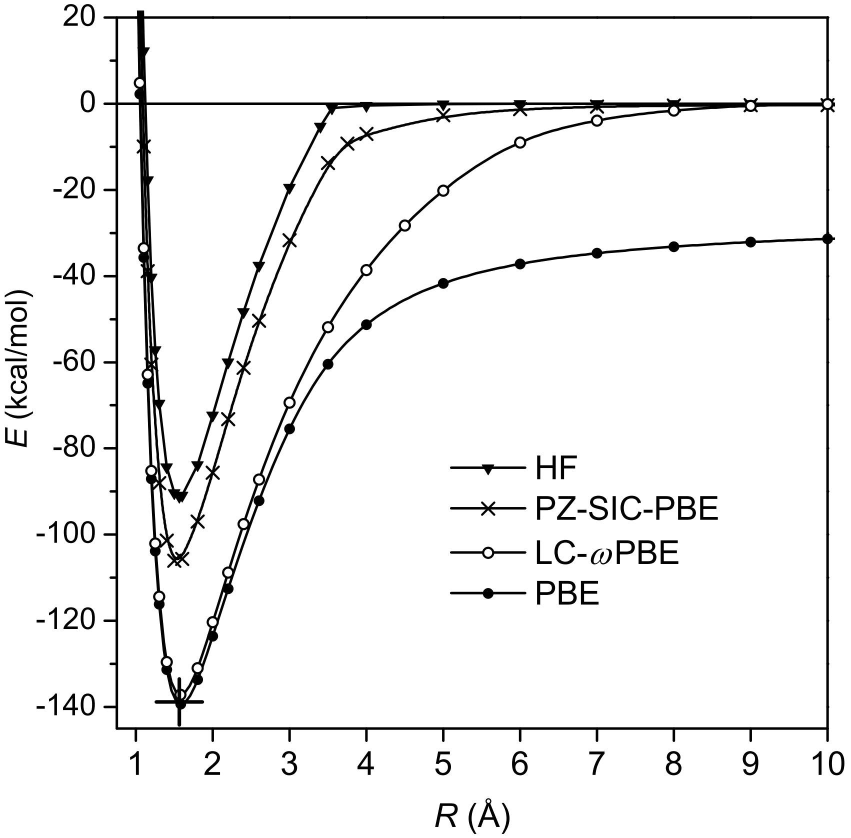

Figure 4.6 : LiF dissociation curves with the zero energy level set to $E(\mathrm{Li}) + E(\mathrm{F})$ in each method. Only the lowest-energy spin-unrestricted solutions are shown. The 6-311+G($3df$) basis set is used. Experimental equilibrium bond length and atomization energy is marked by symbol "+".

Note that Eq. (4.1) may be inaccurate if the predicted R_c is small and other types of interatomic interactions, besides electrostatic, intervene.

Fig. 4.6 shows the computed dissociation curves of LiF and Fig. 4.7 shows how Mulliken charges change with increase in R. In Hartree–Fock, the abrupt charge transfer occurs at $R = 3.5$ Å, which is much shorter than expected. In PZ-SIC-PBE, around $R = 3.5$ Å Mulliken charge drops from 0.90 to 0.26 and then decreases slowly towards zero. In LC-ωPBE, the charge transfer occurs gradually: Mulliken charge smoothly decreases from 0.92 at $R = 5$ Å to nearly zero at $R = 11$ Å. This

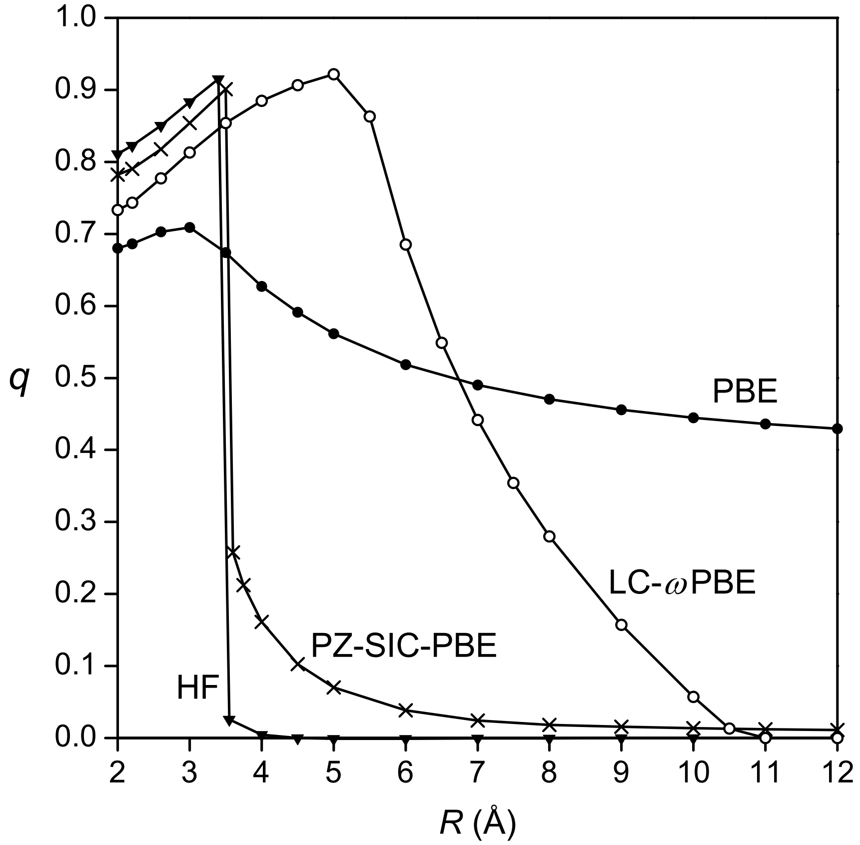

Figure 4.7 : Mulliken charge on the Li atom as a function of the internuclear distance in LiF. The 6-311+G($3df$) basis set is used.

result is quite different from the NaCl case studied in the previous section. In NaCl, LC-ωPBE predicts that charge drops abruptly from $q \approx 1$ to $q = 0$ at $R_c \approx 9$ Å. The qualitative difference between LiF and NaCl dissociation curves in LC-ωPBE stems from the use of a fixed range separation parameter $\omega = 0.4$ bohr^{-1}, which governs the admixture of the long-range HF exchange. As was already mentioned in Section 3.3, the larger the spatial extent of the system is, the more HF exchange is included. R_c in NaCl is larger than in LiF. Also, Na and Cl atoms themselves are larger than Li and F atoms. Therefore, description of the NaCl dissociation in LC-ωPBE is more Hartree–Fock-like. At any rate, among all the studied methods, LC-ωPBE is the only one that accurately predicts the atomization energy of LiF, its equilibrium bond length, and the correct dissociation limit at the same time.

4.5 Dissociation of symmetric radical cations

Proper description of 2-center 3-electron bonds in symmetric radical cations A_2^+ has proven quite challenging for many theoretical methods. In this section, we study four such systems with A = H, He, Ne, and Ar. Failures of semi-local functionals to describe symmetric radical cations are well documented [29, 35, 36, 40, 112, 113]. For such systems, semi-local DFAs predict too long bond lengths and too low energies for the equilibrium structures. We have optimized the geometries of the four radical cations using the aug-cc-pVQZ basis set. As Table 4.2 shows, equilibrium bond lengths are considerably improved in hybrid functionals, as compared to pure

Table 4.2 : Dissociation of symmetric radical cations. The aug-cc-pVQZ basis set is used.

	H_2^+	He_2^+	Ne_2^+	Ar_2^+	ME	MAE
	Equilibrium bond length r_e (Å)					
Reference [a]	1.057	1.081	1.765	2.423		
HF	1.057	1.076	1.855	2.436	0.024	0.027
PBE	1.131	1.176	1.909	2.557	0.112	0.112
PBE0	1.106	1.132	1.802	2.479	0.049	0.049
LC-ωPBE	1.100	1.133	1.779	2.423	0.027	0.027
	Dissociation energy D_e (kcal/mol)[b]					
Reference [a]	64.4	57.0	32.2	30.8		
HF	64.4	45.6	3.8	15.0	−13.9	13.9
PBE	69.1	78.0	73.1	50.2	21.5	21.5
PBE0	67.9	70.6	54.9	42.3	12.8	12.8
LC-ωPBE	67.7	71.9	55.9	35.7	11.7	11.7
	Energy difference of the two dissociation limits, Δ (kcal/mol)[c]					
HF	0.0	14.7	35.8	16.3	16.7	16.7
PBE	−66.7	−95.3	−97.0	−62.7	−80.5	80.5
PBE0	−49.2	−67.7	−63.6	−43.1	−55.9	55.9
LC-ωPBE	−15.2	−34.8	−35.0	−9.4	−23.6	23.6

[a] Ref. [114] for H_2^+, Ref. [115] for He_2^+, Ref. [116] for Ne_2^+, and Ref. [117] for Ar_2^+.

[b] $D_e = E(\mathrm{A}) + E(\mathrm{A}^+) - E(\mathrm{A}_2^+)_{eq}$.

[c] $\Delta = 2E(\mathrm{A}^{1/2+}) - E(\mathrm{A}) - E(\mathrm{A}^+)$. Δ must be zero in the exact theory.

PBE. For the dissociation energies calculated as $D_e = E(\mathrm{A}) + E(\mathrm{A}^+) - E(\mathrm{A}_2^+)_{eq.}$, hybrid functionals give sensible estimates, although overestimated as compared to experiment (see Table 4.2). However, D_e computed in such a way does not reflect the real dissociation profile, since DFAs incorrectly describe the dissociation limit, as discussed below.

The dissociation curve of the one-electron molecule H_2^+ is one of the most dramatic examples of the failure of common density functionals. Common DFAs predict that the electron splits itself equally between two infinitely separated fragments and such a state is much lower in energy then the H atom [29]. Similar problems arise for all symmetric radical cations A_2^+. In the exact theory, at the dissociation limit of A_2^+, the state $\mathrm{A}(a)\cdots\mathrm{A}(b)^+$ is degenerate with its nuclear permutation $\mathrm{A}(a)^+\cdots\mathrm{A}(b)$. Any linear combination of these two states is also a ground state [29], including the delocalized state $\mathrm{A}^{1/2+}\cdots\mathrm{A}^{1/2+}$. Neither HF nor semi-local DFT are able to reproduce this degeneracy. HF predicts a lower energy for a dissociation limit with localized charge (except for the one-electron system H_2^+, for which HF is exact). Common DFAs, on the other hand, predict a much lower energy for the state with delocalized charge.

The value of Δ in Table 4.2 shows the difference in energy of two possible dissociation limits. To evaluate Δ, we find the energy of the system with very large internuclear separation (e.g. 1000 Å). In the exact theory, Δ must be zero, but it is very far from zero for typical density functionals. Δ serves as an indicator of non-linearity of the energy with respect to non-integer electron number. As Table 4.2 shows, Δ is on average closer to zero in LC-ωPBE than in other tested functionals.

Fig. 4.8 shows dissociation curves of Ar_2^+ as predicted by various methods. PBE and PBE0 curves in Fig. 4.8 exhibit a spurious maximum. This maximum is attributed to the SIE in these functionals: at distances R far from equilibrium, two

$Ar^{1/2+}$ fragments erroneously repel one another, introducing a positive Coulombic term of $e^2/(4R)$ to the energy. As a result, for large R, the PBE curve has the shape of $\Delta + e^2/(4R)$. At intermediate R, the PBE curve passes through an artificial transition state. In PBE0, only a quarter of the SIE is compensated by HF exchange. Thus, for large R, the PBE0 curve has the shape $\Delta + 3e^2/(16R)$; the maximum is still present but less distinct. In LC-ωPBE, as well as in HF, the spurious Coulomb repulsion of the two fragments of the same electron is completely compensated by the corresponding long-range HF exchange counterpart. Hence, HF and LC-ωPBE

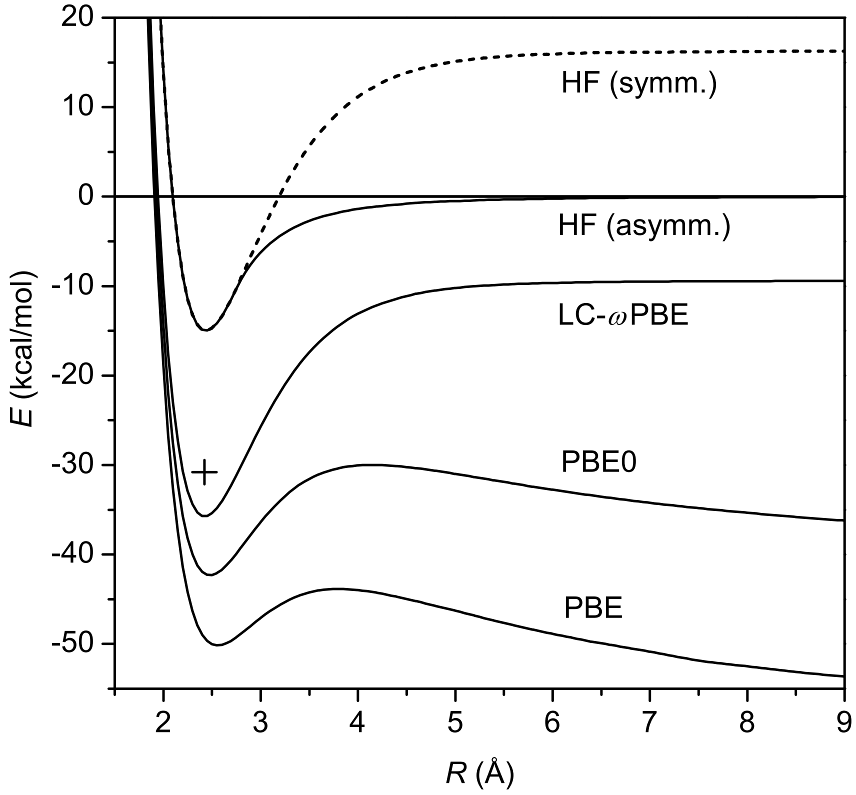

Figure 4.8 : Ar_2^+ dissociation curves obtained with the aug-cc-pVQZ basis set. Zero level is set to $E(Ar) + E(Ar^+)$ in each method. Experimental equilibrium bond length and dissociation energy is marked by symbol "+".

curves in Fig. 4.8 have no maxima and level off at a constant value for $R > 6$ Å. For HF, it is possible to obtain two dissociation curves. The upper (dashed) curve in Fig. 4.8 is obtained by applying the symmetry restriction to the wave function, and corresponds to dissociation into two $\mathrm{Ar}^{1/2+}$ fragments.

Below we study the dissociation limit of Ne_2^+ using atomic calculations with fractional charges. As Fig. 4.9 shows, none of the studied methods is able to reproduce the degeneracy of the dissociation limit of Ne_2^+. PBE, PBE0, and LC-ωPBE assign

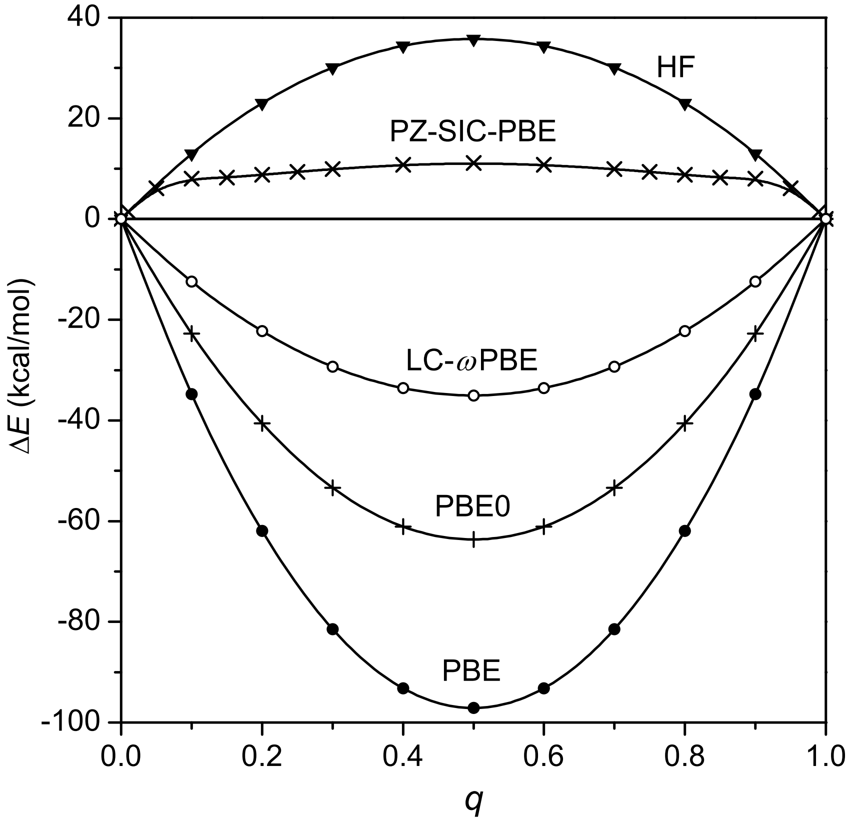

Figure 4.9 : Energy difference $\Delta E = E(\mathrm{Ne}^{+q}) + E(\mathrm{Ne}^{+(1-q)}) - E(\mathrm{Ne}) - E(\mathrm{Ne}^{+})$ in kcal/mol as a function of q. This represents the dissociation limit of Ne_2^+. The aug-cc-pV5Z basis set is used in all calculations except PZ-SIC, where the 6-311+G(3df) basis set is used. The exact result is $\Delta E = 0$ for $0 \le q \le 1$.

too low energy to the symmetric state $\mathrm{Ne}^{+1/2}\cdots\mathrm{Ne}^{+1/2}$, while HF and PZ-SIC-PBE predict the broken-symmetry state $\mathrm{Ne}\cdots\mathrm{Ne}^{+}$ to be lower in energy. The midpoint error in Fig. 4.9 is the smallest (in the absolute value) for PZ-SIC-PBE. Note that most of the curves in Fig. 4.9 have parabolic shape, except for the PZ-SIC-PBE curve which is quite flat. PZ-SIC-PBE yields an S-like curve for the energy of Ne^{+q} as a function of q, so when this dependence is added to its inverse ($\mathrm{Ne}^{+(1-q)}$), there is a

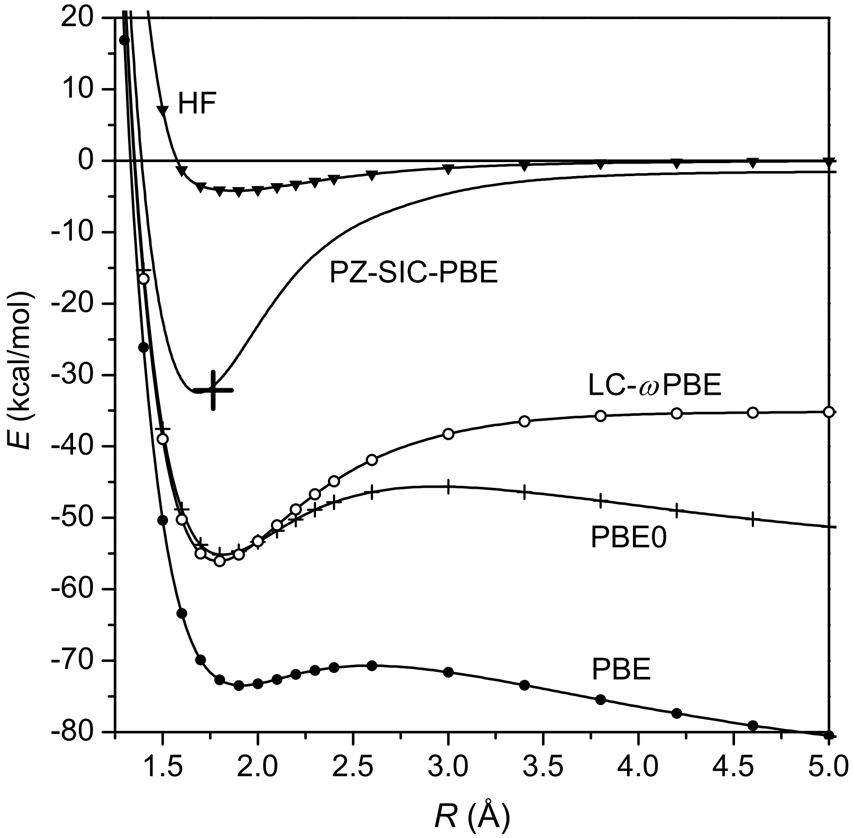

Figure 4.10 : Ne_2^+ dissociation curves with the zero energy level set to $E(\mathrm{Ne}) + E(\mathrm{Ne}^+)$ in each method. The 6-311+G($3df$) basis set is used. Only the lowest-energy solutions are shown. HF and PZ-SIC-PBE predict the dissociation limit to be $\mathrm{Ne}\cdots\mathrm{Ne}^{+}$, whereas all other methods predict $\mathrm{Ne}^{+1/2}\cdots\mathrm{Ne}^{+1/2}$ (see Fig. 4.9). Experimental equilibrium bond length and dissociation energy is marked by the bold symbol "+".

partial cancellation of errors leading to the plot we see in Fig. 4.9.

Fig. 4.10 shows the computed dissociation curves for Ne_2^+. The PBE and PBE0 curves in Fig. 4.10 display a spurious energy barrier, attributed [35, 36] to the erroneous electrostatic repulsion of the $Ne^{+1/2}$ fragments at large R. The LC-ωPBE curve is quite close to the PBE0 curve for distances R close to equilibrium, but LC-ωPBE improves upon PBE0 for larger R by eliminating the long-range SIE and hence removing the spurious maximum. HF yields very small dissociation energy for Ne_2^+. The dissociation energy predicted by PZ-SIC-PBE is the closest to experiment [116]. Overall, the PZ-SIC-PBE curve in Fig. 4.10 is the most accurate one, although the equilibrium bond length is somewhat too short in PZ-SIC-PBE. Perdew–Zunger SIC is known to improve dissociation curves of symmetric radical cations [35, 36, 40].

Comparing Figures 4.8 and 4.10 we see that LC-ωPBE performs better for Ar_2^+ than for Ne_2^+. The Ar atom is larger than the Ne atom (the same can be said about their cations), thus LC-ωPBE includes more HF exchange into a calculation involving Ar, which benefits the Ar_2^+ dissociation curve.

4.6 The effect of scaling down the SIC

In the previous section, we showed that PZ-SIC-PBE works rather well for Ne_2^+ dissociation. Here we test if scaling down the PZ-SIC preserves this good performance.

Figure 4.11 shows the dissociation curves obtained with the scaled-down SIC using the scaling factor of Eq. (2.10). Figure 4.12 shows similar curves for the simplified scaling factor of Eq. (2.13). As can be seen from these plots, even a minor scaling down destroys the good PZ-SIC curve shapes. The equilibrium structure becomes too low in energy and spurious transition states appear on the dissociation curves. In the scaled-down SIC, the dissociation limit $\mathrm{Ne}^{+1/2}\cdots\mathrm{Ne}^{+1/2}$ is far from being degenerate with $\mathrm{Ne}\cdots\mathrm{Ne}^{+}$.

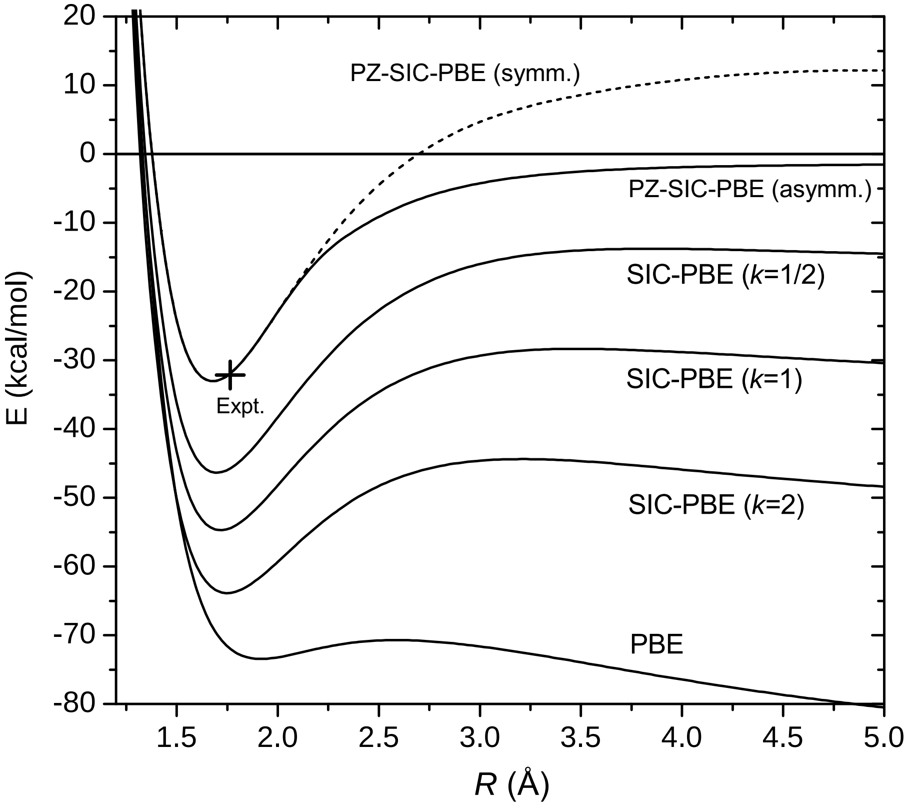

Figure 4.11 : Ne_2^+ dissociation curves calculated with a scaled-down self-interaction correction. The scaling factor of Eq. (2.10) is used. The zero energy level is set to $E(\mathrm{Ne}) + E(\mathrm{Ne}^+)$ in each method. The 6-311+G(3*df*) basis set is used. For PZ-SIC-PBE, two solutions can be found: asymmetric and symmetric. For other methods, the solutions are symmetric, i.e. the dissociation limit is $\mathrm{Ne}^{+1/2}\cdots\mathrm{Ne}^{+1/2}$. Experimental equilibrium bond length and dissociation energy is marked by the bold symbol "+".

As we mentioned in the last paragraph of Section 2.4.2, scaling down the PZ-SIC loses the exact asymptotic behavior of the exchange potential. As we show here, scaling down the SIC also deteriorates the performance for fractionally-charged many-electron systems. The scaled-down SIC is one-electron SIE-free, but not M-electron SIE-free for $M > 2$. When we scale down the self-interaction correction via

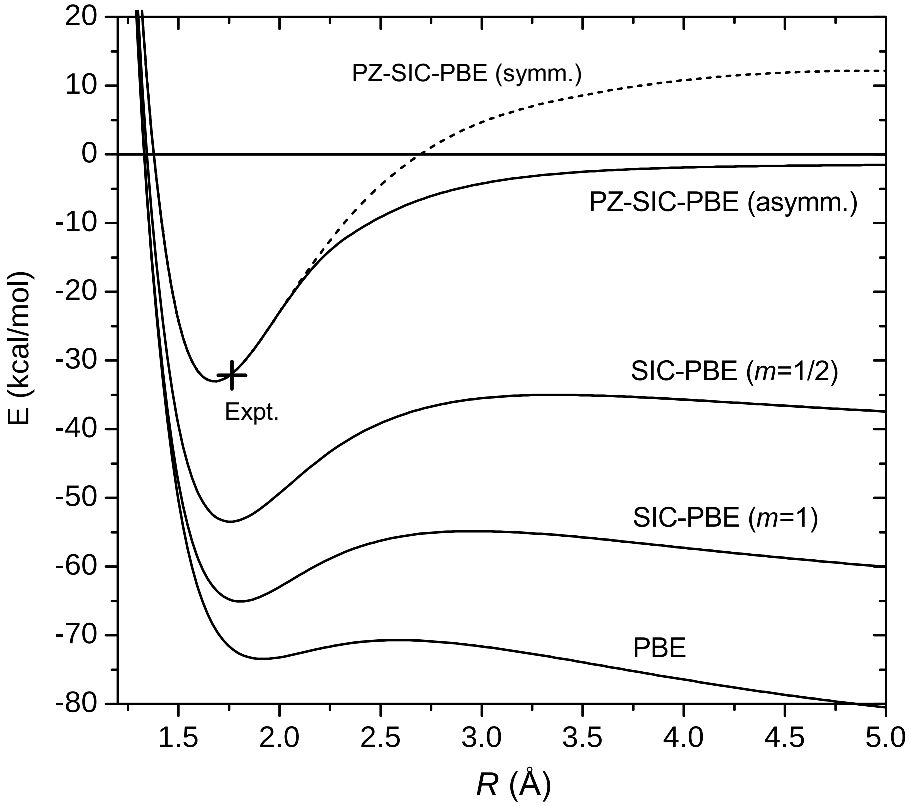

Figure 4.12 : Ne_2^+ dissociation curves calculated with a scaled-down self-interaction correction. The scaling factor of Eq. (2.13) is used. The zero energy level is set to $E(\mathrm{Ne}) + E(\mathrm{Ne}^+)$ in each method. The 6-311+G(3df) basis set is used. For PZ-SIC-PBE, two solutions can be found: asymmetric and symmetric. For other methods, the solutions are symmetric, i.e. the dissociation limit is $\mathrm{Ne}^{+1/2} \cdots \mathrm{Ne}^{+1/2}$. Experimental equilibrium bond length and dissociation energy is marked by the bold symbol "+".

Eq. (2.9), we improve the equilibrium properties and keep the functional exact for any one-electron density, but the resilient fractional-charge error returns.

Chapter 5

Conclusions

Self-interaction error has traditionally been defined as inexactness for one-electron systems. Most of the common approximate functionals are not one-electron SIE-free. This problem affects not only one-electron systems, it manifests itself in many-electron systems as well. Unfortunately, the SIE of a particular xc approximation is very difficult to quantify and correct in a many-electron system. SIE is often blamed for failures of common DFAs to describe charge transfer processes and transition states of chemical reactions.

The most widely known self-interaction correction was proposed by Perdew and Zunger in 1981. The PZ-SIC has not been systematically tested, mainly because it is nontrivial to implement. We implemented the PZ-SIC self-consistently and tested it in combination with a variety of xc functionals. We found that PZ-SIC impairs thermochemical accuracy of common approximate functionals (with the only exception of LSDA) and predicts too short equilibrium bond lengths. PZ-SIC often seems to overcorrect many-electron systems.

We devised a modified self-interaction correction, which is scaled down in many-electron regions. Compared to the original Perdew–Zunger SIC, the new SIC performs much better for thermochemistry and thermochemical kinetics and predicts equilibrium bond lengths much closer to experiment.

The SIE of semi-local functionals is particularly large in systems with non-integer average electron numbers, which causes such problems as instabilities of anions and spurious fractional charges on dissociated atoms. Studies of fractionally-charged systems led to a new definition of SIE for many-electron systems. A method is said to be "M-electron self-interaction-free" if its total energy has a realistic linear variation with electron number N between the integers M–1 and M. Both the original Perdew–Zunger self-interaction correction and our scaled-down version of it are one-electron self-interaction-free, but only the former is nearly many-electron self-interaction-free.

Inexactness of the asymptote of the exchange-correlation potential in common DFAs is regarded as a consequence of SIE. PZ-SIC recovers the exact asymptotic behavior of the xc potential, but this property is lost in the scaled-down SIC. The exact asymptote can be imposed in a hybrid functional by introducing a range-separation into the exchange component and replacing the long-range part of the approximate exchange by the exact (Hartree–Fock-like) exchange counterpart. This "long-range correction" works particularly well in combination with the short-range PBE exchange functional. This hybrid, denoted LC-ωPBE, performs remarkably well for a broad range of molecular properties, whether in equilibrium, transition state, or dissociation limit. It often surpasses in accuracy the well-established global hybrid PBE0. LC-ωPBE is not exactly one-electron SIE free, but it is nearly many-electron SIE-free in many cases.

Appendix A

Self-consistent implementation of the Perdew–Zunger SIC with Gaussian basis sets

We expand molecular orbitals $\{\varphi_i\}$ as linear combinations of Gaussian basis functions $\{\chi_\mu\}$:

$$\varphi_i(\mathbf{r}) = \sum_\mu C_{\mu i}\,\chi_\mu(\mathbf{r}). \tag{A.1}$$

The gradient of Eq. (2.7) can be converted to the new basis by applying the chain rule:

$$\begin{aligned} \frac{\partial E}{\partial C_{\mu i}} &= \int \frac{\partial E}{\partial \varphi_i(\mathbf{r})}\,\chi_\mu(\mathbf{r})\,d\mathbf{r} \\ &= 2(\mathbf{H}^i\mathbf{C})_{\mu i} - \sum_j (\mathbf{SC})_{\mu j}\Big\{(\mathbf{C}^\dagger\mathbf{H}^j\mathbf{C})_{ij} + (\mathbf{C}^\dagger\mathbf{H}^i\mathbf{C})_{ji}\Big\}, \end{aligned} \tag{A.2}$$

where $\mathbf{H}^i_{\mu\nu} = \langle\chi_\mu|H_i|\chi_\nu\rangle$ are the matrix elements of the H_i operator of Eq. (2.5) and $\mathbf{S}_{\mu\nu} = \langle\chi_\mu|\chi_\nu\rangle$ are the overlap matrix elements.

The SIC-DFT gradient of Eq. (A.2) has been implemented in a development version of the Gaussian program [119]. The energy minimization is performed using the Broyden–Fletcher–Goldfarb–Shanno (BFGS) variant of a quasi-Newton method [120]. Cubic interpolation is employed as a line search method. After each minimization cycle orbitals are re-orthogonalized using Löwdin's procedure:

$$\mathbf{C}' = \mathbf{C}\left(\mathbf{C}^\dagger\mathbf{SC}\right)^{-1/2}. \tag{A.3}$$

In the BFGS Hessian update method, a unit matrix is often used as an initial guess for the Hessian matrix. However, we found that convergence can be accelerated by starting from a diagonal Hessian with the diagonal elements calculated by an approximate formula

$$\frac{\partial^2 E}{\partial C_{\mu i}^2} = 2\mathbf{H}^i_{\mu\mu} - 2(\mathbf{C}^\dagger \mathbf{H}^i \mathbf{C})_{ii} - \sum_j (\mathbf{SC})_{\mu j} \Big\{ (\mathbf{H}^j \mathbf{C})_{\mu j} + \ (\mathbf{H}^i \mathbf{C})_{\mu j} \Big\} (1 + \delta_{ij}). \quad \text{(A.4)}$$

Eq. (A.4) is obtained from Eq. (A.2) under the assumption that matrix elements of the H_i operator (2.5) do not change upon variation of orbital coefficients $C_{\mu i}$.

The time needed for the optimization procedure to converge to a minimum strongly depends on the quality of the initial guess for the orbital coefficients. Applying a localization transformation to the canonical self-consistent Kohn–Sham orbitals provides a good estimate to the self-consistent SIC-DFT orbitals [41, 50]. The Boys' localization procedure [64], which minimizes the spatial extension of each orbital, proved to be the most appropriate. However, the Boys' method can be unstable for open-shell systems and molecules containing second row atoms. This problem can be cured by removing a subset of orbitals from the localization set and applying the transformation to the remaining orbitals only. In some particularly difficult cases we resorted to the Pipek–Mezey method [121], which shows no considerable convergence problems, but provides a somewhat worse guess. The Pipek–Mezey procedure minimizes the number of atoms over which an orbital is extended. Thus it is not suited for localizing orbitals located on a single atom such as lone pairs. For multiple bonds, the Pipek–Mezey procedure results in σ–π separation while the Boys' method gives a set of equivalent orbitals. For atoms, the initial guess was prepared by localizing core and valence orbitals separately.

Self-consistent SIC-DFT orbitals from different parent semi-local functionals look similar in the majority of cases. Hence, for a given molecule, self-consistent orbitals obtained with one functional can be used as a good initial guess in minimization of another SI-corrected functional.

We found that the SIC-DFT energy is more sensitive to the grid size than the regular Kohn–Sham DFT and small grids can even lead to convergence problems. Unpruned integration grids with at least 99 radial shells and at least 590 angular points per shell are used in all calculations.

Appendix B

Energy derivatives for the scaled-down SIC

In the scaled-down SIC of Eq. (2.9), the derivative of the total energy with respect to orbital variations under the constraint of orbital orthonormality is given by Eq. (2.7). If the scaling factor of Eq. (2.10) is used, then H_i in Eq. (2.7) is replaced by

$$\begin{aligned} H_i &= -\frac{1}{2}\nabla^2 + v(\mathbf{r}) + \int \frac{\rho(\mathbf{r}')}{|\mathbf{r}-\mathbf{r}'|}\,d\mathbf{r}' + v_{\rm xc}^{\rm DFA}\big([\rho_\alpha,\rho_\beta],\mathbf{r}\big) \\ & \quad -X_i^k\bigg(\int \frac{\rho_i(\mathbf{r}')}{|\mathbf{r}-\mathbf{r}'|}\,d\mathbf{r}' + v_{\rm xc}^{\rm DFA}\big([\rho_i,0],\mathbf{r}\big)\bigg) - \bigg(\frac{\tau^W}{\tau}\bigg)^k\Big(J[\rho_i] + E_{\rm xc}^{\rm DFA}[\rho_i,0]\Big) \\ & \quad -\sum_j \frac{\partial X_j^k}{\partial \rho(\mathbf{r})}\Big(J[\rho_j] + E_{\rm xc}^{\rm DFA}[\rho_j,0]\Big). \end{aligned} \tag{B.1}$$

The derivatives $\partial X_j^k/\partial\rho(\mathbf{r})$ in Eq. (B.1) account for variations in $(\tau^W/\tau)^k$. They are evaluated using the method of Neumann *et al.* [122], which is typically used for obtaining matrix elements of xc potentials of meta-GGA functionals.

If the scaling factor of Eq. (2.13) is used, then H_i in Eq. (2.7) is replaced by

$$\begin{aligned} H_i &= -\frac{1}{2}\nabla^2 + v(\mathbf{r}) + \int \frac{\rho(\mathbf{r}')}{|\mathbf{r}-\mathbf{r}'|}\,d\mathbf{r}' + v_{\rm xc}^{\rm DFA}\big([\rho_\alpha,\rho_\beta],\mathbf{r}\big) \\ & \quad -X_i^m\bigg(\int \frac{\rho_i(\mathbf{r}')}{|\mathbf{r}-\mathbf{r}'|}\,d\mathbf{r}' + v_{\rm xc}^{\rm DFA}\big([\rho_i,0],\mathbf{r}\big)\bigg) - (m+1)\Big(\frac{\rho_i}{\rho}\Big)^m\Big(J[\rho_i] + E_{\rm xc}^{\rm DFA}[\rho_i,0]\Big) \\ & \quad +m\sum_j \Big(\frac{\rho_j}{\rho}\Big)^{m+1}\Big(J[\rho_j] + E_{\rm xc}^{\rm DFA}[\rho_j,0]\Big). \end{aligned} \tag{B.2}$$

The details of the implementation of Eq. (2.7) with Gaussian basis sets can be found in Appendix A.

Bibliography

[1] P. Hohenberg and W. Kohn, Phys. Rev. **136**, B864 (1964).

[2] W. Kohn and L. J. Sham, Phys. Rev. **140**, A1133 (1965).

[3] R. G. Parr and W. Yang, *Density-Functional Theory of Atoms and Molecules* (Oxford University Press, New York, 1989).

[4] J. F. Janak, Phys. Rev. B **18**, 7165 (1978).

[5] J. P. Perdew, A. Ruzsinszky, J. Tao, V. N. Staroverov, G. E. Scuseria, and G. I. Csonka, J. Chem. Phys. **123**, 062201 (2005).

[6] S. H. Vosko, L. Wilk, and M. Nusair, Can. J. Phys. **58**, 1200 (1980).

[7] J. P. Perdew and Y. Wang, Phys. Rev. B **45**, 13244 (1992).

[8] J. P. Perdew, K. Burke, and M. Ernzerhof, Phys. Rev. Lett. **77**, 3865 (1996); **78**, 1396 (1997) (E).

[9] J. Tao, J. P. Perdew, V. N. Staroverov, and G. E. Scuseria, Phys. Rev. Lett. **91**, 146401 (2003).

[10] A. D. Becke, Phys. Rev. A **38**, 3098 (1988).

[11] C. Lee, W. Yang, and R. G. Parr, Phys. Rev. B **37**, 785 (1988); B. Miehlich, A. Savin, H. Stoll, and H. Preuss, Chem. Phys. Lett. **157**, 200 (1989).

[12] T. Van Voorhis and G. E. Scuseria, J. Chem. Phys. **109**, 400 (1998).

[13] A. D. Becke, J. Chem. Phys. **98**, 1372 (1993).

[14] A. D. Becke, J. Chem. Phys. **98**, 5648 (1993).

[15] A. D. Becke, J. Chem. Phys. **104**, 1040 (1996).

[16] J. P. Perdew, M. Ernzerhof, and K. Burke, J. Chem. Phys. **105**, 9982 (1996).

[17] M. Ernzerhof and G. E. Scuseria, J. Chem. Phys. **110**, 5029 (1999).

[18] C. Adamo and V. Barone, J. Chem. Phys. **110**, 6158 (1999).

[19] J. Jaramillo, G. E. Scuseria, and M. Ernzerhof, J. Chem. Phys. **118**, 1068 (2003).

[20] A. Savin, in *Recent Developments and Applications of Modern Density Functional Theory*, edited by J. M. Seminario (Elsevier, Amsterdam, 1996), pp. 327–357.

[21] J. Toulouse, F. Colonna, and A. Savin, Phys. Rev. A **70**, 062505 (2004).

[22] J. Heyd, G. E. Scuseria, and M. Ernzerhof, J. Chem. Phys. **118**, 8207, (2003); **124**, 219906 (2006) (E).

[23] J. Heyd and G. E. Scuseria, J. Chem. Phys. **120**, 7274 (2004).

[24] J. Heyd and G. E. Scuseria, J. Chem. Phys. **121**, 1187 (2004).

[25] J. Heyd, J. E. Peralta, G. E. Scuseria, and R. L. Martin, J. Chem. Phys. **123**, 174101 (2005).

[26] H. Iikura, T. Tsuneda, T. Yanai, and K. Hirao, J. Chem. Phys. **115**, 3540 (2001).

[27] Y. Tawada, T. Tsuneda, S. Yanagisawa, T. Yanai, and K. Hirao, J. Chem. Phys. **120**, 8425 (2004).

[28] I. C. Gerber and J. G. Ángyán, Chem. Phys. Lett. **415**, 100 (2005).

[29] Y. Zhang and W. Yang, J. Chem. Phys. **109**, 2604 (1998).

[30] D. R. Hartree, Proc. Camb. Phil. Soc. **24**, 89; 111; 426 (1928).

[31] E. Fermi and E. Amaldi, Mem. R. Accad. Ital. **6**, 117 (1934).

[32] J. P. Perdew and A. Zunger, Phys. Rev. B **23**, 5048 (1981).

[33] J. P. Perdew, R. G. Parr, M. Levy, and J. L. Balduz, Jr., Phys. Rev. Lett. **49**, 1691 (1982).

[34] J. P. Perdew, in *Density Functional Methods in Physics*, edited by R. M. Dreizler and J. da Providencia (Plenum, New York, 1985), pp. 265–308.

[35] J. Gräfenstein, E. Kraka, and D. Cremer, J. Chem. Phys. **120**, 524 (2004).

[36] J. Gräfenstein, E. Kraka, and D. Cremer, Phys. Chem. Chem. Phys. **6**, 1096 (2004).

[37] J. P. Perdew, A. Ruzsinszky, G. I. Csonka, O. A. Vydrov, G. E. Scuseria, V. N. Staroverov, and J. Tao, submitted. URL: `http://arxiv.org/abs/cond-mat/0702283`.

[38] P. Mori-Sánchez, A. J. Cohen, and W. Yang, J. Chem. Phys. **125**, 201102 (2006).

[39] A. Ruzsinszky, J. P. Perdew, G. I. Csonka, O. A. Vydrov, and G. E. Scuseria, J. Chem. Phys. **125**, 194112 (2006).

[40] A. Ruzsinszky, J. P. Perdew, G. I. Csonka, O. A. Vydrov, and G. E. Scuseria, J. Chem. Phys. **126**, 104102 (2007).

[41] B. G. Johnson, C. A. Gonzalez, P. M. W. Gill, and J. A. Pople, Chem. Phys. Lett. **221**, 100 (1994).

[42] G. I. Csonka, N. A. Nguyen, and I. Kolossvary, J. Comput. Chem. **18**, 1534 (1997).

[43] G. I. Csonka and B. G. Johnson, Theor. Chem. Acc. **99**, 158 (1998).

[44] C. Legrand, E. Suraud, and P.-G. Reinhard, J. Phys. B **35**, 1115 (2002).

[45] I. Ciofini, H. Chermette, and C. Adamo, Chem. Phys. Lett. **380**, 12 (2003); Chem. Phys. **309**, 67 (2005).

[46] J. Garza, J. A. Nichols, and D. A. Dixon, J. Chem. Phys. **112**, 7880 (2000).

[47] J. Garza, R. Vargas, J. A. Nichols, and D. A. Dixon, J. Chem. Phys. **114**, 639 (2001).

[48] S. Patchkovskii, J. Autschbach, and T. Ziegler, J. Chem. Phys. **115**, 26 (2001).

[49] S. Patchkovskii and T. Ziegler, J. Phys. Chem. A **106**, 1088 (2002).

[50] S. Patchkovskii and T. Ziegler, J. Chem. Phys. **116**, 7806 (2002).

[51] J. B. Krieger, Y. Li, and G. J. Iafrate, Phys. Rev. A **45**, 101 (1992); **46**, 5453 (1992); **47**, 165 (1993).

[52] A. Svane, W. M. Temmerman, Z. Szotek, J. Lægsgaard, and H. Winter, Int. J. Quantum Chem. **77**, 799 (2000).

[53] A. Filippetti and N. A. Spaldin, Phys. Rev. B **67**, 125109 (2003).

[54] C. D. Pemmaraju, T. Archer, D. Sánchez-Portal, and S. Sanvito, Phys. Rev. B **75**, 045101 (2007).

[55] M. R. Pederson, R. A. Heaton, and C. C. Lin, J. Chem. Phys. **80**, 1972 (1984); **82**, 2688 (1985).

[56] M. A. Whitehead, in *Recent Advances in Density Functional Methods, Part II*, edited by D. P. Chong (World Scientific, Singapore, 1997).

[57] S. Goedecker and C. J. Umrigar, Phys. Rev. A **55**, 1765 (1997).

[58] V. Polo, E. Kraka, and D. Cremer, Mol. Phys. **100**, 1771 (2002).

[59] V. Polo, J. Gräfenstein, E. Kraka, and D. Cremer, Theor. Chem. Acc. **109**, 22 (2003).

[60] R. Seeger and J. A. Pople, J. Chem. Phys. **65**, 265 (1976).

[61] O. A. Vydrov and G. E. Scuseria, J. Chem. Phys. **122**, 184107 (2005).

[62] E. J. Bylaska, K. Tsemekhman, and F. Gao, Phys. Scr. **T124**, 86 (2006).

[63] C. Edmiston and K. Ruedenberg, Rev. Mod. Phys. **35**, 457 (1963); J. Chem. Phys. **43**, S97 (1965).

[64] S. F. Boys, Rev. Mod. Phys. **32**, 296 (1960); J. M. Foster and S. F. Boys, *ibid.* **32**, 300 (1960).

[65] L. A. Curtiss, K. Raghavachari, P. C. Redfern, and J. A. Pople, J. Chem. Phys. **106**, 1063 (1997).

[66] L. A. Cole and J. P. Perdew, Phys. Rev. A **25**, 1265 (1982).

[67] J. G. Harrison, R. A. Heaton, and C. C. Lin, J. Phys. B **16**, 2079 (1983).

[68] J. Chen, J. B. Krieger, Y. Li, and G. J. Iafrate, Phys. Rev. A **54**, 3939 (1996).

[69] X.-M. Tong and S.-I. Chu, Phys. Rev. A **55**, 3406 (1997).

[70] J. G. Harrison, J. Chem. Phys. **78**, 4562 (1983).

[71] M. R. Pederson and C. C. Lin, J. Chem. Phys. **88**, 1807 (1988).

[72] L. A. Curtiss, P. C. Redfern, K. Raghavachari, and J. A. Pople, J. Chem. Phys. **109**, 42 (1998).

[73] A. D. Becke, J. Chem. Phys. **109**, 2092 (1998).

[74] S. J. Chakravorty, S. R. Gwaltney, E. R. Davidson, F. A. Parpia, and C. F. Fischer, Phys. Rev. A **47**, 3649 (1993).

[75] B. J. Lynch and D. G. Truhlar, J. Phys. Chem. A **107**, 8996 (2003); **108**, 1460 (2004) (E).

[76] B. J. Lynch, Y. Zhao, and D. G. Truhlar, `http://comp.chem.umn.edu/database`.

[77] *CRC Handbook of Chemistry and Physics*, edited by D. R. Lide, 87th ed. (CRC Press, Boca Raton, 2006).

[78] J. P. Perdew, Adv. Quantum Chem. **21**, 113 (1990).

[79] M. R. Norman, Phys. Rev. B **28**, 3585 (1983).

[80] J. G. Harrison, Phys. Rev. B **35**, 987 (1987).

[81] M. R. Pederson, R. A. Heaton, and J. G. Harrison, Phys. Rev. B **39**, 1581 (1989).

[82] U. Lundin and O. Eriksson, Int. J. Quantum Chem. **81**, 247 (2001).

[83] C.-O. Almbladh and U. von Barth, Phys. Rev. B **31**, 3231 (1985).

[84] F. Della Sala and A. Görling, Phys. Rev. Lett. **89**, 033003 (2002).

[85] D. J. Tozer and N. C. Handy, J. Chem. Phys. **109**, 10180 (1998).

[86] M. E. Casida and D. R. Salahub, J. Chem. Phys. **113**, 8918 (2000).

[87] T. Leininger, H. Stoll, H.-J. Werner, and A. Savin, Chem. Phys. Lett. **275**, 151 (1997).

[88] H. Sekino, Y. Maeda, and M. Kamiya, Mol. Phys. **103**, 2183 (2005).

[89] M. Kamiya, H. Sekino, T. Tsuneda, and K. Hirao, J. Chem. Phys. **122**, 234111 (2005).

[90] M. Kamiya, T. Tsuneda, and K. Hirao, J. Chem. Phys. **117**, 6010 (2002).

[91] T. Sato, T. Tsuneda, and K. Hirao, J. Chem. Phys. **123**, 104307 (2005).

[92] J. G. Ángyán, I. C. Gerber, A. Savin, and J. Toulouse, Phys. Rev. A **72**, 012510 (2005).

[93] E. Goll, H.-J. Werner, and H. Stoll, Phys. Chem. Chem. Phys. **7**, 3917 (2005).

[94] P. M. W. Gill, R. D. Adamson, and J. A. Pople, Mol. Phys. **88**, 1005 (1996).

[95] M. Ernzerhof and J. P. Perdew, J. Chem. Phys. **109**, 3313 (1998).

[96] L. A. Constantin, J. P. Perdew, and J. Tao, Phys. Rev. B **73**, 205104 (2006).

[97] A. V. Krukau and G. E. Scuseria (unpublished).

[98] T. Yanai, D. P. Tew, and N. C. Handy, Chem. Phys. Lett. **393**, 51 (2004).

[99] M. J. G. Peach, T. Helgaker, P. Sałek, T. W. Keal, O. B. Lutnæs, D. J. Tozer, and N. C. Handy, Phys. Chem. Chem. Phys. **8**, 558 (2006).

[100] M. J. G. Peach, A. J. Cohen, and D. J. Tozer, Phys. Chem. Chem. Phys. **8**, 4543 (2006).

[101] P. M. W. Gill and R. D. Adamson, Chem. Phys. Lett. **261**, 105 (1996).

[102] Y. Zhao, B. J. Lynch, and D. G. Truhlar, J. Phys. Chem. A **108**, 2715 (2004).

[103] E. V. R. de Castro and F. E. Jorge, J. Chem. Phys. **108**, 5225 (1998).

[104] L. A. Curtiss, K. Raghavachari, P. C. Redfern, and J. A. Pople, J. Chem. Phys. **112**, 7374 (2000).

[105] L. A. Curtiss, P. C. Redfern, K. Raghavachari, and J. A. Pople, J. Chem. Phys. **114**, 108 (2001).

[106] V. N. Staroverov, G. E. Scuseria, J. Tao, and J. P. Perdew, J. Chem. Phys. **119**, 12129 (2003); **121**, 11507 (2004) (E).

[107] Y. Zhao, N. González-García, and D. G. Truhlar, J. Phys. Chem. A **109**, 2012 (2005); **110**, 4942 (2006) (E).

[108] A. D. Boese and J. M. L. Martin, J. Chem. Phys. **121**, 3405 (2004).

[109] J. P. Perdew, A. Savin, and K. Burke, Phys. Rev. A **51**, 4531 (1995).

[110] N. Rösch and S. B. Trickey, J. Chem. Phys. **106**, 8940 (1997).

[111] A. D. Dutoi and M. Head-Gordon, Chem. Phys. Lett. **422**, 230 (2006).

[112] R. Merkle, A. Savin, and H. Preuss, J. Chem. Phys. **97**, 9216 (1992).

[113] B. Braïda, P. C. Hiberty, and A. Savin, J. Phys. Chem. A **102**, 7872 (1998).

[114] L. J. Schaad and W. V. Hicks, J. Chem. Phys. **53**, 851 (1970).

[115] J. Xie, B. Poirier, and G. I. Gellene, J. Chem. Phys. **122**, 184310 (2005).

[116] A. Carrington, D. I. Gammie, J. C. Page, A. M. Shaw, and J. M. Hutson, J. Chem. Phys. **116**, 3662 (2002).

[117] A. Wüest and F. Merkt, J. Chem. Phys. **120**, 638 (2004).

[118] D. C. Langreth and J. P. Perdew, Phys. Rev. B **26**, 2810 (1982); and references therein.

[119] GAUSSIAN Development Version, Revision D.02, M. J. Frisch, G. W. Trucks, H. B. Schlegel, G. E. Scuseria, M. A. Robb, J. R. Cheeseman, J. A. Montgomery, Jr., T. Vreven, K. N. Kudin, J. C. Burant, J. M. Millam, S. S. Iyengar, J. Tomasi, V. Barone, B. Mennucci, M. Cossi, G. Scalmani, N. Rega, G. A. Petersson, H. Nakatsuji, M. Hada, M. Ehara, K. Toyota, R. Fukuda, J. Hasegawa, M. Ishida, T. Nakajima, Y. Honda, O. Kitao, H. Nakai, M. Klene, X. Li, J. E. Knox, H. P. Hratchian, J. B. Cross, V. Bakken, C. Adamo, J. Jaramillo, R. Gomperts, R. E. Stratmann, O. Yazyev, A. J. Austin, R. Cammi, C. Pomelli, J. W. Ochterski, P. Y. Ayala, K. Morokuma, G. A. Voth, P. Salvador, J. J. Dannenberg, V. G. Zakrzewski, S. Dapprich, A. D. Daniels, M. C. Strain, O. Farkas, D. K. Malick, A. D. Rabuck, K. Raghavachari, J. B. Foresman, J. V. Ortiz, Q. Cui, A. G. Baboul, S. Clifford, J. Cioslowski, B. B. Stefanov, G. Liu, A. Liashenko, P. Piskorz, I. Komaromi, R. L. Martin, D. J. Fox, T. Keith, M. A. Al-Laham, C. Y. Peng, A. Nanayakkara, M. Challacombe, P. M. W. Gill,

B. Johnson, W. Chen, M. W. Wong, C. Gonzalez, and J. A. Pople, Gaussian, Inc., Wallingford CT, 2004.

[120] W. H. Press, B. P. Flannery, S. A. Teukolsky, and W. T. Vetterling, *Numerical Recipes* (Cambridge University Press, Cambridge, 1992).

[121] J. Pipek and P. Mezey, J. Chem. Phys. **90**, 4916 (1989).

[122] R. Neumann, R. H. Nobes, and N. C. Handy, Mol. Phys. **87**, 1 (1996).